BIOGEOCHEMICAL AND ECOLOGICAL RESPONSES TO WARMING CLIMATE IN HIGH ARCTIC POLAR DESERTS

A Thesis Submitted to the College of Graduate Studies and Research
In Partial Fulfilment of the Requirements
For the Degree of Doctor of Philosophy
In the Department of Soil Science
University of Saskatchewan
Saskatoon

By

Mitsuaki Ota

PERMISSION TO USE

In presenting this thesis/dissertation in partial fulfilment of the requirements for a Postgraduate degree from the University of Saskatchewan, I agree that the Libraries of this University may make it freely available for inspection. I further agree that permission for copying of this thesis/dissertation in any manner, in whole or in part, for scholarly purposes may be granted by the professor or professors who supervised my thesis/dissertation work or, in their absence, by the Head of the Department or the Dean of the College in which my thesis work was done. It is understood that any copying or publication or use of this thesis/dissertation or parts thereof for financial gain shall not be allowed without my written permission. It is also understood that due recognition shall be given to me and to the University of Saskatchewan in any scholarly use that may be made of any material in my thesis/dissertation. Requests for permission to copy or to make other uses of materials in this thesis (dissertation), in whole or part, should be addressed to:

Head, Department of Soil Science
University of Saskatchewan
Room 5D34, Agriculture Building, 51 Campus Drive
Saskatoon, Saskatchewan S7N 5A8
Canada

OR

Dean
College of Graduate and Postdoctoral Studies
University of Saskatchewan
116 Thorvaldson Building, 110 Science Place
Saskatoon, Saskatchewan S7N 5C9
Canada

DISCLAIMER

Reference in this thesis/dissertation to any specific commercial product, process, or service by trade name, trademark, manufacturer or otherwise, does not constitute or imply its endorsement, recommendation, or favouring by the University of Saskatchewan. The views and opinions of the author expressed herein do not state or reflect those of the University of Saskatchewan and shall not be used for advertising or product endorsement purposes.

ABSTRACT

High Arctic polar deserts cover 26% of the Arctic and are found to store a larger amount of soil organic carbon (SOC) in the permafrost and to emit higher amounts of the main greenhouse gases (GHGs) than previously expected. However, the mechanisms of the main GHG production are not clear. Furthermore, polar deserts are predicted to dramatically transform under rapidly warming temperatures and have uncertainty regarding a potential positive GHG-feedback to the warming climate. Freeze-thaw cycles develop frost-boil landscape and diapirs within frost-boil profiles. Diapirs are cryoturbic nutrient patches and support vascular plants in polar deserts. Frost-boil development and diapirs are expected to increase with the increase in temperatures and the permafrost thaw and are likely key for projected polar-desert evolutions. This dissertation investigated soil properties including the chemical structure of SOC, microbial processes responsible for GHG emissions, and the main GHG emissions associated with diapirism.

Diapirs had increased polysaccharides known to raise soil viscosity, which in turn facilitates diapirism. In addition to this, diapirs contained more recalcitrant SOC, which was consistent with the decreases in gross nitrogen mineralization by 30–48% and in carbon dioxide (CO_2) emissions by 19–38%. Similarly, diapiric frost boils slowed net methane (CH_4) emissions. With higher archaeal *amoA* abundance, diapiric frost boils had a higher magnitude of the emissions leading to a higher estimate of the emissions under dry conditions. On the other hand, a higher estimate of the emissions from diapiric frost boils linked to a higher probability of the emissions under wet conditions. Freeze-thaw treatment increased CO_2 emissions by 1.3–3.5 times and estimation of N_2O emissions by 72–204% but apparently reduced CH_4 consumption more than CH_4 production to increase net CH_4 emissions.

This dissertation found that diapirisms alter SOC components and the main GHG emissions. The higher abundance of polysaccharides and recalcitrant SOC suggests that biological factors are involved in diapirism and that diapirs supply vascular plants with nutrients as a result of a mutualistic relationship. Furthermore, this dissertation suggests that freeze-thaw triggers the main GHG emissions leading to the distinct emission patterns during snowmelt season from later growing season.

ACKNOWLEDGEMENTS

I would like to thank my supervisor, Dr. Steven Siciliano, for your guidance at each stage during my Ph.D. journey. I enjoyed learning western style academic and appreciate your believing in myself regardless of a language barrier. I would also like to thank my advisory committee members, Drs. Sina Adle, Angela Bedard-Haughn, Richard Farrell, Joyce McBeth for all the advice and guidance. In addition to my advisory committee members, I would like to thank Dr. Bobbi Helgason for providing the standard gene for ammonia-oxidizing archaea, Dr. Ken van Rees for your advice and support during the Arctic trip and my Ph.D. journey, and Dr. Katherine Stewart for providing advice on the diffusion disk technique.

Financial support for my project was provided by the Natural Sciences and Engineering Research Council of Canada Discovery Grant (#403046) to Dr. Siciliano. Polar Continental Shelf Program provided logistical field support. Personal financial support was provided by the Dean's Scholarship administered by the College of Agriculture and Bioresources and by the Saskatchewan Innovation and Opportunity Scholarship established by the provincial government.

Many thanks to the Arctic field crew members, Martin Brummell, Amanda Muller, Sarah Hardy, and Nicole Marleau for their assistance with fieldwork and your supports. Thanks to Dr. Greg Henry and his UBC field crew for their support and wonderful memories. I am thankful to the Soil Environmental Toxicology Lab for providing laboratory equipment and assistance, Frank Krijnen and Darren Richman for the greenhouse gas measurements, and Myles Stocki for ^{15}N enrichment analysis.

DEDICATION

This dissertation is dedicated to everyone who made me the person I am today, supported me, and believed in me even when I wasn't sure if it would be possible to explore my Ph.D. journey. I would like to dedicate this dissertation to Dr. Kosuke Noborio, who gave me the opportunity to pursue my Ph.D. here and Dr. Shuichiro Murakami, who taught laboratory skills to me from scratch. I would also like to dedicate this dissertation to my host family, Ed & Marilyn Palmer, who introduced Canadian culture and inspired me and to the teachers at the U of S Language Centre. Finally, I would like to dedicate this thesis to my mom, Keiko Ota and my brother, Narutoshi Ota, who always supported and encouraged me during my Ph.D. journey, and to my best friend, Natsuki Ochiai.

TABLE OF CONTENTS

LIST OF TABLES

LIST OF FIGURES

LIST OF ABBREVIATIONS

AOA	Ammonia-oxidizing archaea
AOB	Ammonia-oxidizing bacteria
AMO	Ammonia monooxygenase
ATR-FTIR	Attenuated total reflectance Fourier transformed mid-infrared
CH_4	Methane
CAVM	Circumpolar Arctic Vegetation Map
CO_2	Carbon dioxide
DL	Detection limit
DOC	Dissolved organic carbon
GHG	Greenhouse gas
GLMM	Generalized linear mixed model
LS	Least squares
N_2	Dinitrogen
NH_3	Ammonia
NO	Nitric oxide
NO_2^-	Nitrite
NO_3^-	Nitrate
N_2O	Nitrous oxide
SOC	Soil organic carbon
SOM	Soil organic matter
SP	Site preference
TDN	Total dissolved nitrogen
vis-NIR	Visible and near-infrared
WFPS	Water-filled pore space

1. INTRODUCTION

The High Arctic is the northernmost region of the Arctic and is defined as a bioclimatic subzone in the Circumpolar Arctic Vegetation Map (CAVM; Walker et al., 2005) that has mean July temperatures ranging from 4–6°C (Burnham & Sletten, 2010; Ping et al., 2008). The dominant ecological zones in the High Arctic are polar deserts, which cover 1,358,000 km^2 or approximately 26% of the land within the Arctic region (Walker et al., 2002). Despite scant vegetation and slow biogeochemical process, the High Arctic polar deserts potentially increase greenhouse gas (GHG) emissions in response to the recent warming climate. Polar deserts occur from sea level to upland (> 200 m) (Bliss et al., 1994) and have annual precipitation of less than 150 mm (Blaud et al., 2015). Due to the harsh environment, cryptogam and forb are the dominant vegetation types in polar deserts and sparsely cover the ground (< 5%) (Gold & Bliss, 1995). The low organic matter input and cold climate were thought to limit biogeochemical cycling in polar deserts. However, polar deserts can tentatively emit GHGs including carbon dioxide (CO_2), nitrous oxide (N_2O), and methane (CH_4) at a rate comparable to the nearby mesic and hydric tundras of which vegetation communities are common at lower Arctic latitudes (Brummell et al., 2012, 2014; Lamb et al., 2011). It should be noted that polar deserts understandably emit less CH_4 compared with the moss wetland community (W1, "Wetland" according to Circumpolar Arctic Vegetation Map; Walker et al., 2002) during the growing season (Brummell et al., 2012). Though the Arctic soils generally emit GHGs as a result of biogeochemical cycling as the topsoil layer overlying the permafrost (*i.e.,* active layer) thaws during the short summer season, the mechanism of GHG production in polar deserts is poorly understood. The Canadian High Arctic is warming at twice the rate of the global average and is expected to increase in temperatures by 6–8°C by 2100 (Allan et al., 2014). The High Arctic has a larger amount of soil organic carbon (SOC) than that was previously estimated by Bliss & Matveyeva (1992), and the estimates of SOC were the most underestimated in polar deserts among the High Arctic vegetation communities (Burnham & Sletten, 2010). Therefore, as

warming temperatures thaw the permafrost and deepen the active layer during the growing season, the SOC released from the permafrost enhances microbial decomposition, leading to GHG emissions. Considering that polar deserts cover a large area, it is critical to evaluate potential feedback with GHG production in the High Arctic polar desert ecosystems in the context of a warming climate.

The ground features of the High Arctic polar deserts deform due to alternate freezing and thawing, which often develop sorted circles (*i.e.,* frost boils) (Bliss et al., 1994; Muc et al., 1989). "Frost boil" is also commonly used to describe the circular patches with sparse vegetation cover which don't have rock fragments at the margins (*i.e.,* non-sorted circles) (van Everdingen, 1998; Walker et al., 2004). In this dissertation, however, frost boils are defined as sorted circles or the patches (< 3 m diameter) which have borders of stones at the margins. In polar deserts, frost-boil development leads to biogeochemical cycling and is related to warming temperatures. The development begins with cracking of the active layer due to thermal contraction in winter (Ping et al., 2015). Seasonal cracking creates circular patterns on the ground which form the margins of frost boils, and then the cracks are filled with cryptogams and herbaceous vegetation (Walker et al., 2004). Also, as the soil freezes, unfrozen soil water, such as film water on soil particles, migrates toward the freezing front (*i.e.,* the boundary between freeze and unfrozen soil) along the thermal gradient and develops ice lenses and segregated ice (Torrance & Schellekens, 2006). Ice lenses and segregated ice increase in size as unfrozen water continues to migrate and increases its volume due to the phase change to ice. The expansion of the volume creates pressure, and due to the underlying permafrost, the pressure forces soil materials upward (*i.e.,* frost heave). The vegetation at the margins reduces thermal conductivity and frost heave compared to the center portion of the patches (Ping et al., 2015). As a result, the centers of frost boils are elevated at a greater rate than the margins and remain barren or host only sparse vegetation as frost heave breaks plant roots (Brady & Weil, 2008; Ping et al., 2015). The active layer contains coarse materials; repeated frost heave eventually moves these materials to the ground surface, and then coarser particles move outward toward the margins due to soil creep whereas finer particles stay in the center portions (Walker et al., 2004). The vegetation and stone rings at the margins cool the active layer due to the insulation effects and raise the permafrost table whereas the central portions with little vegetation increase thermal conductivity and deepen the active layer (Ping et al., 2015; Shilts, 1978). Thus, the permafrost shapes depressions under

frost boils (Ping et al., 2015; Shilts, 1978), and dissolved organic matter derived from the vegetation at the margins moves downward with meltwater leaching (Muller et al., 2017; Schaeffer et al., 2013; Tye et al., 2005) and accumulates above the bowl-shaped permafrost table (Boike et al., 2008; Cannone et al., 2004; Walker et al., 2004). The accumulated nutrients move upward by frost heave; therefore, frost-boil development plays a primary role on nutrient cycling in polar deserts. Furthermore, frost boil development is expected to increase with permafrost thaw and meltwater production (Callaghan et al., 2005; Klaus et al., 2013; Walker et al., 2008) and is key for future GHG emissions from polar deserts under a warming climate.

Diapirism develops in some frost-boil soil profiles, which is also related to warming temperatures. Diapirism is the intrusion of soil materials into the overlying soil layer as a result of a freezing and thawing cycle (Ping et al., 2015; Swanson et al., 1999). The lower part of the active layer (*i.e.,* ice-rich horizon) develops ice lenses and segregated ice and lowers bulk density. As ice-rich horizon thaw, the soil materials intrude into the overlying horizon with higher bulk density, and the diapiric flow is facilitated as the overlying layer is more viscous (Ping et al., 2015; Swanson et al., 1999). Diapirism carries the accumulated nutrients upward, above the bowl-shaped permafrost table moves upward and creates subsurface nutrient patches or diapirs (Bhy horizon). Muller et al. (2017) showed that diapirs occurred in approximately 30% of frost boils and increased soil carbon (C) by 7% and nitrogen (N) by 20%. Diapirism is also expected to increase with permafrost thaw and meltwater production under a warming climate (Klaus et al., 2013; Ping et al., 2015; Swanson et al., 1999). The uppermost part of the permafrost remains frozen most years, however extreme climate conditions thaw the uppermost layer on a decadal scale, which increases water and the resulting saturated materials to lead to diapirism (Ping et al., 2015). By the end of the 21st century, up to 81% of the top 3.5 m of the permafrost is projected to decrease at high northern latitudes depending on scenarios with GHG emissions in this century (*i.e.,* the representative concentration pathways) (IPCC, 2014). Therefore, it is critical to assess how diapirism alters biogeochemical cycling as ecological feedback to a warming climate in the High Arctic polar deserts.

The goal of this dissertation is to address how the High Arctic polar deserts produce GHGs in response to the warming climate. The main objectives are (1) to assess how diapirism alters the soil properties and microbial processes responsible for the GHG emissions in polar deserts, and (2) to assess GHG emission rates associated with diapirism. Furthermore, this

dissertation assesses how freeze and a subsequent thaw alter GHG emissions in relation to diapirism to expand the picture of the diapirism's role during the growing season. I hope this dissertation will contribute to the robust understanding of the ecological feedbacks to a projected warming climate in the High Arctic polar deserts.

1.1 Dissertation Organization

This dissertation consists of six chapters, including three research chapters for submission to peer-reviewed journals. Chapter 1 is an introduction to address the scientific question and the objectives of the dissertation. The following literature review in Chapter 2 is an overview of the key concepts for the research chapters and focuses on the High Arctic polar desert ecosystem, cryoturbation as an edaphic factor (*i.e.,* frost-boil development and diapirism), C and N cycles associated with the major GHGs, and an analytical approach for zero-inflated data (*i.e.,* the hurdle model). Chapter 3–5 are the research chapters and consist of preface, abstract, materials and methods, results, and discussion. Chapter 3 also contains a conclusion section according to the guidelines of the journal in which the manuscript was submitted. Please note that the information about frost-boil development and diapirism is repeated in the research chapters as they are central to the dissertation.

Chapter 3 summarizes soil properties such as SOC, dissolved organic C and N, soil phosphorus, pH, and electrical conductivity and examines C and N mineralization rates associated with diapirism. Together with, I also assess if diapirism alters the chemical structure of SOC (*i.e.,* the quality of SOC). Chapter 4 assesses the archaeal *amoA* gene—carried by ammonia-oxidizing archaea—abundance associated with diapirism and determines nitrous oxide production under conditions favouring nitrification and denitrification. As the nitrous-oxide data are zero-inflated and are difficult to perform common statistical methods such as general linear modeling, I take the hurdle model approach to reveal the effects of covariates such as diapirism on nitrous oxide production. Chapter 5 assesses carbon dioxide, nitrous oxide, and methane productions after freeze and a subsequent thaw in relation to diapirism. I use data on each of these gases obtained from Chapter 4 and compare it with each of the corresponding gas data in Chapter 5. The key findings of the research chapters are summarized in Chapter 6 as a synthesis chapter. Chapter 6 also focuses on ecological implications of diapirism for future research on the High Arctic polar deserts.

2. LITERATURE REVIEW

2.1 High Arctic Polar Desert Ecosystem

High Arctic polar deserts generally have dry soils with sparse plant communities. The development of the plant communities is primarily limited by N availability that increases with soil moisture in polar deserts. The plant community covers approximately 5% of the ground surface and mainly consists of herb-cryptogam with a limited presence of woody species (Bliss et al., 1994; Callaghan et al., 2005). In typically dry areas, Bliss et al. (1994) found that vascular plants covered 0.4–1.1% of the ground and that cryptogams covered up to 8% at Alexandra Fjord, Ellesmere Island. Similarly, total plant cover ranged from 2.5–4.5% in dry areas, but vascular plants accounted for 70% of the total at Truelove, Devon Island (Bliss et al., 1994). Despite the low biological productivity, polar deserts also have exceptional areas where surface soils remain moist during most of the growing season due to topography (Bliss et al., 1994; Gold & Bliss, 1995; Stewart et al., 2014). For example, areas located downslope from persistent snow banks continuously receive water supply from melting snow during the growing season and support well-developed plant communities comparable to wet tundras of the Low Arctic (Bliss et al., 1994; Gold & Bliss, 1995). Cryptogams form thin (< 1 cm) crust layers of cyanobacteria, crustose lichens, moss, protists, and fungi (*i.e.,* biological soil crusts) on the soil surface (Boulanger-Lapointe et al., 2014; Gold & Bliss, 1995). In such areas, vascular plants cover 5–13% and biological soil crusts cover 5–72% of the ground surface in the polar deserts at Alexandra Fjord and Truelove (Bliss et al., 1994). Gold & Bliss (1995) compared plant water relations between barren (noncrusted) sites and biological soil crust and vascular plant community (crusted) sites. The crusted sites had consistently higher water contents by up to 7.7% in top 10 cm soil and approximately threefold higher vascular plant cover than the noncrusted sites; however, water stress for established plants was minor in both sites (Gold & Bliss, 1995). For instance, midday maximal stomatal conductance—indicative of plant water status—of *Saxifraga oppositifolia* did not differ between the crusted and the noncrusted sites

(Gold & Bliss, 1995). Indeed, at noncrusted sites, the subsurface soil remained effectively saturated, and thus soil moisture was available for some polar-desert plants such as *Saxifraga oppositifolia*, *Dryas integrifolia*, and *Sasix Arctica* as these species can grow roots down near the permafrost layer (20–40 cm) (Gold & Bliss, 1995; Muller et al., 2017). Consistently, another study showed few responses of a polar semi-desert plant community to water addition (Callaghan et al., 2005). On the other hand, cryptogams benefit from surface moisture and increase N fixation activities in polar deserts where total soil N is often scarce (0.04%) (Callaghan et al., 2005; Gold & Bliss, 1995; Stewart et al., 2014). As biological soil crusts form, soil N can double; thus, greater floristic richness in polar-desert ecosystem results from greater soil N concentrations enhanced by surface soil moisture availability (Bliss et al., 1994; Callaghan et al., 2005; Gold & Bliss, 1995; Stewart et al., 2014). Therefore, cryptogam development is likely of great consequence for the projected transformation of polar-desert ecosystems under a warming climate (Callaghan et al., 2005; Gold & Bliss, 1995; Lamb et al., 2011; Stewart et al., 2013).

The amount of SOC stock is critical for GHG-production feedbacks to rapidly warming temperatures in the permafrost region. SOC stocks in the northern circumpolar region are disproportionately large—approximately 30–40% of the global SOC to a depth of 3 m—considering the small landmass (*i.e.,* 15% of the global land surface) and the low vegetation (*i.e.,* 10–20% of the global vegetation C pool) generally because decomposition rates are slow under the low temperature (Ping et al., 2015). As temperatures continue to warm, increased microbial activity and additional SOC released by permafrost thaw can enhance GHG emissions and seasonal GHG budgets (Burnham & Sletten, 2010; Elberling et al., 2010; Schuur et al., 2015; Voigt et al., 2017). Conventionally, SOC in the High Arctic was estimated solely based on the upper 25 cm depth (Bliss & Matveyeva, 1992). However, the depth of the active layer is variable across the High Arctic landscapes ranging from 20 cm in organic-rich soils to 100 cm in mineral soils, and cryoturbation buries SOC to the depth of the active layer (Burnham & Sletten, 2010; Callaghan et al., 2005; Gillespie et al., 2014; Kaiser et al., 2007; Wild et al., 2013). Burnham & Sletten (2010) assessed SOC stock in the entire active layer across the High Arctic ecosystems, including polar desert, polar semi-desert, and mire, and estimated that the High Arctic contains approximately 12 Pg of SOC. The estimation is more than fivefold greater than Bliss & Matveyeva (1992) (Burnham & Sletten, 2010). Similarly, Hugelius et al. (2014) estimated SOC

stock to be 10 ± 3 Pg in the 0–0.3 m and 24 ± 8 Pg in the 0–1 m depth ranges in the High Arctic. By the vegetation type, polar deserts are found to store over 127 times more SOC than the previous estimation by Bliss & Matveyeva (1992) whereas polar semidesert and mire are found to store approximately eight times and 1.5 times more, respectively (Burnham & Sletten, 2010). The huge underestimation in polar deserts is primarily because SOC distribution is subject to cryoturbation and accumulates in the deep active layer (Burnham & Sletten, 2010). Burnham & Sletten (2010) found that polar deserts contained 57% of the total SOC below 25 cm, whereas polar semideserts and mires contained 31% and 16% below 25 cm, respectively as they are more densely vegetated and less affected by cryoturbation. In the 0–3 m depth range, the High Arctic is estimated to have 30–50% of the SOC in the upper 0.3 m and to store 34 ± 16 Pg, which accounts for 3% of the SOC stock in a depth of 3 m in the northern circumpolar permafrost region (Hugelius et al., 2014). Despite the low estimates of SOC compared to other Arctic regions, it is important to note that the estimates are based on very limited pedon data, and thus highly remain uncertain (Hugelius et al., 2014). For example, though robust estimates of SOC stock require a minimum of 30 sample sizes in the High Arctic region to cover the variabilities in SOC due to cryoturbation and vegetation type, the estimates are obtained from only eight pedons (Hugelius et al., 2014). Furthermore, among the eight pedons, the number of pedons for cryoturbated permafrost soils (*i.e.,* Turbels) was one whereas the numbers for organic permafrost soils (*i.e.,* Histels) and for non-cryoturbated permafrost-affected mineral soils (*i.e.,* Orthels) were six and one (Hugelius et al., 2014; Soil Survey Staff, 1999). In addition to the higher SOC stock than previously expected, high-latitude regions have warmed at a higher rate than the global average (Schuur et al., 2015). Indeed the sensitivity of permafrost to temperature change is variable depending on scenarios with GHG emissions in the 21st century across the Arctic regions (IPCC, 2014; Slater & Lawrence, 2013). Canadian Archipelago is still projected to sustain the permafrost even under the most intense scenario in 2099 (Slater & Lawrence, 2013). However, Slater & Lawrence (2013) excluded the majority part of Ellesmere Island and Devon Island as glaciers where polar deserts present. Furthermore, frost-boil development increases the thermal conductivity of the center portions of frost boils (Ping et al., 2015; Shilts, 1978). Therefore, with the frost-boil landscape, Canadian High Arctic polar deserts may have less sustainable permafrost in Canadian Archipelago and may have stronger positive feedback loops (Ping et al., 2015) than previously thought.

2.2 Cryoturbation as an Edaphic Factor

Frost-boil development led by frost heave interacts with aboveground vegetation and subsequently initiates nutrient cycling in frost-boil ecosystems. The center portion of the frost boil has a higher rate of frost heave and is commonly more barren or sparsely vegetated than the margins with a lower frost-heave rate (Ping et al., 2015; Wilson & Humphreys, 2010). At the same time as frost heave limits vascular plant growth, vegetation colonization limits frost heave of nonsorted circles (Wilson & Humphreys, 2010). Similarly, Kade & Walker (2008) showed an increase in frost heave rate by 26% after removing vegetation from nonsorted circle in Alaska. Frost heave plays a critical role in developing biogeochemical cycles within frost boils which involves (1) net upward movement of soil materials with frost heave, (2) outward movement of soil materials toward the margin at the frost-boil surface by soil creep, and (3) downward movement of soil materials including dissolved organic matter from the more vegetated margin area by soil movement and leaching (Walker et al., 2004). Maximum heave on frost boils (*i.e.,* the center portion) varies from less than 1 cm to more than 20 cm (Walker et al., 2004), and thus the degree of frost heave is critical for variations in the rates of a biogeochemical cycle and subsequently GHG production in frost-boil ecosystems. Polar-desert frost boils may have relatively higher amounts of frost heave. Due to the lack of surface thermal insulation, circle centers freeze faster than the margins and attract unfrozen water from the margins, and thus allow more ice lensing to develop and increase the amount of frost heave (Ping et al., 2015; Walker et al., 2004). With the influence of water movement, frost-boil development is likely linked to biogeochemical cycling in the High Arctic polar deserts.

Cryoturbation redistributes soil organic matter (SOM) and enhances the sequestration of SOM within the active layer. Cryoturbated SOM accounts for approximately 400 Gt of C and increases its contribution to SOM stock until shrub tundra dominates the landscape as the greater thermal insulation reduces frost heave, and thus is more significant in the northern Arctic than in southern Low Arctic (Ping et al., 2015; Wild et al., 2014). Previous studies show that cryoturbation and burying of soil horizons slow C and N mineralization in Arctic regions (Gillespie et al., 2014; Kaiser et al., 2007; Wild et al., 2013), which cannot be explained solely by lower soil temperature in subsurface soils (Kaiser et al., 2007). Wild et al. (2013) indicated that cryoturbated horizons strongly reduced protein depolymerization rate (*i.e.,* the rate-limiting step in soil N cycling) in eastern Greenland and north-eastern Siberia, which appeared to slow N

mineralization rate. The reduction in protein depolymerization in those cryoturbated horizons may link to a low abundance of fungi since fungi produce extracellular enzymes such as proteases to degrade complex organic molecules (Wild et al., 2013). Extracellular enzymes may be a key mechanism for cryoturbated organic matter degradation. Cumulative SOM-derived respiration in the cryoturbated horizon increased two-fold without microbial growth or change in microbial community composition after adding protein or amino acids to the horizon (Wild et al., 2014). Thus, it was likely that the input of N was used for producing extracellular enzymes to decompose cryoturbated organic matter (Wild et al., 2014). In addition to the microbial capacity to decompose cryoturbated organic matter, chemical speciation of SOM in cryoturbated horizon differs from those in other horizons, which may alter the bioavailability of cryoturbated organic matter. Gillespie et al. (2014) found the accumulation of ketones and the loss of carbohydrate, phenolic, and carboxylic compounds in the cryoturbated horizons that had lower cumulative C mineralization than surface organic horizons. Carbohydrates and carboxylic compounds represent labile OC derived from plant and microbial biomass and are lost by mineralization whereas ketones accumulate as microbes consume carboxylates and phenols in labile SOM (Gillespie et al., 2014). Therefore, the organic matter subducted by cryoturbation likely is a refractory pool of SOM in the soil profile (Gillespie et al., 2014).

Diapirism also redistributes SOM and is a key component of a biogeochemical cycle in Arctic ecosystems where the climate is relatively harsh such as the High Arctic polar desert. Diapirism is, however, driven by unstable bulk density caused by differences in water content between the ice-rich layer and the overlying soil layer instead of segregated ice and ice lens formation which leads to frost heave (Ping et al., 2015; Swanson et al., 1999). Until recently, few studies assessed soil properties and the GHG production associated with diapirism in Canadian High Arctic polar desert ecosystems where frost boils dominated the landscape (Brummell et al., 2015; Muller et al., 2017; Ota et al., 2020). Approximately 30% of frost boils have an abrupt increase in SOC (> 0.2 log % SOC)—indicative of diapirism—based on visible near-infrared reflectance at depths ranging from 10–30 cm within the frost-boil profile (Muller et al., 2017). The survey also found that frost boils typically develop spatially variable diapirs with 5–15 cm thickness below the center portions, supporting Swanson et al. (1999) (Muller et al., 2017). Diapirs increase total soil C by 7% and have 11–20% greater total soil N compared with those at the corresponding depths within control frost boils that were not indicative of diapirism (Muller

et al., 2017). Despite the increase in soil C, diapirs decrease net CO_2 production within frost boils (Brummell et al., 2015). In addition to this, highly contorted diapiric horizons and mechanical models for diapirism suggest that as the overlying horizon becomes more viscous, the increase in viscosity facilitates diapiric intrusion that is initiated by the unstable bulk density (Swanson et al., 1999). Thus, similar to the SOM in the buried horizons in other Arctic regions (Gillespie et al., 2014; Kaiser et al., 2007; Wild et al., 2013), diapirs may sequester the SOM and enrich altered chemical components. Nevertheless, diapirism is likely a critical nutrient source for plant growth in the High Arctic polar desert. Muller et al. (2017) showed that *Salix arctica* (arctic willow)—the dominant-vascular plant species at the study site—increased root biomass and N uptake from diapirs. Therefore, diapirism may be critical for sustaining polar desert ecosystems where plant-available nutrients are generally low, and vegetation is further challenged by cold temperatures and low precipitation (Brummell et al., 2012; Schimel & Schaeffer, 2012).

Warming temperatures create favourable conditions for frost-boil development and diapirism in the High Arctic polar deserts by increases in plant biomass and precipitation (Callaghan et al., 2005; Klaus et al., 2013; Walker et al., 2008). Over the last 30 years, temperatures in high-latitude regions have increased 1.8°C—two-fold higher than the global average—and are anticipated to increase by 6–8°C by 2100 in the Canadian High Arctic (Allan et al., 2014; Schuur et al., 2015). Warmer and more productive bioclimate subzones (C and D) in the CAVM (Walker et al., 2005) have higher rates of frost heave compared with the other CAVM bioclimate subzones; however, warming climate is expected to shift zonal climate boundaries toward the north (Walker et al., 2008). As plant biomass and soil organic matter increase on frost-boil centers, frost-boil development in the CAVM subzone C and D will likely decrease (Walker et al., 2008). Similarly, plant colonization and increases in precipitation may increase frost-boil development in the High Arctic polar deserts. Vascular plant species are most sensitive to temperatures between 3–8°C, which suggests that species composition primarily changes in polar deserts as the temperatures increase during the growing season (Callaghan et al., 2005). Due to the lower rate of frost heave (Ping et al., 2015; Walker et al., 2004; Wilson & Humphreys, 2010), plant colonization is likely to occur at the margins of frost boils and inter-boil area. In addition to this, Klaus et al. (2013) showed a three to five increase in differential frost heave (*i.e.,* the difference in frost heave between the center portion of frost boil and inter-boil) along the precipitation gradient in northernmost Sweden. Thus, the High Arctic polar desert

may increase frost-boil development as the contrast of vegetation becomes stronger between the center portion of frost boils and the margins with the increase in soil moisture with precipitation.

Warming temperatures may also increase the magnitude of diapir formation as permafrost degrades. Diapirism is thought to mainly occur during rate events of major permafrost degradation that thaws the uppermost part of the permafrost (*i.e.,* ice-rich horizon) on the decadal scale (Ping et al., 2015; Swanson et al., 1999). With the projected increase in air temperatures in the Canadian High Arctic (Allan et al., 2014), the intense thaw will likely to more frequently occur to form diapirs especially within polar-desert frost boils as sparse or barren patches have high heat conductivity. Furthermore, increases in precipitation can more cause unstable bulk density between the ice-rich horizon and the overlying horizon (Klaus et al., 2013; Swanson et al., 1999), and thus can increase the magnitude of diapirism.

2.3 C and N Cycles Involved in the Major GHGs

CO_2, N_2O, and CH_4 are the major GHGs and are critical in the context of climate change. In well-mixed GHGs, these CO_2, N_2O, and CH_4 account for 80% of the total radiative forcing and greatly contribute to the net change in the energy balance of the Earth system (Ciais et al., 2013; Myhre et al., 2013). All of the three GHGs have increased in the atmosphere since the pre-industrial era. The atmospheric CO_2 concentration has increased by 48% and has reached 412.5 ppm (Ciais et al., 2013; Dlugokencky & Tans, 2021)(Ciais et al., 2013). The atmospheric N_2O concentration has increased by 22% and has reached 331.9 ppb (Ciais et al., 2013; Dlugokencky, 2021b) (Ciais et al., 2013). Though the concentration is relatively small, N_2O is 298 times stronger GHG than CO_2 on a 100-year time horizon based on the global warming potential approach (*i.e.,* time-integrated radiative forcing relative to an equal mass of CO_2) (Ciais et al., 2013; Myhre et al., 2013). Furthermore, N_2O is a severe ozone-depleting substance and has a long atmospheric residence time (*i.e.,* 121 years) (Myhre et al., 2013; Ravishankara et al., 2009). The atmospheric CH_4 concentration has increased by 160% and has reached 1879.1 ppb (Ciais et al., 2013; Dlugokencky, 2021a). Based on the global warming potential approach, CH_4 is 34 times stronger GHG than CO_2 per unit mass on a 100-year time horizon. Therefore, I focus on CO_2, N_2O, and CH_4 as the major GHGs in this dissertation.

The capacity of vegetation to uptake atmospheric CO_2 during the growing season is closely related to the annual C budget in Arctic regions; thus patterned-ground landscape is critical for the C budget as it decreases vegetation cover. During the growing season, net CO_2

exchange is the balance between biological respiration and photosynthetic CO_2 uptake; Arctic ecosystems are mainly small net CO_2 sources during other seasons due to the small uptake rate or the absence of photosynthesis (Luërs et al., 2014). The amount of aboveground vegetation, especially vascular vegetation determines the strength of CO_2 assimilation by the ecosystem, and thus controls variations in net CO_2 exchange in Arctic ecosystems (Wilson & Humphreys, 2010). In a Siberian Arctic polygonal tundra, the tundra acted as an annual CO_2 sink of 72 g m^{-2} based on eddy covariance measurements (Wille et al., 2008). Also, Corradi, Kolle, Walter, Zimov, & Schulze (2005) assessed an annual CO_2-C balance of −38 g C m^{-2} in a north-east Siberian tussock tundra based on eddy flux measurements in summer and a winter respiration model. However, as frost heave limits plant vegetation (Ping et al., 2015; Wilson & Humphreys, 2010), nonsorted circles decrease the capacity of the CO_2 uptake in tundra landscape (Walker et al., 2008). Despite the similar tundra types and identical climates, the tundra area with 36% cover of nonsorted circles decreased C sink by more than 50% compared with the other with few nonsorted circles (*i.e.,* < 1%) (Walker et al., 2008). In the High Arctic, photosynthetic CO_2 uptake has a similar magnitude to that of CO_2 release by autotrophic and heterotrophic respirations during the growing season (Lloyd, 2001). Consistently, Luërs et al. (2014) reported the annual CO_2 budget of approximately 0 g C m^{-2} in the High Arctic polar semi-desert based on eddy covariance flux measurements. Though the dominance of CO_2 assimilation is much lower compared with more vegetated Arctic ecosystems (Corradi et al., 2005; Wille et al., 2008), the vegetation cover at the measurement site was 60% (Luërs et al., 2014) and is much higher than that at my research site (*i.e.,* < 10%) (Muller et al., 2017), which belongs to polar desert ecosystems. Furthermore, the research site develops a frost-boil landscape and likely limits photosynthetic CO_2 uptake. Therefore, heterotrophic respiration may contribute to the CO_2 budget relatively higher in the research site.

Instead of the C budget, CH_4 emissions largely contribute to GHG budgets in Arctic regions. Compared with CO_2, the magnitude of CH_4 flux is low. Wille et al. (2008) reported that the annual CH_4 flux was 3.15 g m^{-2} in the Arctic polygonal tundra based on eddy covariance flux measurement whereas the annual CO_2 uptake was 72 g m^{-2}. As a result, the CH_4 emissions accounted for about 14% of the C balance of the tundra ecosystem. The minor contribution to the C balance was also found in a Siberian wetland where the CH_4 emissions contributed to 19% of the total C uptake (Friborg et al., 2003). However, as CH_4 has a high global warming potential,

small CH_4 emissions offset CO_2 GHG sink strength. As the global warming potential of CH_4 and CO_2 was considered in the Arctic polygonal tundra with a small influence of CH_4 emissions on the C budget, the GHG balance even became a source of 6.8 g CO_2 equivalent m^{-2} for a 100-year time horizon (Wille et al., 2008). Similarly, the Siberian wetland became a source of GHG with consideration of the global warming potential (Friborg et al., 2003). Therefore, CH_4 is also a key component of C cycling in Arctic ecosystems especially from the perspective of GHG budgets. Since High Arctic polar deserts are expected to have a relatively low capacity for CO_2 uptake, it is critical to investigate the CH_4 emissions from polar deserts to assess if the ecosystems are GHG sources.

Suitable conditions for CH_4 production possibly exist in the High Arctic polar deserts and may be regulated by the bioavailability of SOC. CH_4 is generally produced in the methanogenic process as the end product of SOC degradation under strictly anaerobic conditions (*i.e.,* < 200 mV redox potential) (Brady & Weil, 2008; Conrad, 2007). Since dihydrogen (H_2) or acetate plus CO_2 are only suitable substrates for the methanogenic process, the biodegradability of SOC is critical for the supply of the substrates, and thus CH_4 production (Conrad, 2007). Polar deserts remain the subsurface soil effectively saturated throughout the growing season with the presence of the permafrost layer (Gold & Bliss, 1995) and may have a methanogenic process. Furthermore, in the frost-boil landscape, diapirism increases subsurface SOC (Muller et al., 2017). Diapirism may link to CH_4 production and regulate the production rate with its bioavailability in the High Arctic polar deserts.

Nitrification and denitrification are key biological processes for N_2O production in Arctic soils. Nitrification is an oxidizing process of ammonia (NH_3) to nitrate (NO_3^-) via nitrite (NO_2^-) (Hu et al., 2015; Marushchak et al., 2011). In the first step of nitrification (*i.e.,* ammonia oxidation), N_2O is mainly produced as a by-product as the intermediate hydroxylamine converts to NO_2^- (Hu et al., 2015). Denitrification is a multistep respiratory process that reduces the oxidized forms of N (*i.e.,* nitrate (NO_3^-) or nitrite (NO_2^-)) to the gaseous forms of N (*i.e.,* nitric oxide (NO), N_2O, or dinitrogen (N_2)) (Hu et al., 2015). Previous studies show that other processes such as nitrifier-denitrification (Wrage et al., 2001), coupled nitrification-denitrification (Verhoeven et al., 2018), and dissimilatory nitrate reduction to ammonium (Silver et al., 2001) also contribute to N_2O production in soils and share intermediates and/or products with nitrification and denitrification. Nevertheless, approximately 70% of global N_2O emissions

from soils are attributed to nitrification and denitrification processes (Butterbach-Bahl et al., 2013). Therefore, this dissertation focuses on denitrification and nitrification for N_2O sources.

The reaction steps in nitrification and denitrification processes are regulated by the corresponding enzymes. The essential enzyme related to N_2O production in nitrification is ammonia monooxygenase (AMO), which catalyzes the first step of nitrification or ammonia oxidation (Hu et al., 2015). The subunit A of AMO is encoded by *amoA* gene, and the gene is carried by ammonia-oxidizing bacteria (AOB) and ammonia-oxidizing archaea (AOA) (Prosser & Nicol, 2012). Ammonia oxidation is the rate-limiting step, and thus the rates are directly related to rates of N_2O production by nitrification (Hu et al., 2015). Denitrification involves four reductases—nitrate reductase for the first step ($NO_3^- \rightarrow NO_2^-$), nitrite reductase for the second step ($NO_2^- \rightarrow NO$), nitric oxide reductase for the third step ($NO \rightarrow N_2O$), and nitrous oxide reductase for the fourth step ($N_2O \rightarrow N_2$) (Hayatsu et al., 2008). The final step is known to be the only biological N_2O consumption, and thus the availability of nitrous oxide reductase determines the net balance of N_2O production as N_2O is either an intermediate or the final product (Brummell et al., 2014; C. M. Jones et al., 2013). Nitrous oxide reductase is encoded by *nosZ* gene; however, the gene is not carried by all denitrifying microbes. Denitrifying fungi and some bacteria lack *nosZ* gene, which results in N_2O being the final product in their denitrification systems (Hu et al., 2015; Jones et al., 2013).

The enzymatic activities and the corresponding gene expression in both nitrification and denitrification are subject to soil conditions. Nitrification and denitrification are aerobic and anaerobic processes, oxygen levels in soil influence N_2O releases from both processes. Though direct measurement of soil oxygen level is rarely reported, soil moisture level or water-filled pore space (WFPS) is commonly used as an inversely correlated measurement of oxygen availability in soil (Hu et al., 2015). Well et al. (2008) demonstrated that 88% of the total N_2O emitted from microcosm was derived from ammonia oxidation using ^{15}N compounds. On the other hand, oxygen inhibits the expression of *nosZ* gene more than other denitrifying genes encoding the other reductases (Hu et al., 2015). N_2O production through denitrification becomes dominant from 60–70% WFPS and decreases at near saturation (*i.e.,* > 80% WFPS) where N_2O is reduced to N_2 (Hu et al., 2015; Ma et al., 2007). Soil pH influence both nitrification and denitrification processes. As soil is more acidic, NH_3 becomes a less dominant form as NH_4^+ has a pKa value of 9.25 (Siljanen et al., 2019). Generally, AOA has a higher affinity of AMO than

AOB (Prosser & Nicol, 2012). Siljanen et al. (2019) showed that AOA mainly performed ammonia oxidation in peat soils with low soil pH ranging from 2.81–4.06 and indicated AOA as the dominant contributor of N_2O in the soils. N_2O production via denitrification increases with low pH possibly because acidic conditions affect the assembly of nitrous oxide reductase in the periplasm and inhibit the enzymatic activity (Wrage et al., 2001). Moreover, acidic condition inhibits the expression of *nosZ* gene relatively more than other denitrifying genes encoding the corresponding reductases, leading to accumulation of N_2O and an increase in N_2O/N_2 ratio (Hu et al., 2015; Šimek & Cooper, 2002). Therefore, soil properties such as soil moisture and pH are the major determinants of N_2O source and sink in soils.

Nitrification contributes to N_2O emissions under dry conditions and facilitates denitrification-derived N_2O under wet conditions in the Arctic ecosystems. Generally, in permafrost-affected soils, vegetated regions have smaller flux rates than barren or sparsely vegetated regions during the growing season (median: ~30 μg N_2O-N m^{-2} d^{-1} vs. median: ~455 μg N_2O-N m^{-2} d^{-1}) (Voigt et al., 2020). Specially and temporally high N2O emissions also occur and reach 6556 μg N_2O-N m^{-2} d^{-1} in permafrost peatlands and 4429 μg N_2O-N m^{-2} d^{-1} in the High Arctic (Lamb et al., 2011). In the High Arctic lowland ecosystem, Ma et al. (2007) showed *in situ* N_2O emissions correlated with NH_4^+ but not with NO_3^- and demonstrated that N_2O production is mainly through nitrification under aerobic conditions (≤ 55% WFPS) using acetylene inhibition assay and ^{15}N enriched incubations. The dominance of nitrification in N_2O production has been explained as fungi outcompete denitrifiers for available NO_3^- to limit denitrification (Siciliano et al., 2009) and by that the main form of soil N is NH_4^+ which provides the substrate for ammonia oxidizers (*i.e.,* ammonia) as High Arctic soils are typically aerobic (Brummell et al., 2014). Brummell et al. (2014) showed a positive relationship between N_2O production and CO_2 production in High Arctic polar desert sites, which suggested that the increase in N mineralization leads to CO_2 production and NH_4^+, and thus to N_2O through nitrification. On the other hand, higher soil moisture increases N_2O production by denitrification. Marushchak et al. (2011) found high N_2O emissions from the permafrost peatlands which had high NO_3^- concentration and soil moisture (≥ 70% WFPS) and suggested that denitrification is the dominant pathway of N_2O production. However, Marushchak et al. (2011) also found the negative correlations of the N_2O emissions with soil moisture, which was explained by less NO_3^- availability for denitrification due to the decrease in nitrification with low oxygen level. Indeed,

in natural unfertilized ecosystems, inorganic N is predominantly derived from N mineralization and N-fixation. As a result, ammonia-oxidation is the first step of N transformation in the Arctic soils, and thus denitrification largely depends on nitrification for NO_2^- and NO_3^- (Siljanen et al., 2019). Therefore, nitrification is critical not only for direct N_2O production but also for fueling denitrification for N_2O release in Arctic ecosystems.

2.4. Hurdle Model

Ecological data set, in practice, commonly contains zeros, which can cause statistical problems due to the violations of the underlying assumptions. The high number of zeros increases the variance and highly skews the distribution (*i.e.,* left-censored distribution) (Huang et al., 2019; Zuur et al., 2009). Without the replacement of zeroes, log-transformation cannot fix the skewness (Zuur & Ieno, 2016). As a result, the increase in the number of zeros increases the chance of biased parameter estimates by common statistical approaches such as linear regression modelling or simple *t*-tests (Huang et al., 2019; Zuur et al., 2010; Zuur & Ieno, 2016). Indeed, linear regression modelling is reasonably robust against the violation of normality, and thus, to some extent, the presence of zeros does not mean that linear regression must not be applied (Zuur et al., 2010; Zuur & Ieno, 2016). In N cycling studies, for example, some gross N transformation rates often result in negative values, which are commonly either omitted or truncated to zero since gross negative values are ecologically impossible (Bedard-Haughn et al., 2013; Piper et al., 2015). The source of negative values includes violation of methodological assumption, methodological errors, environmental variability, and negligible N transformation rates (Bedard-Haughn et al., 2013; Piper et al., 2015). Piper et al. (2015) considered negative values within the range of three standard deviations from the mean as the negligible rates and truncated them to zero and omitted negative values outside the range as likely the other errors; general linear models were still capable of coping with the gross N transformation rates. However, once data set contains an excessive number of zeros (*i.e.,* zero inflation), ignoring zero inflation causes linear regression modelling to likely produce biased parameter estimates (Zuur et al., 2010; Zuur & Ieno, 2016). Gabler & Siemann (2013) investigated the effects of environmental factors on an invasive species (*Tridadica sebifera*). The biomass data for *T. sebifera* contained approximately 76% zeros, and a linear regression approach without dealing with the excess zeros caused a problem with the heterogeneity of variance (Gabler & Siemann, 2013; Zuur et al., 2009; Zuur & Ieno, 2016). Furthermore, the generalized linear models

predicted various negative fitted values and the maximum fitted value of approximately 0.35 whereas the range of the biomass was from 0– approximately 2.5 (Zuur & Ieno, 2016). Therefore, excess zeros caused the problem with the estimated parameters and standard errors, and an alternative approach to linear regression needed to be considered for zero-inflated data (Zuur et al., 2010; Zuur & Ieno, 2016).

The statistical approach for zero-inflated data depends on the consideration of the source of zeros and is well developed in count data. Previous studies classify zero count into true zero count resulting from certain covariate effect, and false zero count that is recorded as zero due to experimental, observation, or random errors (Kuhnert et al., 2005; Martin et al., 2005). Zero-inflated models are a combination of a Bernoulli and a count processes and separately model true and false zeros (Zuur & Ieno, 2016). Namely, the Bernoulli part models false zeros that do not comply with the covariates in the count part, and the count part such as Poisson or negative binomial distributions models true zeros that comply with the covariates (Hofstetter et al., 2016; Zuur & Ieno, 2016). For example, in dental epidemiology, Hofstetter et al. (2016) applied a zero-inflated negative binomial model for a DMF index—representing the number of decayed (D), missing (M), and filled (F) teeth—for caries (*i.e.,* whose feature is strongly positively skewed distribution due to a large stack of zero counts. The Bernoulli part represented individuals without caries whereas the negative binomial part represented those at risk for dental caries (Hofstetter et al., 2016). The negative binomial distribution includes zero; thus the negative binomial part modelled some of the zeros (*i.e.,* true zeros) that follow the covariates (Hofstetter et al., 2016; Zuur & Ieno, 2016). Therefore, the Bernoulli part estimated excess zeros (*i.e.,* false zeros) that were above the estimated zeros based on the negative binomial distribution (Hofstetter et al., 2016; Zuur & Ieno, 2016). Another approach for zero-inflated data is zero-altered or hurdle models (Zuur & Ieno, 2016). Hurdle models consist of a Bernoulli and a zero-truncated count (*i.e.,* zero-truncated Poisson or zero-truncated negative binomial distributions) processes and model zero values in only a Bernoulli part, and thus do not discriminate true and false zeros (Hofstetter et al., 2016; Zuur & Ieno, 2016). Therefore, hurdle models estimate the probability of presence versus absence in the Bernoulli process and, once the object presents (*i.e.,* crossing the threshold or hurdle), estimate the abundance of the object in the zero-truncated process (Zuur & Ieno, 2016). Hofstetter et al. (2016) also used a hurdle model with negative binomial distribution for modelling the DMF index. The Bernoulli part modelled observing

individuals with caries (*i.e.,* presence) whereas the zero-truncated negative binomial part modelled the number of caries for individuals with caries (Hofstetter et al., 2016). As the differences between the zero-inflated model and the hurdle model are generally small, the zero-inflated negative binomial and the negative binomial hurdle model showed comparable fit to the DMF index and had similar results (Hofstetter et al., 2016). Therefore, the choice between zero-inflated and hurdle models depends on theoretical considerations of the data and statistical inferences.

The hurdle model is applicable for zero-inflated continuous data in ecological and environmental studies. Zuur & Ieno (2016) reviewed the zero-inflated biomass data for *T. sebifera* in the pot study (Gabler & Siemann, 2013) and argued that it would be more meaningful to consider the biomass is present or absent in a pot than to clearly separate true and false zeros in the Bernoulli part. Thus, the probability density of the presence or the absence of *T. sebifera* was expressed by

$$P(Y_i = y_i|\pi_i) = \begin{cases} 1 - \pi_i & y_i = 0 \\ \pi_i & y_i = 1 \end{cases} \quad \text{(Eq. 2.1)}$$

where: y_i and π_i were the presence/absence value of the biomass and the probability of the presence at i^{th} observation, respectively (i = 1, …, 400) (Zuur & Ieno, 2016).

The probability of presence π_i was given by

$$logit(\pi_i) = \gamma_0 + \gamma_1 \times X_{i1} + \cdots + \gamma_K \times X_{iK} \quad \text{(Eq. 2.2)}$$

where: logit stood for the logistic link function, γ_0 was the intercept, γ_K and X_{iK} were the K^{th} coefficient and covariate (K = 1, …, 5) at i^{th} observation, respectively (Zuur & Ieno, 2016).

To model the nonzero biomass data, Zuur & Ieno (2016) used gamma distribution, which is reasonable for highly skewed data but is suitable for only positive data, and thus was appropriate for the hurdle model. The probability distribution function of a gamma distribution was expressed by

$$f(Y|\mu,r) = P(Y = y_i|\mu_i,r) = \frac{1}{\Gamma(r)} \times (r/\mu_i)^r \times {y_i}^{r-1} \times exp(-y_i \times r/\mu_i) \quad \text{(Eq. 2.3)}$$

where: y_i and μ_i were the amount of the biomass and the estimated mean biomass, respectively once *T. sebifera* was present ($y_i > 0$), and the symbol Γ is defined as $\Gamma(r+1) = r!$, and r is dispersion statistic defined as the sum of squared Pearson residuals divided by the residual degree of freedom (Zuur & Ieno, 2016).

The estimated mean biomass μ_i was expressed by

$$log(\mu_i) = \beta_0 + \beta_1 \times X_{i1} + \cdots \beta_K \times X_{iK} \quad \text{(Eq. 2.4)}$$

where: β_0 was the intercept, and β_K and X_K were the K^{th} coefficient and covariate (K = 1, …, 5) at i^{th} observation (Zuur & Ieno, 2016).

By combining Eq. 2.1 and Eq. 2.3, density function of the hurdle model using the gamma distribution was expressed by

$$P(Yi = y_i|\beta,\gamma) = \begin{cases} 1 - \pi_i & y_i = 0 \\ \pi_i \times f_{gamma}(Y|\beta) & y_i > 0 \end{cases} \quad \text{(Eq. 2.5)}$$

where: the $f_{gamma}(.)$is the density function of a gamma distribution expressed in Eq. 2.3 (Zuur & Ieno, 2016).

As a result, the expected mean and variance of the biomass variable that follows the hurdle model were expressed in Eq. 2.6 (Zuur & Ieno, 2016).

$$E(y_i) = \pi_i \times \mu_i \qquad \text{and} \qquad var(y_i) = \frac{\pi_i \times r + \pi_i - \pi_i^2 \times r}{r} \times \mu_i^2 \quad \text{(Eq. 2.6)}$$

Note that if the biomass was equal to zero, the expected value was equal to the corresponding π_i (Zuur & Ieno, 2016).

Huang et al. (2019) applied the hurdle model for a soil remediation study. Soil environmental pollutants commonly exist at lower concentrations than detection limits (*i.e.,* DLs) of analytical instruments, which results in highly skewed left-censored data (Huang et al., 2019). Furthermore, the distinction between true and false zeros below DLs is unknown; thus, the hurdle model is sensible for modelling for the left-censored pollutant data (Huang et al., 2019; Zuur & Ieno, 2016). The hurdle model included the Bernoulli and a gamma components, however, the threshold or the hurdle to be crossed was the DL (Huang et al., 2019). As a result, lower concentrations above the DL were assigned to the presence (*i.e.,* one), and those below the DL were assigned to the absence (*i.e.,* zero) (Huang et al., 2019). Furthermore, as the lower boundary of integration of gamma probability density function is zero, the density function of hurdle model in Eq. 2.5 and the expected mean in Eq. 2.6 were modified by

$$P(Yi = y_i|\beta,\gamma) = \begin{cases} 1 - \pi_i & -DL \leq y_i \leq 0 \\ \pi_i \times f_{gamma}(Y|\beta) & y_i > 0 \end{cases} \quad \text{(Eq. 2.7)}$$

$$E(y_i) = \pi_i \times (\mu_i + DL) \quad \text{(Eq. 2.8)}$$

in the study, respectively (Huang et al., 2019).

Note that if the concentration was below the DL, the expected value was equal to the corresponding $\pi_i \times DL$, which means that as a censored real concentration is closer to the DL, the probability estimate from the Bernoulli part would become closer to one; thus, the expected mean value would be close to the DL (Huang et al., 2019).

Huang et al. (2019) adopted a likelihood function developed by Haslauer et al. (2017) to assess if the gamma distribution parameters (*i.e.,* shape and scale) obtained by maximum likelihood estimation improve gamma fitting to the left-censored pollutant data. The shape (α) and scale (β) parameters are expressed in Eq. 2.9 using dispersion statistic r and mean estimate μ of gamma distribution (Zuur & Ieno, 2016).

$$\alpha = r \quad \text{and} \quad \beta = {}^{\mu}/_{\alpha} \quad \text{(Eq. 2.9)}$$

Using the shape (α) and scale (β) parameters, the probability distribution function of a gamma distribution is also expressed in Eq. 2.10 (Zuur & Ieno, 2016).

$$f(Y|Y > 0, \alpha, \beta) = \frac{1}{\beta^{\alpha} \times \Gamma(\alpha)} \times Y^{\alpha-1} \times exp(-Y/\beta) \quad \text{(Eq. 2.10)}$$

Huang et al. (2019) compared a gamma fitting based on the shape and scale parameters that maximize the original gamma likelihood in Eq. 2.11 with Haslauer-modified gamma fitting based on the likelihood function in Eq. 2.12 that incorporates the proportion of true zero p_0 (*i.e.,* samples with no contamination) to account for multiple DLs (Haslauer et al., 2017)

$$\ln L(\alpha, \beta, y) = \sum_{k=1}^{k=m} \ln f(\alpha, \beta, y_k) + n \ln F(\alpha, \beta, DL) \quad \text{(Eq. 2.11)}$$

$$ln(\alpha, \beta, p_0, y) = \sum_{k=1}^{k=m} \ln[(1 - p_0) f(\alpha, \beta, y_k)] + n \ln[p_0 + (1 - p_0) F(\alpha, \beta, DL)] \quad \text{(Eq. 2.12)}$$

where: $F(.)$ was the cumulative distribution function.

As the Haslauer-modified gamma model provided a better estimate than the original gamma model under some treatments, Huang et al. (2019) recommended using both of the gamma models during data exploration.

3. COULD CRYOTURBIC DIAPIRS BE KEY FOR UNDERSTANDING ECOLOGICAL FEEDBACKS TO CLIMATE CHANGE IN HIGH ARCTIC POLAR DESERTS?

3.1 Preface

High Arctic polar deserts emit the main GHGs at rates comparable to mesic Arctic regions; however, the mechanism of GHG emissions is not well described. Furthermore, polar deserts are found to store a larger amount of SOC in the permafrost than previously expected and have a potential positive feedback loop of the GHG emissions under a rapidly warming climate. Repeated freeze-thaw cycle creates frost-boil landscape and diapirs—subsurface nutrient patches enriched in C and N—within frost-boil profiles. As temperatures warm polar deserts, permafrost thaw and meltwater production are expected to further develop frost boils and diapirs. In this chapter, I investigate how diapirs alter key soil properties including the chemical structure of SOC, N transformation rates, and C mineralization. I discuss a potential ecological role of diapirs in polar-desert ecosystems and implications of diapirism-GHG production feedbacks to projected warming temperatures.

This Chapter has been published, with minor formatting changes, as Ota M., S.D. Mamet, A.L. Muller, E.G. Lamb, G. Dhillon, D. Peak, S.D. Siciliano. Could cryoturbic diapirs be key for understanding ecological feedbacks to climate change in high arctic polar deserts? 2020. Journal of Geophysical Research: Biogeosciences 125: 1–13. SD Mamet provided critical assistance with the statistical analyses and helpful advice on the data presentations and created Fig. 3.1 and 3.4. AL Muller was responsible for the field survey for block assignment and frost-boil profiles in the study site and provided critical advice. Dr. Lamb provided critical advice and comments on this paper. G Dhillon provided critical assistance with the instrument for SOC speciation and with the data analysis. Dr. Peak provided the instrument for the speciation and critical advice. Dr. Siciliano provided necessary operating funds and critical advice to develop the concept of this paper and data analysis.

3.2 Abstract

High Arctic polar deserts cover 26% of the Arctic. Increasing temperatures are predicted to significantly alter polar desert freeze-thaw and biogeochemical cycles, with important implications for greenhouse gas emissions. However, the mechanisms underlying these changing cycles are still highly uncertain. Cryoturbic, carbon-rich Bhy horizons (diapirs) in frost boils are key nutrient sources for *Salix arctica*. I hypothesized that diapirism leads to organic carbon characteristics that alter microbial pathways, which then control root foraging and greenhouse gas production. During July and August 2013, I characterized soil properties and examined gross nitrogen transformation rates in frost boils both with and without diapirs in two High Arctic polar deserts (dolomite and granite) near Alexandra Fjord (78°51′N 75°54′W), Ellesmere Island, Nunavut, Canada. Diapiric frost boils had 18% higher soil organic carbon in the dolomitic and 9% higher in the granitic deserts, and 29% higher total dissolved nitrogen in the dolomitic desert. However, diapirs decreased gross nitrogen mineralization rates by 30% in the dolomitic and by 48% in the granitic deserts. Attenuated total reflectance Fourier transformed mid-infrared spectroscopy revealed greater concentrations of polysaccharides and recalcitrant carbon in diapiric versus non-diapiric frost boils. These increased polysaccharide concentrations likely facilitate diapirism as soil viscosity increases with polysaccharides. Lower microbial activity or ectomycorrhizae that are found to colonize *S. arctica* in a High Arctic site adjacent to Alexandra Fjord (Kohn & Stasovski, 1990) may accumulate total dissolved nitrogen in diapirs. My results suggest geomorphologic-plant-microbe interactions may underlie important patterns of geochemical cycling in Arctic systems. Thus, polar desert frost boils should represent a key focus of future investigations of climate change in Arctic systems.

3.3 Plain Language Summary

Arctic ecology and climate are intricately interconnected. During short summers, the upper soil layers thaw, allowing biological activities. Recent warming in polar deserts has influenced key thaw processes and plant-microbe interactions with soil nutrients. Polar desert ecosystems cover 26% of the Arctic and are expected to transform dramatically with further warming, with important implications for climate-ecology feedbacks. To evaluate feedbacks in polar deserts, I focused on cryoturbic diapirism (buoyant nutrient patches above the permafrost), which is expected to increase with warming. I investigated soil properties and microbial activities in frost boils (density-driven circulations of sediments above the permafrost). I found

that diapirism increased recalcitrant soil organic carbon, which decreased microbial activities. Interestingly, I found that microbes and/or plants may augment diapirism by enhanced polysaccharide production increasing soil viscosity. Despite low organic carbon quality, the dominant vascular plant species, *Salix arctica*, increased root biomass and nitrogen uptake from diapirs, suggesting a mutualistic relationship between *S. arctica* and microbes. Under warming air temperatures, permafrost degradation releases stored organic matter, which may enhance nutrient cycling via diapirism. Therefore, my study suggests that diapirism may reflect an ecological change in the High Arctic polar deserts and may further occur in non-diapiric frost boils in response to global warming.

3.4 Introduction

High Arctic polar deserts are widespread in the North, covering 26% of the Arctic (1,358,000 km^2; Walker et al., 2002) and support sparse vegetation limited by nutrient availability, moisture, and temperature (Arft et al., 1999; Gold & Bliss, 1995; Henry et al., 1986). However, polar deserts can produce greenhouse gases (GHGs) at rates comparable to mesic arctic environments (Brummell et al., 2012, 2014; Lamb et al., 2011) and store large amounts of carbon in organic permafrost soils (Burnham & Sletten, 2010; Hugelius et al., 2014). Widespread permafrost warming is underway (Biskaborn et al., 2019), which increases permafrost thaw and organic matter decomposition, providing more stored nutrients to microbes and increasing GHG production in polar deserts. Though polar deserts are predicted to transform dramatically under a rapidly warming climate (Lamb et al., 2011; Stewart et al., 2013), their biogeochemical and ecological feedbacks to climate change are unclear. Accurate predictions of GHG emissions from polar desert soils under projected warming require a more robust understanding of cryogenic mechanisms contributing to enhanced nutrient cycling and GHG production.

Freeze-thaw (cryoturbation) processes generate distinct features in arctic soil that regulate biogeochemical cycling. For instance, liquid water migrates to frozen water along the soil thermal gradient to develop segregated ice, which thrusts soil material upward above the permafrost layer (*i.e.,* frost heave). Frost heave sorts soil materials by size, producing repeated circular patches or frost boils (< 3 m diameter) at the ground surface, with finer materials in the centers and larger materials in the margins. Frost boils are common in polar deserts (Muc et al., 1989), with surfaces that are either barren or sparsely vegetated (Muller et al., 2017; van

Everdingen, 1998). Frost boil cryoturbation may control biological production of GHGs from nutrient cycling, as organic matter leaches downward from the surface and then moves upward with frost heave (Walker et al., 2004). Diapirism intrudes soil materials from the top of the permafrost table (ice-rich horizon) into the overlying horizon. Within frost boils, surface meltwater leaching (Muller et al., 2017; Schaeffer et al., 2013; Tye et al., 2005) can accumulate in ice-rich horizons above concavities in the permafrost table (Boike et al., 2008; Cannone et al., 2004; Walker et al., 2004); therefore, diapirism can carry nutrients upward creating nutrient-rich soil horizons (Bhy). Diapiric nutrient intrusions occur when this nutrient-enriched low bulk density (higher buoyancy) Bhy horizon "floats" through the higher bulk density overlying layer into the upper soil (Swanson et al., 1999). The nutrient flow is facilitated as the overlying layer is more viscous (Swanson et al., 1999). These Bhy horizons contain approximately 7% more carbon (C) and 20% more nitrogen (N) than non-diapiric frost boils and may develop in approximately 30% of frost boils (Muller et al., 2017). Frost boil development and diapirism are expected to increase with increasing temperatures, permafrost thaw, and meltwater production (Callaghan et al., 2005; Klaus et al., 2013; Walker et al., 2008), with important implications for future biogeochemical cycling in arctic ecosystems.

How plant and soil biology interact with diapirism and how this interaction may contribute to GHG production from frost boil systems are not clear. Muller et al. (2017) found that *Salix arctica* (arctic willow) roots actively targeted Bhy horizons for N, though microbial C respiration was lower in diapiric relative to non-diapiric frost boils (Brummell et al., 2015). In other arctic regions, C and N mineralization was lower in cryoturbated relative to noncryoturbated horizons (Gillespie et al., 2014; Kaiser et al., 2007; Wild et al., 2013). Therefore, diapiric nutrients may be also less bioavailable for microbes. The lower bioavailability may be due to the release of recalcitrant C from plants actively colonizing frost boils (*e.g., Betula nana*; Lynch et al., 2018). Vegetation certainly influences SOC quality by altering both the aliphatic and aromatic content of SOC in the High Arctic (Szymański, 2017) and microbial carbon use efficiency (Lynch et al., 2018). Alternatively, organic detritus may be occluded in the aggregates of Bhy horizons, inhibiting microbial metabolism of soil organic carbon (SOC; Brummell et al., 2015; *sensu* Schimel & Schaeffer, 2012). It may be also because cryoturbated SOC accumulates ketones that increase recalcitrance (*i.e.,* lowers quality), becoming more resistant to biodegradability than SOC of noncryoturbated soils (Gillespie et al.,

2014) despite similar C/N ratios (Ernakovich et al., 2015). Thus, in frost boil systems, the question of GHG production related to diapiric SOC characteristics is still open.

Nitrous oxide (N_2O) is a critical GHG in the High Arctic polar deserts. N_2O has considerable global warming potential (> 300 times that of CO_2; Intergovernmental Panel on Climate Change (IPCC), 2014) and is a dominant ozone-depleting substance (Ravishankara et al., 2009). N_2O production also decreases soil N; therefore, N_2O emissions may not only accelerate permafrost degradation via warming air temperatures but also directly disturb polar desert ecosystem functioning due to the reduction of N supply. The major biological pathways involved in N_2O production are nitrification and denitrification. Soil N is present mainly as ammonia (Brummell et al., 2014), and organic carbon is limited in aerobic polar deserts soils (relative to other terrestrial areas). Thus, total N_2O production may be driven chiefly by nitrification (Hayatsu et al., 2008; Stein, 2011; Zumft, 1997) as has been seen in other arctic ecosystems (Ma et al., 2007; Siciliano et al., 2009). When ammonium produced through N mineralization is oxidized to nitrite, nitrification produces N_2O as a by-product. In turn, soil organic matter bioavailability can indirectly control N_2O production (Marushchak et al., 2011) in polar deserts. However, little is known about the links between diapirism, mineralization, and nitrification. Given that frost boil development and diapirism are predicted to increase with climate warming and the uncertainty in SOC-diapirism and diapirism-N_2O production feedbacks, further investigation into cryogenic-biological processes is warranted. Here I propose that key SOC characteristics link to diapirism and control both root foraging and GHG production. I hypothesize that (1) frost boil diapirism increases key soil properties such as soil organic C and N, which leads to altered microbial nutrient (*i.e.,* C and N) cycling, and (2) frost boil diapirism decreases SOC quality for soil microbes, which links to GHG emissions. Confirming these hypotheses would help explain how desert frost boils influence GHG emissions and why *S. arctica* aggressively forages for nutrients in frost boils (Muller et al., 2017).

3.5 Materials and Methods

3.5.1 Site description

This study was conducted during July and August 2013 in a Canadian High Arctic polar desert near Alexandra Fjord (78°51′N, 75°54′W), Ellesmere Island (Fig. 1). The study area was broadly classified as a cryptogam, herb barren community, characterized by dry soil, sparse herbaceous cover, lichens, mosses, and liverworts (Walker et al., 2002). The study site is

characterized by two distinctive desert types derived from granitic and dolomitic parent material, respectively (hereafter, I use "desert" to refer to parent material). Soils are characterized as Regololic Turbic Cryosols with limited horizon development (Brummell et al., 2012). The granitic desert (650 m.a.s.l.) was located on a gentle gradient (2–5°), immediately upslope of the dolomitic desert (500 m.a.s.l.) to the east and downslope of a glacier (750 m.a.s.l.) to the northwest. These polar desert plant communities are described as noncarbonated mountain complexes (B3b, "Mountain") in the granitic desert and as cryptogam, herb barren (B1, "Barren") in the dolomitic desert (Brummell et al., 2012) according to the CAVM (Walker et al., 2002). Mean growing season temperatures range from 3–8 °C, and the growing season lasts from early June to mid-August (Beamish et al., 2016). Annual precipitation is < 50 mm. Gravimetric soil water content in the area ranged from 9–13%, fine soil particles comprised 55% of the soil, and biological soil crusts covered 3% of the ground (Boulanger-Lapointe et al., 2014; Muller et al., 2017). C content ranged from ~0.3% in granitic to 3.8% in dolomitic deserts, and N content ranged from ~0.03–0.13% (Bliss et al., 1994; Muller et al., 2017). Soil pH ranged from 5.5 in the granitic desert to 7.9 in the dolomitic desert (Bliss et al., 1994). Poorly to well-developed frost boils are common across the site due to pronounced annual freeze-thaw cycles (Muller et al., 2017). I sampled soil from organic-rich horizons within diapiric and non-diapiric frost boils in each desert. To account for environmental gradients and vegetation cover within each desert, this study employed a randomized block design to encompass the full range of geomorphological (frost boil size, interboil area, frost-boil connectivity and development, slope orientation) and vegetation (see above) characteristics within each site. The dolomitic and granitic sites were divided into five and twelve blocks, respectively (Fig. 3.1). The unbalanced design occurred due to the more varied geomorphology, aspect, and slope on the granitic site. Frost boils were randomly selected from each block using two perpendicular transects (17–50 m in length and 3–4 m in width); within each, the center point and the orientations were chosen randomly. To assess if these were diapiric frost boils (*i.e.,* Bhy horizon present), the SOC within each soil profile was quantified using a field-portable visible and near-infrared (vis-NIR) reflectance spectrophotometer with a soil probe attachment (Guy et al., 2015). Soil spectra were collected at 8-nm resolution over a spectral range from 2,225–350 nm by inserting the vis-NIR spectrophotometer probe into a 3.3 cm diameter pilot hole in the center of each of the selected frost boils (Muller et al., 2017). Frost boils were classified as diapiric if there was an abrupt

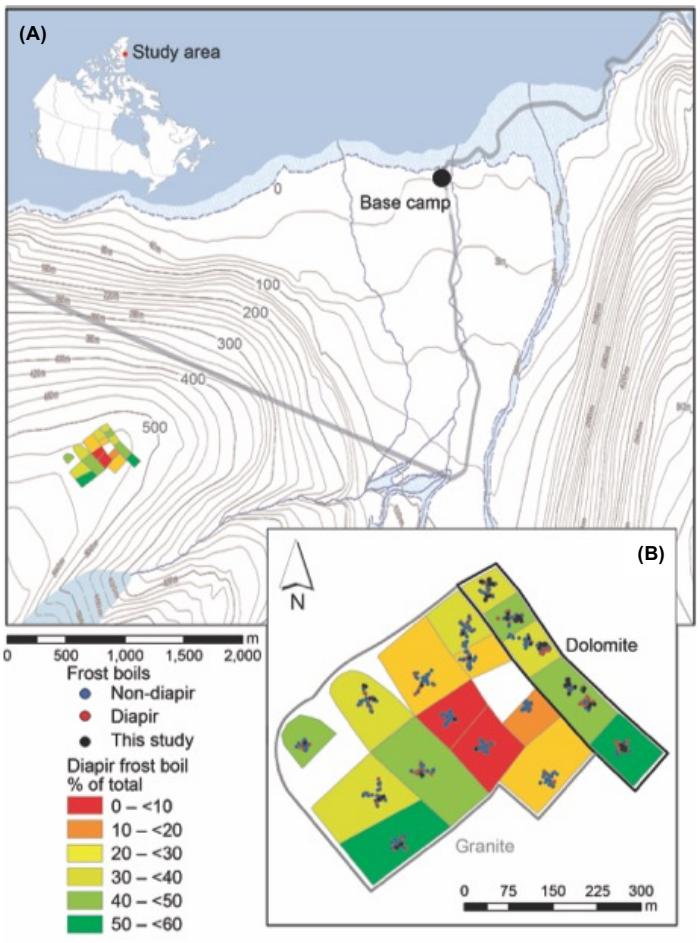

Fig. 3.1(A) Overview of the study area at Alexandra Fjord dome, Nunavut. Contour interval is 20 m. Basemap source: Natural Resources Canada (http://atlas.gc.ca/toporama/en/index.html). (B) Randomized complete block experimental design of soil sampling in the dolomitic and the granitic deserts. Block color indicates the proportion of diapiric frost boils relative to the number surveyed (%). The thick black line encloses dolomitic blocks (n = five) and the thick gray line granitic blocks (n = 12).

increase of at least 0.2 log % SOC in the subsurface—indicative of a diapiric Bhy horizon and non-diapiric in the absence of increasing SOC concentrations with depth as shown in Fig. A3.1 (Muller et al., 2017). Pits were excavated into diapiric and non-diapiric frost boils to expose the soil profile. Excavated soil was placed on a tarp and returned to the pit following sampling for minimum disturbance of the excavation. In diapiric frost boils, I extracted two soil pairs of 200 cm^3 from each SOC peaks using a 100 cm^3 metal core hammered horizontally for gross N transformation assays, and then 1 kg of soil was taken using a shovel for other measurements. In non-diapiric frost boils, two pairs of 200 cm^3 and 1 kg soil samples were taken at the same depths as the paired diapiric frost boils. The depth of the SOC peaks ranged from 10–25 cm below ground surface in the dolomitic desert and from 15–30 cm in the granitic desert. The soil sampling was completed on five dates from July 12–Aug. 10 (n = 40) within the dolomitic desert and from July 13–Aug. 14 in 2013 (n = 40) within the granitic desert. Gross nitrogen transformation assays were conducted on soil samples in the field. The 1 kg soil samples were frozen and shipped to the University of Saskatchewan for further analyses. The soil samples may have undergone some impact that alters soil properties and DNA through the disturbance such as the breakdown of soil aggregates. Nevertheless, my study assumes that both diapiric and non-diapiric soil samples experienced the same degree of impact and that the effect of diapirism would be still testable for further analyses.

3.5.2 Soil properties

SOC was determined by the dry combustion method on a Leco-2000 carbon analyzer (Leco Corporation, St. Joseph, Michigan, USA). Soils were pretreated with concentrated HCl fumes to remove carbonates (Dhillon et al., 2015). Nonpurgeable dissolved organic carbon (DOC) and total dissolved nitrogen (TDN) were extracted by 5 mM $CaCl_2$ solution in deionized water (Chantigny et al., 2008) and measured using a TOC-V combustion analyzer (Shimadzu Corporation, Kyoto, Japan) with a nitrogen module and furnace temperature set to 720 °C. Soil phosphorus (P) was determined by sodium bicarbonate extraction (Schoenau & O'Halloran, 2008). Soil pH and electrical conductivity were measured in 1:5 soil:0.01 M $CaCl_2$ and in 1:2 soil:water extract (Miller & Curtin, 2008), respectively. Gravimetric water content was measured using an MJ33 Moisture Analyzer (Mettler Toledo, Columbus, Ohio, USA).

3.5.3 Gross N transformation assay

Soil N transformations were measured as gross rates: mineralization, nitrification, NH_4^+ consumption, and NO_3^- consumption using the ^{15}N isotope-dilution technique as described by Hart et al. (1994). For gross rates of mineralization and NH_4^+ consumption, a pair of 200 cm^3 soil cores was taken from each frost boil, and 10.4 mL of $(^{15}NH_4)_2SO_4$ solution (15 µg/mL N at 98% ^{15}N enrichment) was injected into the cores. For gross nitrification and NO_3^- consumption rates, another pair of 200 cm^3 soil cores was taken and labeled by injecting 10.4 mL of $K^{15}NO_3$ solution (15 µg/mL N at 98% ^{15}N enrichment). To label the NH_4^+ and NO_3^- pools homogeneously, each solution was injected at eight points in each core using an 18-gauge side-port needle. One of the paired cores was vigorously mixed within 30 min of injection, and 25 g of soil was sub-sampled for 2 M KCl extraction (time zero hour). The other core was incubated in a shaded cooler box on site for 48 hours to keep samples cool and in the dark, and 25 g of soil was subsampled using 2 M KCl extraction (time 48 hours). Soil extracts were filtered through filter paper (2.7 µm pore size Grade GF/D, Whatman, Maidstone, UK), then frozen and shipped to the laboratory at the University of Saskatchewan. Total N (*i.e.,* $^{14}NH_4^+$ and $^{15}NH_4^+$ or $^{14}NO_3^-$ and $^{15}NO_3^-$) in the 2 M KCl extract was analyzed calorimetrically using a Technicon Autoanalyzer (Seal Analytical, Southampton, UK). The diffusion disk technique (Stark & Hart, 1996) was used to prepare samples for analysis of ^{15}N enrichment in the extract. As soil N level is low in polar deserts, N carrier solution was added for accurate analysis by mass spectroscopy (Hart et al., 1994). For the 2 M KCl extracts for gross mineralization and NH_4^+ consumption assays, 10 mL of each was subsampled, and 30 µg of ^{14}N was added to the subsample as a form of NH_4Cl in 1 mL of 2 M KCl. To collect $^{15}NH_4^+$ and, $^{14}NH_4^+$ an acid trap (filter paper disk acidified by $KHSO_4$ and sealed by polytetrafluoroethylene) was added, and 0.3 g of MgO added to raise pH (Bedard-Haughn et al., 2004; Stewart et al., 2013). Diffusion samples were incubated at room temperature for seven days with daily gentle shaking. For the 2 M KCl extracts for gross nitrification and NO_3^- consumption assays, 30 µg of ^{14}N was added to the subsample as a form of KNO_3 in 1 mL of 2 M KCl. The $^{15}NO_3^-$ and $^{14}NO_3^-$ were collected as $^{15}NH_4^+$ and $^{14}NH_4^+$ using a reducing agent (Devarda's alloy; Stewart et al., 2013). The prepared samples were analyzed using an ECS4010 elemental analyzer (Costech Analytical Technologies, Valencia, California, USA) coupled to a Delta V mass spectrometer with Conflo IV interface (Thermo Scientific, Bremen, Germany). Gross N transformation rates were calculated following Hart et al. (1994). A small

number of negative rates were calculated. Negative rates can be due to laboratory errors or can arise when rates are very low. I assumed that negative values outside the range of three standard deviations from the mean were laboratory errors and treated them as missing values, whereas negative values within three standard deviations of the mean were truncated to zero and retained (Piper et al., 2015). I removed two gross mineralization rates and truncated twenty-four values to zero. For gross NH_4^+ consumption rates, I removed one value and truncated fourteen values to zero. For gross nitrification and NO_3^- consumption rates, I removed nine values and converted nineteen values to zero.

3.5.4 Respiration assay

Cumulative CO_2 (normalized to SOC: $\mu g \cdot CO_2\text{-}C \cdot mg^{-1}$ soil C and normalized to dry soil mass: $\mu g \cdot CO_2\text{-}C \cdot g^{-1}$ dry soil) were determined by laboratory incubation. Soil samples were packed in a polystyrene core (2.8 × 1.4 cm internal diameter) with a bulk density of 1.3 g/cm^3 based on the field measurements in the active layer at the study site (Brummell et al., 2014). Autoclaved distilled water was added to the core to adjust water content to 60% water-filled pore space (Linn & Doran, 1984). Each core was placed in a 100 mL glass bottle (VWR International, Radnor, Pennsylvania, USA). The cap was equipped with a brass compression tube straight adapter for 1/4″ OD tubing × 1/8″ male pipe (McMaster-CARR Supply Company, Elmhurst, Illinois, USA) sandwiching Thermogreen™ LB-2 septa (9.5 mm; Sigma-Aldrich Co., St. Louis, Missouri, USA) for gas sampling. The cap was closed tightly by sandwiching a steam-resistant EPDM 3/16″ O-Ring (McMaster-CARR Supply Company, Illinois, USA) with vacuum grease. Immediately after each cap was closed, gas sampling was conducted for time zero hour using a standard 20 mL polypropylene syringe fitted with a 25-gauge needle. To prevent ambient air from coming into the syringe due to decreases in internal pressure, 15 mL of zero-air was injected into the bottle prior to gas sampling, and then 15 mL of the headspace was collected and injected into a pre-evacuated 12 mL Exetainer® vial (flushed with zero-air prior to evacuation; Labco, Lampeter, UK). After gas sampling for time zero hour, each bottle was incubated in the dark at 10°C. During the incubation period, headspace gas was sampled at 24, 48, 96, 168, and 240 hours. Gas samples were analyzed using a gas chromatograph (Bruker 450 GC, BioSpin, Milton, Ontario, Canada) equipped with a thermal conductivity detector for CO_2 (Bruker Biosciences Co., Billerica, Massachusetts, USA). CO_2 concentrations ($\mu l\ L^{-1}$) were adjusted to represent concentrations prior to adding 15 mL N_2 and further converted to a mass unit ($\mu g\ CO_2$-

C) using the Ideal Gas Law. Cumulative CO_2 at time = t (µg CO_2-C mg^{-1} soil C) was calculated using

$$Cumulative\ CO_2\ t\ (\mu g\ CO_2 - C\ mg^{-1}\ soil\ C)\ =\ (C_t\ -\ C_0)/(ds\ \times\ SOC) \qquad \text{(Eq. 3.1)}$$

where Co = CO_2 mass at time zero (µg CO_2-C); Ct = CO_2 at time t (µg CO_2-C); ds = dry soil mass (mg); and SOC = soil organic carbon (mg mg^{-1} dry soil).

Cumulative CO2 at time = t (µg CO_2-C g^{-1} dry soil) was calculated using

$$Cumulative\ CO_2\ t\ (\mu g\ CO_2 - C\ g^{-1}\ dry\ soil)\ =\ (C_t\ -\ C_0)/(ds/1000) \qquad \text{(Eq. 3.2)}$$

where Co = CO_2 mass at time zero (µg CO_2-C); Ct = CO_2 mass at time t (µg CO_2-C); and ds = dry soil mass (mg).

The cumulative CO_2 at time 240 hours was used for the respiration assay. To check the quality of the incubation system, each series of cumulative CO_2 from time zero to 240 hours were plotted against time, and series with poor linearity (*i.e.,* $R^2 < 0.85$) were removed from further analysis.

3.5.5 ATR-FTIR

The chemical structure of the SOC was analyzed using attenuated total reflectance Fourier transformed mid-infrared (ATR-FTIR) spectroscopy. Soil samples were dried and finely ground to < 250 µm. To obtain ATR-FTIR spectra from the ground samples, I used a Bruker Optics Equinox 55 FTIR spectrometer equipped with a Mercury Cadmium Teluride detector. Spectra were collected with 256 scans per spectrum at 4 cm^{-1} resolution over a spectral range from 4,000–400 cm^{-1}. The baseline of the spectrum was corrected using OPUS (ver. 6.5, Bruker Optik GmbH, Ettlingen, Germany). Ambient air was used as background. The wavenumber range of 1,800–900 cm^{-1} was considered for the analysis of SOC functional groups in this study. Spectral deconvolution was performed by fitting Gaussian curves within this wavenumber range, following Dhillon et al. (2017). The Fityk software package (version 1.2.1; Wojdyr, 2010) was used for the deconvolution of the spectra. The absorbance of each deconvoluted band was normalized by dividing the area of individual bands within 1,800–900 cm^{-1} wavenumber region, by the sum of the total area of all bands in this region.

3.5.6 Statistical analyses

All statistical analyses were performed using R version 3.3.3 (R Core Team, 2017). To test the effect of diapirism on each soil property, gross N transformation rates, cumulative CO_2, and normalized absorbance from ATR-FTIR, mixed models were fitted with frost boil type (diapiric versus non-diapiric) as a fixed effect and block nested within sampling time as a random effect. The linear mixed model analysis was conducted using the nlme R package version 3.1-131 (Pinheiro et al., 2017). The varIdent function was used in the lme function to allow different variances per stratum (Zuur et al., 2009). The optimal varIdent variance structure was selected using the Akaike information criterion and the likelihood ratio testing approach (Zuur et al., 2009) for each of the analyses. For the analysis of ATR-FTIR data, the mixed model included the same varIdent variance structure as the one for SOC analysis. Heterogeneity of variance was checked by plotting residuals against fitted values for each model. Measurements were considered as outliers and removed if they were greater than 2.5 standard deviations from the mean. The relationships between gross mineralization rate and gross nitrification rates were tested using Spearman's rank correlation separately for each desert. Correlations were considered significant at $p < 0.05$.

3.6 Results

3.6.1 Soil properties

Diapiric frost boils had greater SOC than non-diapiric frost boils in both deserts ($p < 0.01$), which confirmed the vis-NIR-based frost-boil classification in the field (Table 1). Also, diapiric frost boils had higher TDN ($p = 0.03$) compared to non-diapiric frost boils within the dolomitic desert. In the granitic desert, however, TDN was comparable between frost boil types ($p = 0.70$). Besides SOC and TDN, no other soil properties were significantly different between diapiric and non-diapiric frost boils in both deserts ($p > 0.05$). SOC was 38% higher in diapiric and 27% higher in non-diapiric frost boils in the dolomitic relative to granitic deserts. Dolomitic desert dissolved organic carbon was 15% higher in diapiric and 21% higher in non-diapiric frost boils compared to the granitic desert. Additionally, the dolomitic desert had higher soil pH in both diapiric and non-diapiric frost boils than the granitic desert. The electrical conductivity of both diapiric and non-diapiric frost boils in the dolomitic desert was more than three times higher than in the granitic desert. The soil P of the dolomitic desert was 61% lower in diapiric frost boil

and was 58% lower in non-diapiric frost boil relative to each of the frost boils within the granitic desert.

Table 3.1 Mean values of the soil properties in diapiric and non-diapiric frost boils within the dolomitic and granitic deserts.

	Dolomite			Granite		
Soil property	Diapir[a]	Non-diapir[b]	*p*	Diapir[c]	Non-diapir[d]	*p*
SOC[e] (g kg^{-1} dry soil)	6.48 (0.77)	5.49 (0.64)	***	4.71 (0.51)	4.32 (0.35)	***
TDN[f] (mg kg^{-1} dry soil)	0.49 (0.068)	0.38 (0.023)	*	0.54 (0.043)	0.53 (0.039)	ns
DOC[g] (mg kg^{-1} dry soil)	2.54 (0.18)	2.72 (0.16)	ns	2.21 (0.13)	2.24 (0.089)	ns
P[h] (mg kg^{-1} dry soil)	163 (23.7)	175 (23.0)	ns	419 (42.1)	416 (39.7)	ns
pH	7.5 (0.024)	7.6 (0.021)	ns	5.8 (0.087)	5.9 (0.063)	ns
EC[i] (µS/cm)	193 (29.3)	217 (28.1)	ns	51.8 (3.01)	47.0 (3.91)	ns
GWG[j] (%)	10.9 (0.36)	11.2 (0.28)	ns	11.2 (0.81)	11.7 (0.48)	ns

Values in parentheses are $\pm$ 1 SE.
a (n = 15) for all the soil properties
b (n = 24) for all the soil properties
c (n = 16) for all the soil properties except for DOC in which (n = 15)
d (n = 23) for all the soil properties
e SOC = Soil organic carbon
f TDN = Total dissolved nitrogen
g DOC = Dissolved organic carbon
h P = Phosphorus
i EC = Electrical conductivity
j GWG = Gravimetric water content
* and *** indicate significance at the $p \leq 0.05$ and $p \leq 0.001$ levels of probability.
ns denotes no significant difference.

3.6.2 Gross N transformation rates

Diapiric frost boils had lower gross mineralization rates than non-diapiric frost boils. In the granitic desert, gross mineralization rates were 48% lower in diapiric relative to non-diapiric frost boils ($p = 0.03$; Fig. 3.2A). Mineralization rates did not differ between diapiric and non-diapiric frost boils in the dolomitic desert ($p = 0.43$). Gross NH_4^+ consumption rates were lower in diapiric than in non-diapiric frost boils within the granitic desert (−43%; $p = 0.02$; Fig. 3.2B). By contrast, gross NH_4^+ consumption rates did not differ in diapiric relative to non-diapiric frost boils within the dolomitic desert ($p = 0.21$). Diapiric frost boils did not differ in nitrification rates from non-diapiric frost boils within the granitic desert ($p = 0.54$; Fig. 3.2C), despite having significantly lower gross NH_4^+ consumption rates (Fig. 3.2B). The relationship between gross mineralization rate and gross nitrification rate was insignificant in both deserts (Dolomite; $p = 0.14$, granite; $p = 0.37$). The isotope dilution techniques may have ended up increasing the size NO_3^- pool since little NO_3^- is available in arctic ecosystems (Jones & Kielland, 2012); therefore, I excluded interpretation of gross NO_3^- consumption rates.

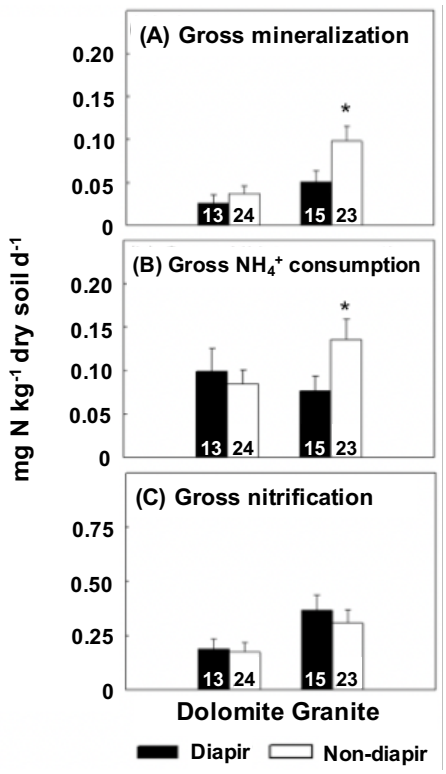

Fig. 3.2 Gross mineralization, NH_4^+ consumption, and nitrification rates in diapiric and non-diapiric frost boils in dolomitic and granitic deserts. Numbers in each column indicate sample sizes. Error bars represent standard errors of the mean. Note the change in y-axis scale between (A, B) and (C). * indicates $p < 0.05$ significance.

3.6.3 Soil respiration

Cumulative CO_2 was lower in diapiric than in non-diapiric frost boils within both deserts (Fig. 3.3A and Fig. 3.3B). In the dolomitic desert, diapiric frost boils had significantly lower cumulative CO_2 (μg CO_2-C·mg^{-1} soil C) over the 10-day incubation period (−38%; $p = 0.01$). Cumulative CO_2 per g dry soil was 19% lower in diapiric compared to non-diapiric frost boils ($p = 0.07$). However, one non-diapiric frost boil had a value of 2.2 standard deviations from the mean, which affected the statistical analysis. Without this potential outlier, the cumulative CO_2 per g dry soil was 21% lower in diapiric compared to non-diapiric frost boils ($p = 0.03$). Nonetheless, here I included the value to present the cumulative CO_2 (Fig. 3.3B). In the granitic desert, the cumulative CO_2 per mg SOC did not differ between diapiric and non-diapiric frost boils ($p = 0.52$) nor did cumulative CO_2 per g dry soil ($p = 0.44$).

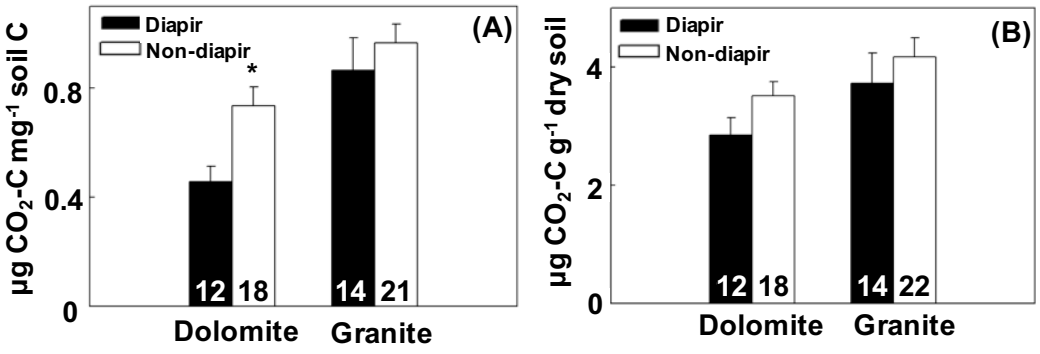

Fig. 3.3 Mean cumulative CO_2 per: (A) soil organic carbon and (B) dry soil mass. The number on each bar specifies the sample size. Error bars represent standard error of the mean. * indicates $p < 0.05$ significance.

3.6.4 ATR-FTIR

Soil organic matter was chemically different between diapiric and non-diapiric frost boils in each desert (Table 2). In the dolomitic desert, ATR-FTIR bands > 1,200 cm^{-1} were obfuscated due to carbonate-rich soil, so I excluded these bands. Normalized absorbance was greater in diapiric than non-diapiric frost boils at 1,158, 1,100, and 1,033 cm^{-1} ($p < 0.01$). Absorbances at 1,158, 1,100, and 1,033 cm^{-1} can be attributed to polysaccharides or chemically similar compounds such as carbohydrates (Ernakovich et al., 2015; Tatzber et al., 2007), which are highly viscous (Hayes, 2009). In the granitic desert, the normalized absorbance at 1,646, 1,100, and 1,033 cm^{-1} was greater in diapiric than non-diapiric frost boils ($p < 0.01$). The normalized

absorbance at 1,158 cm^{-1} was significantly lower in diapiric frost boils ($p < 0.01$). Bands at 1,646 cm^{-1} can be assigned to a combination of recalcitrant carbon such as lignin and humics (Calderón et al., 2011). Similar to the dolomitic desert, absorbances at 1,158, 1,100, and 1,033 cm^{-1} suggest the presence of polysaccharides or carbohydrate-like substances (Ernakovich et al., 2015; Tatzber et al., 2007). Si–O stretching of mineral bands may overlap with the organic band; thus, I excluded bands below 1,000 cm^{-1} from chemical interpretation in both deserts (Calderón et al., 2011; Haberhauer et al., 2000).

Table 3.2 Results from the linear mixed effect model including the varIdent variance structure used for SOC analysis, for the analysis of ATR-FTIR peaks.

	Dolomite[a]		Granite[b]	
ATR-FTIR bands (cm^{-1})	Mean difference[c]	*p* value	Mean difference	*p* value
1,033	−2.69	***	−2.32	***
1,100	−1.28	***	−0.14	***
1,158	−0.19	***	0.36	***
1,442	—[d]	—	−0.02	0.47
1,646	—	—	−0.05	***
1,721	—	—	−0.03	0.42

a 15 diapiric and 24 non-diapiric frost boils
b 16 diapiric and 23 non-diapiric frost boils
c Negative values of mean difference indicate a decrease in ATR-FTIR peak from diapiric to non-diapiric frost boils.
d The absence of data due to obfuscated band.
*** indicates significance at the $p \leq 0.001$ level of probability.

3.7 Discussion

My results suggest a large biological contribution to diapir formation and SOC quality in High Arctic polar deserts. Conventionally, diapiric formation has been explained solely based on soil physical perspectives such as unstable bulk density and viscosity (Muller et al., 2017; Swanson et al., 1999). A previous study showed that SOC was 7% higher in diapiric compared to non-diapiric frost boils (Muller et al., 2017); here I confirmed the vis-NIR classifications and demonstrated that diapiric frost boils increased polysaccharides, which could increase soil viscosity (Hayes, 2009). This alteration of SOC composition may be related to microbes. Polysaccharides are major microbial cell wall components (Rodrigues et al., 2011), and microbes

produce polysaccharides to protect their cells from environmental stresses such as drying (Arco et al., 2005). Diapir formation by microbial polysaccharides may be consistent with that only approximately 30% of frost boils at the site had diapiric ejections (Muller et al., 2017), diapiric and non-diapiric frost boils are interspersed on the landscape, and diapirism occurred independently of parent material (granitic or dolomitic). Soil polysaccharides, however, are also derived from dead plant roots and root exudates (Akhtar et al., 2018). I, therefore, propose that soil microbes and/or plants in diapiric frost boils likely produce polysaccharides at a greater rate than in non-diapiric frost boils, increasing the viscosity of the soil layer overlying an ice-rich horizon and initiating a geomorphological cascade leading to diapirism (Fig. 3.4). In addition to polysaccharide enrichment, my study suggests that SOC in Bhy horizons is more recalcitrant than in non-diapiric frost boils—consistent with previous studies (Gillespie et al., 2014; Kaiser et al., 2007; Wild et al., 2013). However, previous work at the study site showed that the dominant-vascular plant species, *Salix arctica*, was both more abundant and produced more deep roots on diapiric frost boils compared to non-diapiric frost boils (Muller et al., 2017). Therefore, despite the recalcitrant C in Bhy horizons and its slow breakdown into available nutrients for plant roots, some plant species may still actively forage for nutrients in diapirs.

Infrared analysis suggested that the increase in polysaccharides may link to diapiric injections. ATR-FTIR bands indicating polysaccharides had higher absorbance in diapiric versus non-diapiric frost boils within both deserts (dolomitic: 1,158, 1,100, and 1,033 cm^{-1}; granitic: 1,100 and 1,033 cm^{-1} within the granitic desert) although the band near 1,158 cm^{-1} had lower absorbance in diapiric compared to non-diapiric frost boils within the granitic desert. Polysaccharides are a binding agent in soil aggregation (Calderón et al., 2011) and increase soil viscosity (Hayes, 2009). As Swanson et al. (1999) showed, the enriched polysaccharides may increase the viscosity of soil and then the underlying soil material may intrude into the overlying layer. Also, the band at 1,644 cm^{-1} had higher absorbance in diapiric relative to non-diapiric frost boils. This absorbance disparity may be due to recalcitrant SOC. For instance, Calderón et al. (2011) found absorbance within the 1,630 cm^{-1} band increased as C mineralization increased and suggested that the band represented recalcitrant SOC like lignin and humics. The band assignment interpretation agrees with Gillespie et al. (2014), who suggested that cryoturbated organic horizons that had previously lost labile organic matter become resistant to further decomposition. Therefore, diapirism may inject previously decomposed and recalcitrant SOC

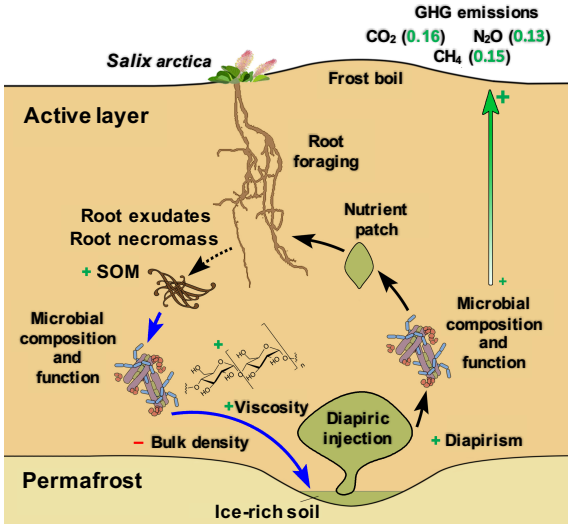

Fig. 3.4 Conceptual diagram of soil movement and microbial and nutrient dynamics within frost boils. Arrows in blue indicate the pathway suggested from the results in this paper, and the dotted arrow indicates a pathway that is hypothesized to exist but not yet demonstrated. Polysaccharides that increase soil viscosity may be of microbial or plant origins. Pluses of disparate size on the arrow connecting microbial composition and function to greenhouse gas (GHG) emissions indicate the increasing influence of microbes closer to the soil surface (Brummell et al., 2012, 2014). Numbers in parentheses indicate CO_2 fluxes in $\mu mol \cdot m^{-2}\ s^{-1}$ and $nmol \cdot m^{-2}\ s^{-1}$ for N_2O and CH_4.

into the upper soil, which is consistent with both the lower C and N mineralization rates (Fig. 3.2A and 3.3) and reduced soil respiration (Brummell et al., 2015) in diapiric frost boils at the study sites. Reduced microbial activity due to recalcitrant SOC (Kaiser et al., 2007; Wild et al., 2013) suggests that, despite high levels of soil C in these diapiric injections, this C is comparatively stabilized and therefore not a key driver of soil nitrogen cycling. Moreover, new (*i.e.,* easily biodegradable) carbon inputs, potentially from thawing permafrost, may select for microbes that are better suited to decompose old recalcitrant SOC by using the fresh carbon as an energy source (the "priming effect"; Fontaine et al., 2011). Projected warming may offset the balance between microbial taxa able to mine nutrients from SOC under low-soluble nutrient conditions (K-strategists) over species that feed only on fresh C and immobilize nutrients from the soil solution (r-strategists; Fontaine et al., 2003). This could have implications for soil nitrogen cycling; however, further monitoring would be necessary to test this hypothesis in polar deserts.

The gross N transformation assay characterized the processes that supply N for plants within this polar desert frost-boil system. Gross N mineralization rates were slower in diapiric compared to non-diapiric frost boils within the granitic desert (Fig. 3.2A), which was consistent

with the results of Kaiser et al. (2007) and Wild et al. (2013). In addition, N immobilization rates of the desert may be also reduced in diapiric frost boils, as the gross NH_4^+ consumption rates were lower in diapiric versus non-diapiric frost boils (Fig. 3.2B). Since gross nitrification rates differed from gross mineralization rates (albeit insignificantly), it is more likely that NH_4^+ produced by mineralization is immobilized by microbes before the NH_4^+ enters the nitrification pathway involved in N_2O production in polar deserts (Fig. 3.2A–3.2C). With slower anabolic and catabolic processes, however, diapiric frost boils may gradually accumulate N as suggested by higher TDN in diapiric frost boils in the dolomitic desert (Table 1). Alternatively, the increase in TDN may be due to a mutualistic relationship between *S. arctica* and microbes, as *S. arctica* is colonized by ectomycorrhizal fungi (Kohn & Stasovski, 1990) and capable of higher N uptake from Bhy horizons (Muller et al., 2017). Though mutualistic relationships between *S. arctica* and microbes might stimulate N_2O production in diapiric frost boils, it is unlikely that diapirism itself drives N_2O production by providing NH_4^+ for nitrifying organisms. Furthermore, diapir is unlikely a suitable C source for denitrification due to its recalcitrant nature.

My study supports that diapirism maintains plant vegetation under nutrient limiting conditions and suggests that diapirism provides an insight into the feedback of the global warming in polar deserts. Muller et al. (2017) demonstrated higher N uptake by *S. arctica* in diapiric compared to non-diapiric frost boils. However, my study suggests that *S. arctica* might not rely on N mineralization for its N supply. Despite the recalcitrant SOC, *S. arctica* is more abundant on diapiric frost boils, with more root biomass at depth, compared to non-diapiric frost boils (Muller et al., 2017). Therefore, *S. arctica* may establish a mutualistic relationship with microbes to utilize nutrients in Bhy horizons. Although the root biomass could be a source of fresh organic matter to stimulate microbial activity, the rates of N and C mineralization in my study did not indicate increased microbial activity (Fig. 3.2A and 3.3). Without plant-microbe interactions, diapirism may not contribute to GHG emissions and could even mitigate GHG production by slowing microbial activity in polar deserts. However, rising air temperatures can further thaw and thicken the active layer, introducing previously stored SOC into the nutrient cycle within frost boils. Gillespie et al. (2014) showed that the permafrost stored more labile SOC compared to the SOC in the upper soil layer. Furthermore, Pautler et al. (2010) showed that permafrost thaw provided fresh soil organic matter to increase microbial activity, accelerating decomposition. In addition to labile SOC, the further permafrost thaw may stimulate N cycling in

frost boils. For example, organisms and genes responsible for denitrification and N_2-fixation are stored in the permafrost (Altshuler et al., 2019). Under wetter soil conditions, the increased rates of N cycling might stimulate denitrification and increase N_2O production. The degree of linkage between N_2-fixation and denitrification varies across ecosystem types (Stewart et al., 2013). In the study sites, the increase in N_2O production via denitrification might be higher in the granitic desert than in the dolomitic desert since lower pH can lead to incomplete denitrification (Šimek & Cooper, 2002). Therefore, once stored soil organic matter and organisms enter into the geochemical cycling in frost boils, diapirism may contribute to positive feedback with GHG production in polar desert ecosystems. My study suggests that diapirism may represent a key mechanism underlying ecological change in the High Arctic, and further investigation is necessary for accurate and timely projections of polar desert evolution under climate change.

3.8 Conclusions

Diapiric frost boils had greater TDN in the dolomitic desert. On the other hand, gross N mineralization and respiration assays showed that diapiric frost boils had lower microbial activity than non-diapiric frost boils. The lower C and N mineralization rates were consistent with ATR-FTIR results, showing that diapiric frost boils contained more recalcitrant SOC than non-diapiric frost boils in the granitic desert. ATR-FTIR data also indicated that diapiric frost boils had greater polysaccharides than non-diapiric frost boils in both deserts. Polysaccharides are a binding agent in soil aggregation and increase viscosity, which facilitates diapirism. Furthermore, as ~30% of frost boils developed diapirism independently of parent material at the site and as soil polysaccharides include dead roots and root exudates, the polysaccharides may be of biological origin (microbes and/or plants). Increased diapiric viscosity intrudes underlying recalcitrant SOC into the overlying horizon, which may then slow microbial activity due to low biodegradability. Lower anabolic and catabolic microbial activity may accumulate TDN in diapiric frost boils as was seen in the dolomitic desert. Alternatively, TDN accumulation may be related to a mutualistic relationship between *S. arctica* and microbes. The mutualistic relationship may stimulate microbial activity (contrary to polysaccharide influence), but diapirism unlikely contributes to GHG production without plant-microbe interactions. Alternatively, as increasing air temperatures thicken the active layer, diapirism could introduce more stored fresh soil organic matter into geochemical cycling. The labile organic matter might allow microbes to mine recalcitrant carbon of diapiric organic to increase GHG production. The

permafrost thaw could also stimulate N cycling, which might increase N_2O from incomplete denitrification pathway. My study suggests that further investigation of diapirism is a key for accurate projections of polar desert feedbacks to a rapidly warming climate.

4. BIOLOGY AND CARBON LABILITY OF SUB-SURFACE NUTRIENT PATCHES IN HIGH ARCTIC POLAR DESERTS DRIVES THE PROBABILITY AND MAGNITUDE OF NITROUS OXIDE EMISSIONS

4.1 Preface

In Chapter 3, I found diapirs slow C and N mineralization, which linked to the higher amount of recalcitrant C. In this chapter, I investigated the effect of diapirs on N_2O emissions under soil moisture conditions favouring nitrification and denitrification under a laboratory-controlled incubation. I employed the hurdle model to deal with zero-inflated continuous data of the N_2O emission. Furthermore, I investigate the abundance of archaeal *amoA*—the dominant ammonia oxidizer in the study site—and ^{15}N site preference of the emitted N_2O and discuss how recalcitrant diapiric C alters N_2O emissions under different soil moisture conditions. I also discuss the probability and magnitude of N_2O emissions from polar desert soils.

This chapter has been published as Ota, M., S.D. Siciliano. 2020. Biology and carbon lability of sub-surface nutrient patches in High Arctic polar deserts drives the probability and magnitude of nitrous oxide emissions. Soil Biology & Biochemistry 150: 1–8. This manuscript was reformatted for inclusion in this dissertation. Dr. Siciliano provided critical advice and discussion about the laboratory incubation system and the statistical approach using the hurdle models for zero-inflated continuous data.

4.2 Abstract

High Arctic polar deserts cover 26% of the Arctic. Climate change is expected to increase cryoturbation in these polar deserts, including frost boils and diapirs. Diapirism—cryoturbic intrusion into the overlying horizon—creates subsurface nutrient patches with low biodegradability and is thought to regulate greenhouse gas emissions, including the potent nitrous oxide. Although nitrous oxide emissions have been observed in polar deserts at a rate comparable to vegetated tundra ecosystems, the underlying mechanism by which nitrous oxide is produced in these environments remains unclear. In this study, I investigated ammonia-oxidizing archaea, which were detected in a previous study, and used stable isotope techniques to characterize the pattern of nitrous oxide emissions from frost boils. Ammonia-oxidizing archaea would be tightly linked to nitrous oxide emissions under aerobic conditions whereas low degradable diapiric nutrient would limit denitrification under wet conditions. I hypothesized that (1) diapirism (*i.e.,* diapiric frost boil) would not primarily drive nitrous oxide emissions and therefore abundance of ammonia-oxidizing archaea would be linked to the increase in nitrous oxide emissions under dry conditions favouring nitrification, and (2) diapirism decreases nitrous oxide emissions relative to non-diapiric frost boil under wet conditions that favour denitrification because of the recalcitrant nature of diapiric organic carbon. I used soil samples collected from two High Arctic polar deserts (dolomite and granite) near Alexandra Fjord (78°51′N, 75°54′W), Ellesmere Island, Nunavut, Canada from July–August 2013. Ammonia-oxidizing archaea did not differ in abundance between diapiric and non-diapiric frost boils within the dolomitic desert; however, within the granitic desert *amoA* abundance was 22% higher in diapiric frost boils. In both deserts, the increased abundance of archaeal amoA genes was linked to increased nitrous oxide emissions under dry conditions. Under higher soil moisture conditions favouring denitrification, diapiric frost boils emit N_2O with higher probability, but at a lower rate, than non-diapiric frost boils. For example, in the dolomitic desert, diapirism increased the probability of N_2O emissions by 104% but decreased the LS means value of the emission rate by 36%. Similarly, diapirism increased the emission probability by 26% but decreased the LS means value by 68% within the granitic desert. Under wet conditions, site preference values suggested that fungal and bacterial denitrification were important nitrous oxide emission processes. My study shows that diapirism is a key cryoturbation process for nitrous oxide emissions in polar

deserts primarily through diapirism's alteration of emission probability and the magnitude of the emissions.

4.3 Introduction

The High Arctic is the northernmost zone in the Arctic region and mostly consists of polar desert ecosystems, covering approximately 1,358,000 km^2 or 26% of the Arctic (Brummell et al., 2014). Vascular vegetation cover in polar deserts is typically less than 5%, and thus polar deserts are highly susceptible to changes in climatic conditions (Voigt et al., 2017). Polar deserts have substantially higher amounts of organic carbon (C) in the permafrost layer than previously estimated (Burnham & Sletten, 2010; Hugelius et al., 2014). As the climate warms and the permafrost table becomes deeper each summer, the stored C becomes accessible to microbes. Soil organic C stored in the permafrost layer is more labile than that in the upper soil layer (Gillespie et al., 2014). As a result, greenhouse gas emissions in polar deserts can be substantial (Voigt et al., 2017), similar to emissions recorded in non-desert mesic Arctic ecosystems (Brummell et al., 2012, 2014; Lamb et al., 2011). Greenhouse gas emissions from polar deserts arise from the geomorphological and microbiological characteristics of cryoturbation. Cryoturbation creates frost boils (Walker et al., 2004) and diapirs (Swanson et al., 1999), which are key landscape and soil profile characteristics in polar deserts (Muc et al., 1989; Muller et al., 2017). Frost boils are repeated circular patches (*i.e.,* 1–3 m in diameter), with barren or sparse vegetation cover and rock fragments near the center relative to the margin (Fig. 4.1A) (Muller et al., 2017; van Everdingen, 1998). Thermal conductivity is greater in the center of the frost boil, leading to soil material migrating to the surface at a higher rate in the center of frost boil relative to the margin. Likewise, the permafrost surface under the center becomes more depressed (Fig. 4.1B) (Ping et al., 2015; Shilts, 1978). Deep within these frost boils, soil nutrients accumulate in an ice-rich horizon above the bowl-shaped permafrost table (Boike et al., 2008; Cannone et al., 2004; Walker et al., 2004) by meltwater leaching (Muller et al., 2017; Schaeffer et al., 2013; Tye et al., 2005) (Fig. 4.1B). In about 30% of frost boils (Muller et al., 2017), soil materials from the ice-rich horizon are extruded into the overlying horizon to create a nutrient-rich patch or diapir, which I've termed a Bhy horizon based on the Canadian system of soil classification (Expert Committee on Soil Survey, 1987) (Fig. 4.1B). In this paper, I defined frost boils with diapirs as diapiric frost boils and frost boils without diapirs as non-diapiric frost boils. The extrusion is termed diapiric flow and occurs as the overlying horizon has lower bulk density and becomes

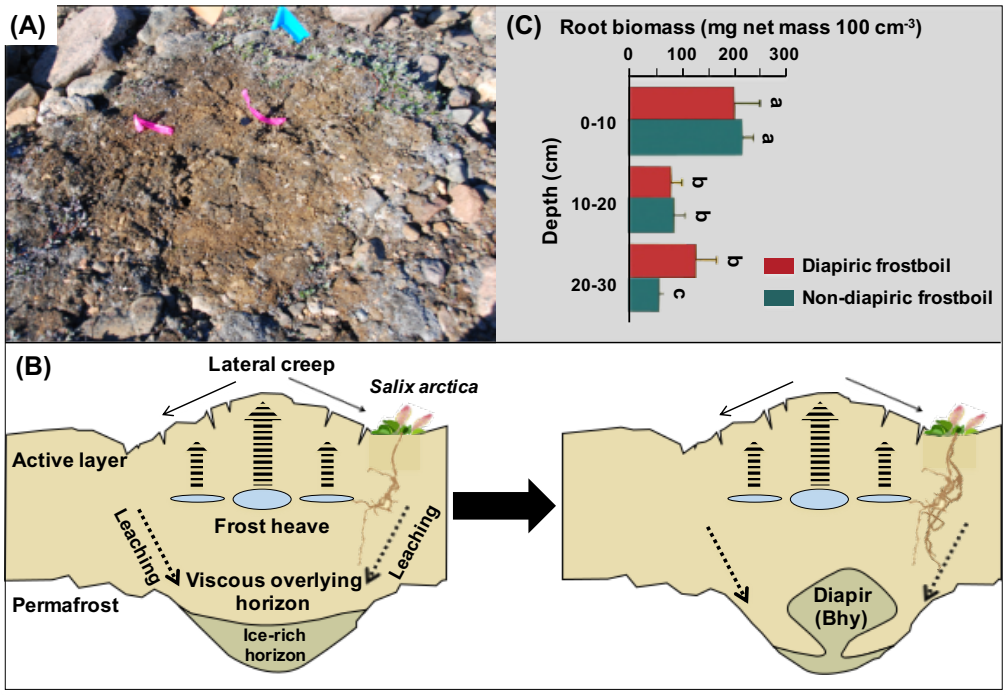

Fig. 4.1 Frost boil (A), mean root biomass (mg net mass 100 cm^{-1}) ± standard error at different depths in diapiric and non-diapiric frost boils (B), and cross-section of frost boil illustrating the form of diapir together with frost-boil development (C). Note: A, B, and C were adapted from Appendix S2: Fig. S2, Fig. 1, and Appendix S2: Fig. S1, respectively, in Muller et al. (2017).

more viscous than the ice-rich horizon (Swanson et al., 1999). These Bhy horizons have 9–18% more organic C than other subsurface horizons (Muller et al., 2017), and as has been observed in cryoturbated horizons in other Arctic regions (Gillespie et al., 2014; Kaiser et al., 2007; Wild et al., 2013), this organic C is resistant to biodegradation (Brummell et al., 2015; Ota et al., 2020). The Bhy horizon also acts as a nutrient patch for *Salix arctica*, the dominant shrub in these ecosystems (Muller et al., 2017). As *Salix arctica* increases root biomass and nitrogen uptake from diapirs (Fig. 4.1C), diapirism is a key source of nitrogen for the vegetation community (Muller et al., 2017). Diapirism is expected to increase as rising temperatures increase permafrost thaw and meltwater production (Callaghan et al., 2005; Klaus et al., 2013; Walker et al., 2008). However, it is not clear how the nitrogen in the Bhy horizon is related to N_2O production by the soil microbial community.

N_2O has a high global warming potential (Intergovernmental Panel on Climate Change, 2014) and depletes the ozone layer (Ravishankara et al., 2009). Furthermore, N_2O emissions reduce limited soil nitrogen (N), which is primarily derived from N_2-fixation. The range of N_2O flux rates (0.06–16 kg N_2O-N ha^{-1} yr^{-1}; Brummell et al., 2012; Lamb et al., 2011) is higher than

average rates of N_2-fixation in Arctic regions (0.2–2 kg N ha^{-1} yr^{-1}; Stewart et al., 2014). It is important to note that the N_2O flux rates mean that a temporal magnitude of the emissions can be equivalent to the large flux rate and not that the output of N is higher than the input in Arctic soils. Nitrification and denitrification are the dominant sources of N_2O in soils, and their relative contributions change with soil moisture. Optimal soil moisture content for N_2O production via nitrification is near 45% water-filled pore space (WFPS) whereas that for N_2O production via denitrification is over 70% WFPS (Hu et al., 2015; Marushchak et al., 2011). Siciliano et al. (2009) and Ma et al. (2007) demonstrated that nitrification is the dominant source of N_2O emitted from upland Arctic soils (0–15 cm depth). This is presumably because in the typically aerobic soils in the High Arctic, soil N mainly presents as ammonium that provides the substrate for ammonia oxidizers (*i.e.,* ammonia) (Brummell et al., 2014; Hayashi et al., 2016) and soil organic C is limited compared to other terrestrial ecosystems. Under wet conditions with available C, N_2O production in Arctic soils is via denitrification (Gil et al., 2017; Marushchak et al., 2011).

N_2O production in frost boils could be due to nitrification or denitrification. Polar deserts are dry in the upper soil horizons; however, Bhy horizons form at depths ranging from 10–30 cm within frost boils (Muller et al., 2017; Ota et al., 2020). Thus, some Bhy horizons can have high soil moisture once they form close to the permafrost layer. The recalcitrant Bhy organic C may not be readily available for denitrifiers and thus favour nitrification. Therefore, Bhy horizons may produce N_2O production via nitrification or denitrification. The intent of this study is to outline the dominant pathways of N_2O production in the High Arctic diapirs.

Analysis of N_2O isotopomers (Toyoda & Yoshida, 1999) has been used to assess N_2O sources. Site preference (SP)—the difference in ^{15}N enrichment between the central and terminal positions in an N_2O molecule (*i.e.,* $\delta^{15}N^{\alpha} - \delta^{15}N^{\beta}$)—provides robust information of the N_2O pathways, as SP value is theoretically independent of ^{15}N enrichment of precursors and depends on N_2O producing process (Gil et al., 2017). The SP for N_2O production under soil conditions favouring nitrification (Well et al., 2008) or denitrification (Park et al., 2011; Well & Flessa, 2009; Well et al., 2006) differs from pure culture studies (Gil et al., 2017). The difference in N_2O SP between soil incubation and pure culture studies is caused by the influences of different microbial community structures and/or interactions of microbe and soil properties on SP (Park et al., 2011; Well & Flessa, 2009). Furthermore, SP values overlap among ammonia-oxidizing

archaea (AOA), ammonia-oxidizing bacteria (AOB), and fungal denitrifiers (Hu et al., 2015), which are all typically active in soils. Despite these limitations, SP values can identify temporal shifts in overall microbial pathways of N_2O production (Gil et al., 2017), such as changes caused by diapir presence and soil moisture. Thus, SP is an ideal indicator to evaluate the microorganisms responsible for N_2O production in Bhy horizons.

Typically, incubation studies of N_2O emissions from polar desert soils have many values near or below the detection limit. As a result, measurements become highly skewed, zero-inflated continuous data, making common statistical approaches, including paired t tests and general linear modeling (GLM), difficult to perform. To overcome this difficulty, I used the hurdle models for the analysis of zero-inflated data. The hurdle models include a Bernoulli component that models whether the data cross the detection limit based on covariates, and GLM components that model the data above the detection limit (Huang et al., 2019). The combination of the Bernoulli and GLM gamma components allows a hurdle model to evaluate how covariates such as soil moisture or diapirism explain the variation in a response variable like N_2O emissions.

The objective of this study was to evaluate how diapirism influenced N_2O emissions from frost boils in two High Arctic polar deserts. I hypothesized that diapirism would not be the proximal driver of N_2O emissions under dry conditions and thus, that (1) AOA abundance would have a positive relationship with N_2O emissions under dry conditions favouring nitrification, and in contrast, (2) diapiric frost boils decrease N_2O emissions relative to non-diapiric frost boils under wet conditions favouring denitrification due to the recalcitrant nature of organic carbon in Bhy horizon. To achieve the objective based on the hypotheses, I examined AOA abundance, N_2O emitted from diapiric and non-diapiric frost boils and SP of the N_2O under both dry and wet conditions. I further examined the N_2O emission data in the context of AOA abundance and the soil moisture levels for the first time to assess how the High Arctic polar desert emits N_2O in relation to diapirism. As diapirism is expected to increase under a warming climate, a better understanding of the effect of diapirism on N_2O emissions will help accurate prediction of positive feedback with N_2O emissions from High Arctic polar deserts.

4.4 Materials and Methods

4.4.1 Study site and soil sampling

The study site was located in a Canadian High Arctic polar desert near Alexandra Fjord (78°51′N, 75°54′W), Ellesmere Island. Soil samples were obtained from July to August 2013. Field description and soil sampling methods are detailed in Ota et al. (2020). Briefly, the site is composed of dolomitic and granitic deserts. The CAVM (Walker et al., 2002) shows the plant communities in the dolomitic desert as cryptogam, herb barren and in the granitic desert as noncarbonated mountain complexes. Mean growing season temperatures are low (3–8°C) and annual precipitation is < 50 mm. For soil sampling, a randomized block design was used to include variability of frost boils and vegetation cover. Dolomitic and the granitic deserts were divided into five and 12 blocks, respectively. Soil samples (1 kg each) were collected from subsurface organic-rich horizons in frost boils (*i.e.,* diapiric frost boils) and from non-organic-rich horizons in paired control frost boils (*i.e.,* non-diapiric frost boils). The depths ranged from 10–25 cm in the dolomitic and from 15–30 cm in the granitic deserts. Subsurface soil organic carbon was quantified using a visible and near-infrared reflectance spectrophotometer (Guy et al., 2015). The soil samples were frozen and shipped to the University of Saskatchewan.

4.4.2 DNA extraction

Soil DNA was extracted using FastDNA SPIN Kit (QBiogene, Carlsbad, California) following the manufacture's instruction. The DNA concentration of each extract was quantified using Qubit 4 Fluorometer (Life Technologies, Darmstadt, Germany) and was standardized to 5 ng/μL. Some extracts yielded low DNA concentrations ranging from 0.1–4.9 ng/μL.

4.4.3 Quantification of archaeal *amoA* gene

Archaeal *amoA* gene assay used primers CrenamoA23f (5′-ATGGTCTGGTWAGACG-3′) (Tourna et al., 2008) and CrenamoA61648x (5′-GCCATCCABCKRTANGTCCA-3′) (Schauss et al., 2009). To construct a standard curve, recombinant *Escherichia coli* DH5αT1R strains carrying an archaeal *amoA* gene fragment (624 bp) from fosmid 54d9 (Treusch et al., 2005) were inoculated into 3.0 mL LB broth with 50 μg/mL ampicillin and were incubated at 37°C for 16 h. Plasmid DNA was extracted using Qiagen QIAprep Spin Miniprep (QIAGEN, Venlo, Netherlands) kit following the manufacturer's instructions. The extracted plasmid was quantified using Qubit 4 Fluorometer and linearized with the HindIII restriction enzyme (Thermo Fisher Scientific, Waltham, Massachusetts). Using the linearized plasmid with the archaeal *amoA* gene fragment, a dilution series (10^1–10^6 *amoA* gene copies) was created for a standard curve.

Based on the slope of the standard curve, the efficiency ranged from 85–93%. The r^2 values for the standard curve were 0.99. Reactions (20 µL) contained 12.5 µL of QuantiTect SYBR Green PCR Master Mix (QIAGEN, Venlo, Netherlands), 0.2 mg mL^{-1} of bovine serum albumin, 0.75 µM of each primer, and 2 µL of the standardized DNA template (DNA concentration = 5 ng/µL) or quantified extract (DNA concentration < 5 ng/µL). The thermal conditions were 5 min at 95°C, followed by 45 cycles of 45 s at 95°C,45 s at 55°C with a touching down to 50°C in 10 cycles followed by 35 cycles at 50°C, and 45 s at 72°C, and a final elongation step for 1 min at 80°C.

4.4.4 Cumulative N_2O (ng N_2O-N g^{-1} dry soil d^{-1})

Soil samples were slowly thawed in ice and packed in a polystyrene core (2.8 × 1.4 cm internal diameter) with a bulk density of 1.3 g cm^{-3} (Brummell et al., 2014). Soil cores were pre-incubated for three weeks at 10°C in the dark before water or ^{15}N was added. To prevent soil cores from drying, each core was put in a drum vial during pre-incubation. Soil moisture was adjusted to 45% WFPS or 75% WFPS by adding autoclaved distilled water. ^{15}N was added as either $^{15}NH_4NO_3$ or $NH_4{}^{15}NO_3$ solution at approximately 1.3 atom%^{15}N. The amount of N was 10% of the total dissolved N in each soil, which was measured in a previous study (Ota et al., 2020). Final soil moisture was 45% WFPS for $^{15}NH_4NO_3$ addition and 75% WFPS for $NH_4{}^{15}NO_3$ addition. As nitrification and denitrification simultaneously occur, it is challenging to separate these major N_2O-producing pathways based solely on soil moisture. However, nitrification (*i.e.,* ammonia oxidation) could contribute to 88% of total N_2O emitted from soil at 45% WFPS (Well et al., 2008) and denitrification could be the main N_2O-producing pathway over 70% WFPS (Gil et al., 2017). Therefore, I considered 45% WFPS as a condition favouring nitrification and 75% WFPS as a condition favouring denitrification pathways for the first investigation of N_2O emissions associated with diapirism.

Three cores of each sample were placed in a 100-mL glass bottle (VWR International, Radnor, Pennsylvania). The cap was equipped with a brass compression tube straight adapter for 1/4” OD tubing × 1/8” male pipe (McMaster-CARR Supply Company, Elmhurst, Illinois), sandwiching ThermogreenTM LB-2 septa (9.5 mm) (Sigma-Aldrich Co., St. Louis, Missouri) for gas sampling. The cap was closed tightly by sandwiching a steam-resistant EPDM 3/16” O-Ring (McMaster-CARR Supply Company, Elmhurst, Illinois) with vacuum grease. Immediately after each cap was closed, gas sampling was conducted for time zero h using a standard 50 mL

polypropylene syringe fitted with a 25-gauge needle. To prevent ambient air from entering the syringe due to decreases in internal pressure, 46 mL of zero-air was injected into the bottle prior to gas sampling and then 46 mL of the headspace was collected. Next, the 16 mL of the headspace gas was injected into a pre-evacuated 12-mL Exetainer vial for N_2O quantification (Labco, Lampeter, Wales, UK), and the rest of 30 mL gas was injected into a pre-evacuated 22-mL thread test tube for N_2O isotopologue analysis. Both vials were flushed with zero-air prior to evacuation. After gas sampling for time zero h, each bottle was incubated in the dark at 10°C. During the incubation period, headspace gas was sampled at day nine and day 14.

Quantification of N_2O was performed using a Bruker 450 gas chromatograph (Bruker Biosciences, Billerica, Massachusetts) equipped with ^{63}Ni electron capture detector. Analysis of $\delta^{15}N^{bulk}$, $\delta^{15}N^{\alpha}$, and $\delta^{15}N^{\beta}$ of N_2O were conducted using a cavity ring-down spectroscope, the Picarro G5131-*i* isotopic N_2O analyzer (Picarro, Santa Clara, CA). ^{15}N SP was obtained by subtracting $\delta^{15}N^{\beta}$ from $\delta^{15}N^{\alpha}$. Please see Appendix 1 for details of calculations of corrected $\delta^{15}N^{bulk}$ and ^{15}N SP values.

N_2O measurements ($\mu L\ L^{-1}$) were adjusted to represent concentrations prior to adding 46 mL zero-air and then were converted to a mass unit (ng N_2O-N) using the Ideal Gas Law. Cumulative N_2O was represented by the slope of a line containing cumulated N_2O values and sampling time points. There was definite accumulation in the controls (*i.e.,* bottle with no soil cores for the background concentrations) (n = four). Therefore, the 95% confidence interval for the slopes of the controls was used for the threshold (*i.e.,* detection limit) of N_2O accumulation.

4.4.5 Statistical analysis

All statistical analyses were performed using R version 3.3.3 (R Core Team, 2017). To test the effect of diapirism on archaeal *amoA* gene abundance, a mixed model was fitted including frost boil type (diapiric versus non-diapiric) as a fixed effect and was block-nested within sampling time as a random effect. Linear mixed model analysis was performed using the nlme R package version 3.1–131 (Pinheiro et al., 2017). To allow different variances per stratum, the varIdent function was used in the lme function (Zuur et al., 2009). The optimal varIdent variance structure was selected using the Akaike information criterion and the likelihood ratio testing approach (Zuur et al., 2009) to select the appropriate model. Heterogeneity of variance was checked by plotting residuals against fitted values for each model.

The hurdle model was used to analyze cumulative N_2O under 45% WFPS, 75% WFPS, and $^{15}NH_4NO_3$ and $NH_4{}^{15}NO_3$ treatments. A generalized linear mixed model (GLMM) for the Bernoulli distribution modeled whether the data were censored ("zero") or uncensored ("one"), and a GLMM for gamma distribution modeled left-censored data above the detection limit (*i.e.,* the amount of N_2O emission). GLMM analysis was performed using the lme4 package (Bates et al., 2015). Fixed terms of maximal models for 45% WFPS and $^{15}NH_4NO_3$ were selected from archaeal *amoA* abundance, total organic carbon, and total dissolved carbon, nitrogen, and frost boil type (diapiric versus non-diapiric) after testing for collinearity (Zuur et al., 2009). The random terms included block nested within sampling time. Maximal models of 75% WFPS and $NH_4{}^{15}NO_3$ included the same fixed and random terms, except that the archaeal *amoA* abundance variable was excluded from the fixed term. Minimum adequate models for each of the treatments were selected using the Akaike information criterion and the likelihood ratio testing approach (Zuur et al., 2009). The effect of diapirism on the amount of N_2O emission was assessed using least-squares means (LS means) (Lenth, 2016) from GLMM for gamma distribution. Effects were declared significant at $p < 0.05$. Finally, the selected GLMMs for the Bernoulli and gamma distributions were combined to estimate the predicted values.

There were extremely high predicted values from non-diapiric frost boils of the granitic desert with 75% WFPS (1.2 ng N_2O-N g^{-1} dry soil d^{-1}) and from diapiric frost boils of the granitic desert with $^{15}NH_4NO_3$ treatment (5.6 ng N_2O-N g^{-1} dry soil d^{-1}), each of which was replaced the mean value for that treatment combination.

4.5 Results

4.5.1 Archaeal *amoA* gene abundance

Diapirism increased archaeal *amoA* abundance in frost boils, but only within the granitic desert (Fig. 4.2). Specifically, within the granitic desert, diapiric frost boils increased the fitted value of the gene abundance by 22% compared to non-diapiric frost boils ($p < 0.001$). The diapiric frost boils had two values that greatly deviated from the others (2.5×10^7 and 2.7×10^7 copy numbers g^{-1} dry soil), and the non-diapiric frost boils had one deviating value (6.1×10^7 copy numbers g^{-1} dry soil). Because excluding these values did not change the statistical result, I included them for the fitted values. On the other hand, within the dolomitic desert, the fitted value of the gene abundance did not significantly differ between the diapiric and non-diapiric

frost boils. The diapiric frost boils had one value that greatly deviated from the others (3.1×10^7 copy numbers g^{-1} dry soil), and the non-diapiric frost boils had one value that deviated significantly (2.4×10^7 copy numbers g^{-1} dry soil). Again, because excluding these values did not change the statistical result, I included them to provide the fitted values.

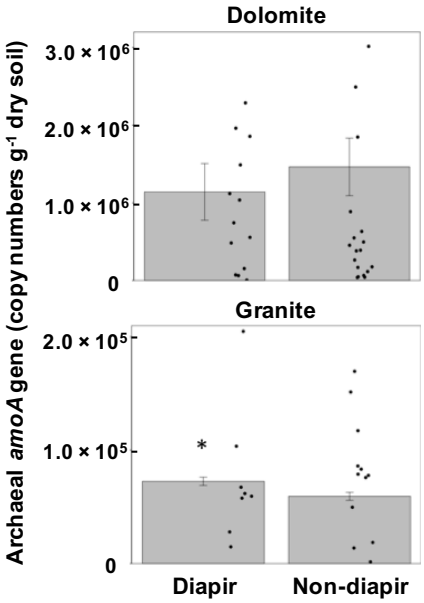

Fig. 4.2 Fitted values of Archaeal *amoA* gene abundance with standard errors in diapiric and non-diapiric frost boils within each of the dolomitic (15 diapiric and 24 non-diapiric frost boils) and the granitic (16 diapiric and 22 non-diapiric frost boils) deserts. Bar charts indicate the mean fitted values, and jitter plots indicate raw data. * indicates $p < 0.05$ significance between diapir and non-diapiric frost boils. Within the dolomitic desert, diapiric frost boils had two values above the y-axis limit (*i.e.,* 3.2×10^6), and non-diapiric frost boils had six. In the granitic desert, diapiric frost boils had eight values exceeding the y-axis (*i.e.,* 2.1×10^5), and non-diapiric frost boils had 10 values.

4.5.2 N_2O emissions

N_2O emissions in deserts result from the combination of two distinct processes: (i) a Bernoulli process, in which covariates cause emissions to occur, and (ii) a continuous process, in which covariates alter emission magnitude once the emissions occur. Overall, the data from each treatment were highly zero-inflated or under-detected within both deserts. The percentage of N2O emissions that was less than the detection limit ranged from 59–87% under 45% WFPS treatment, 47–74% under 75% WFPS treatment, 38–79% under $^{15}NH_4NO_3$ treatment, and 19–54% under $NH_4{}^{15}NO_3$ treatment. The emissions below the detection limit provide key information on the cause of emissions.

4.5.2.1 Bernoulli process

The probability of N_2O emissions increased with diapirism under soil moisture conditions favouring denitrification, but only within the dolomitic desert. Within the dolomitic desert, diapiric frost boils increased the probability of emissions by 104% relative to non-diapiric frost boils at 75% WFPS ($p = 0.048$) (Fig. A4.1A). Under $NH_4{}^{15}NO_3$ treatment, diapiric frost boils increased the probability by 60% relative to non-diapiric frost boils but the effect of diapirism was slightly less significant ($p = 0.052$). The granitic desert had a similar trend and the probability increased by 26% in diapiric frost boils compared to non-diapiric frost boils at 75% WFPS ($p = 0.7$) (Fig. A4.1B) and increased by 10% under $NH_4{}^{15}NO_3$ treatment ($p = 0.6$). In contrast, diapirism did not increase the probability of N_2O emissions under conditions favouring nitrification within either the dolomitic ($p = 0.3$) or granitic ($p = 0.7$) desert (Fig. A4.1C, D). Also, the probability of N_2O emissions did not differ between diapiric and non-diapiric frost boils under $^{15}NH_4NO_3$ treatment within either desert.

Under $^{15}NH_4NO_3$ treatment, higher archaeal *amoA* abundance significantly increased the probability of N_2O emissions within the granitic desert ($p = 0.01$). Besides diapirism and archaeal *amoA* abundance, none of the covariates was significant for a binomial process at any treatment within either of the deserts.

4.5.2.2 Continuous process

Diapirism increased the amount of N_2O emissions from frost boils under soil moisture conditions favouring nitrification but decreased that of emissions under soil moisture favouring denitrification. At 45% WFPS, the diapiric frost boils increased LS means of N_2O emissions by 33% compared to the non-diapiric frost boils within the granitic desert ($p < 0.001$) but not within the dolomitic desert (Fig. A4.2A, B). Similarly, under $^{15}NH_4NO_3$ treatment, the diapiric frost boils increased the N_2O emissions compared to the non-diapiric frost boils within the granitic desert ($p < 0.001$) but not within the dolomitic desert ($p = 0.2$). On the other hand, the diapiric frost boils decreased the LS means of N_2O emissions by 36% compared to the non-diapiric frost boils at 75% WFPS within the dolomitic desert ($p = 0.039$) and decreased by 68% within the granitic desert ($p < 0.001$) (Fig. A4.2C, D). Under $NH_4{}^{15}NO_3$ treatment, diapiric frost boils also significantly increased LS means value for the emissions compared to non-diapiric frost boils within the granitic desert ($p = 0.003$) but not within the dolomitic desert ($p = 0.7$).

Archaeal *amoA* abundance significantly increased with N_2O emissions under soil moisture favouring nitrification. At 45% WFPS, archaeal *amoA* abundance significantly increased the amount of N_2O emissions within both the dolomitic desert ($p < 0.001$) and the granitic desert ($p < 0.001$). Also, under $^{15}NH_4NO_3$ treatment, the amount of N_2O emissions significantly increased with archaeal *amoA* abundance within both the dolomitic desert ($p < 0.001$) and the granitic desert ($p < 0.001$). At 75% WFPS, the amount of total organic carbon significantly decreased the N_2O emissions within the dolomitic desert ($p < 0.001$) and had a similar pattern within the granitic desert ($p = 0.07$). However, when the microcosms were fertilized, the amount of total organic carbon significantly increased the emissions under $NH_4{}^{15}NO_3$ treatment within both the dolomitic desert ($p = 0.03$) and the granitic desert ($p < 0.001$).

4.5.2.3 Predicted values

Predicted values were consistent with the continuous process under soil moisture conditions favouring nitrification and with the Bernoulli process under soil moisture conditions favouring denitrification. At 45% WFPS treatment within the granitic desert, diapiric frost boils had a 51% higher mean predicted value than non-diapiric frost boils (Fig. 4.3A). Also, the pattern of predicted values reflected the results of the continuous process under $^{15}NH_4NO_3$ treatment, where the diapiric frost boils had a 35% higher mean predicted value than the non-diapiric frost boils (Fig. 4.3B). At 75% WFPS, the pattern reflected the Bernoulli process rather than the continuous process. Within the dolomitic desert, the mean predicted value of the diapiric frost boils was 49% higher than that of the non-diapiric frost boils (Fig. 4.3C). Similarly, within the granitic desert, the mean predicted value of diapiric frost boils was 18% higher than that of non-diapiric frost boils (Fig. 4.3C). Under $NH_4{}^{15}NO_3$ treatment within the dolomitic desert, diapiric frost boils had a 50% higher mean predicted value than non-diapiric frost boils, and within the granitic desert, diapiric frost boils had a 26% higher mean predicted value (Fig. 4.3D).

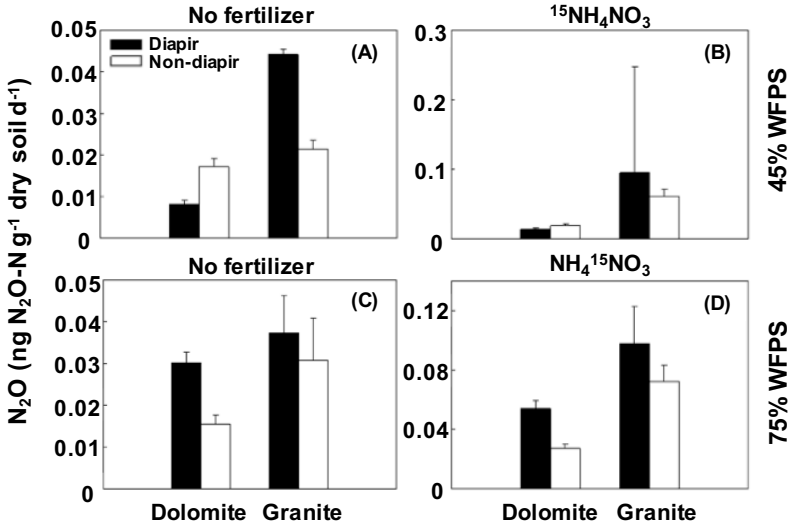

Fig. 4.3 Predicted values and standard errors of N_2O emission from diapiric and non-diapiric frost boils within each of the dolomitic (14 diapiric and 21 non-diapiric frost boils at 45% WFPS; 15 diapiric and 23 non-diapiric frost boils at 75% WFPS; 14 diapiric and 24 non-diapiric frost boils under $^{15}NH_4NO_3$ treatment; 15 diapiric and 24 non-diapiric frost boils under $NH_4{}^{15}NO_3$ treatment) and the granitic (16 diapiric and 21 non-diapiric frost boils at 45% WFPS; 16 diapiric and 23 non-diapiric frost boils at 75% WFPS; 16 diapiric and 21 non-diapiric frost boils under $^{15}NH_4NO_3$ treatment; 16 diapiric and 23 non-diapiric frost boils under $NH_4{}^{15}NO_3$ treatment) deserts. The predicted values and standard errors were obtained using the hurdle model incorporating GLMMs with the Bernoulli and gamma components.

4.5.3 ^{15}N SP of N_2O emitted from frost boils

SP of N_2O mainly changed with soil moisture levels rather than with the presence of diapirs in the frost boils. Within the dolomitic desert, SP increased by 43% in the 75% WFPS treatment compared to the 45% WFPS treatment ($p = 0.01$) (Fig. 4.4A). In contrast, within the granitic desert, SP decreased by 15% in the wetter 75% WFPS compared to the drier 45% WFPS ($p = 0.1$) (Fig. 4.4A). The pattern of SP values associated with soil moisture did not change with N addition, but they became more pronounced within the granitic desert (Fig. 4B).

The ranges of the SP values shifted as soil moisture altered from the condition favourable for nitrification to denitrification within each of the deserts. The SP values ranged from 10.6–21.2‰ at 45% WFPS within the dolomitic desert. The range increased at 75% WFPS and was from 10.8–34.6‰. Similarly, those ranged from 13.4–31.6‰ under $^{15}NH_4NO_3$ treatment and from 12.4–43.5‰ under $NH_4{}^{15}NO_3$ treatment. Within the granitic desert, on the other hand, the range of the SP values decreased at 75% WFPS. The SP values ranged from 13.5–34.0‰ at 45% WFPS and from 6.7–25.6‰ at 75% WFPS. Similarly, the range under $^{15}NH_4NO_3$ treatment was

from 12.0–83.0%, and that under $NH_4{}^{15}NO_3$ treatment was from 2.8–39‰. The $^{15}NH_4NO_3$ treatment had 10 large SP values ranging from 40.0–83.0‰. Except for this, the rest of the SP values ranged from 12.0–37.2‰ and had a similar range to that at 45% WFPS. Under $NH_4{}^{15}NO_3$ treatment, the range was from 2.8–39.0‰.

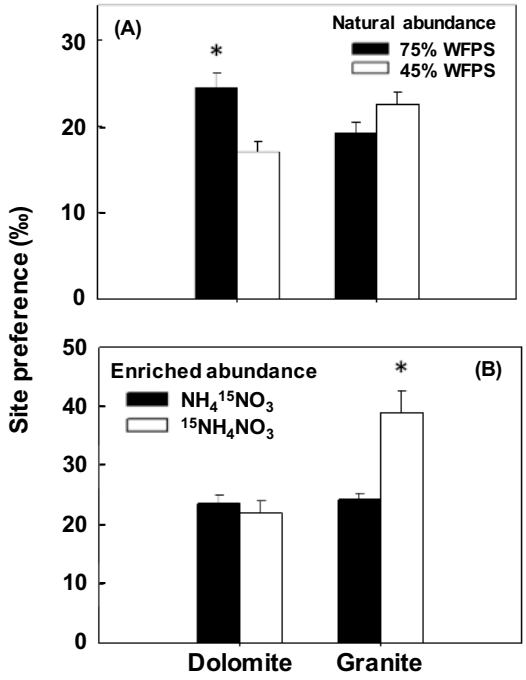

Fig. 4.4 Mean values of site preference (SP) with standard errors at 45% WFPS and 75% WFPS (A) and under $^{15}NH_4NO_3$ and $NH_4{}^{15}NO_3$ treatments (B) within the dolomitic (n = eight at 45% WFPS, and n = 14 at 75% WFPS; n = 10 under $^{15}NH_4NO_3$, and n = 22 under $NH_4{}^{15}NO_3$ treatments) and the granitic (n = 17 at 45% WFPS, and n = 15 at 75% WFPS; n = 23 under $^{15}NH_4NO_3$, and n = 30 under $NH_4{}^{15}NO_3$ treatments) deserts. * indicates $p < 0.05$ significance between the treatments.

4.6 Discussion

Under low soil moisture conditions favourable for nitrification, diapiric frost boils emit higher amounts of N_2O than non-diapiric frost boils. This increase is likely related to the increase in AOA and is consistent with the first hypothesis that AOA abundance would have a positive relationship with N_2O emissions under dry conditions. The geochemical features of diapiric frost boils may be favourable for AOA. AOA dominate in this study site (Brummell, 2015), and others have reported that AOA are an order of magnitude more prevalent than AOB (Alves et al., 2013) in frost boils from another Arctic region. The prevalence of AOA in diapirs is interconnected with the recalcitrant nature of Bhy horizons. In these horizons, N mineralization is slowed (Ota

et al., 2020), providing a low NH_3 environment favoured by AOA. For example, Koper et al. (2010) showed that NH_3 concentrations higher than 2 μM inhibited soil AOA growth. Consistent with the first hypothesis, all ranges of the SP values of N_2O under conditions favouring nitrification entirely agreed with those ranging from 13.1–34.0‰ through AOA ammonia oxidation from pure culture study (Hu et al., 2015).

The SP results suggest that fungal denitrification is the dominant source of N_2O in dolomitic High Arctic deserts under wet conditions. As noted in the introduction, absolute values of SP in soils can be difficult to ascribe to a specific process. However, as I altered conditions to favour denitrification processes, SP increased in dolomitic deserts (*i.e.,* 10.8–34.6‰ at 75% WFPS and 12.4–43.5‰ under $NH_4{}^{15}NO_3$ treatment). Typically, fungal denitrification SP values range from 23–40‰ (Hu et al., 2015), which is slightly higher than those through nitrification and through AOA ammonia oxidation (Hu et al., 2015; Well et al., 2008) and is higher than bacterial denitrification SP values ranging from 1–21‰ (Park et al., 2011; Well et al., 2006). In contrast, bacterial denitrification is likely the dominant source of N_2O in granitic deserts as SP values decreased (*i.e.,* 6.7–25.6‰ at 75% WFPS and 2.8–39‰ under $NH_4{}^{15}NO_3$ treatment) and are more comparable to the range through bacterial denitrification if I altered conditions to favour denitrification. The differences in denitrifier communities between deserts reflect the balance of several simultaneous mechanisms influencing fungal versus bacterial denitrification: (i) fungi can outcompete bacteria for available nitrate in Arctic soils and thereby limit bacterial denitrification (Siciliano et al., 2009), (ii) fungal denitrification activity is tightly linked to soil formate concentrations, a common root exudate (Ma et al., 2008), and (iii) bacteria can produce N_2O via nitrifier denitrification in Arctic ecosystems (Ma et al., 2007). I would caution that the statements do not imply that *only* fungal denitrification occurs in the dolomitic deserts; under laboratory conditions, fungal denitrification was the dominant but not sole process. Similarly, bacterial denitrification was not the *only* process in the granitic desert.

The estimated values of N_2O emissions in this study are substantially lower than some surface flux measurements in the field (Brummell et al., 2014, 2012). These lower estimated values might be related to plant-microbe interactions. For example, root exudates can stimulate denitrification (Stewart et al., 2014) or fungal N_2O emissions (Ma et al., 2008). The dominant shrub in the study site, *Salix arctica*, increases root biomass in Bhy horizons (Fig. 4.1C) (Muller et al., 2017). Therefore, diapiric frost boils might increase more N_2O emissions through plant-

microbe interactions than non-diapiric frost boils at the field level. However, as N_2O resides in the subsurface, it may be consumed. Brummell et al. 2015 showed that *nosZ*—coding nitrous oxide reductase—prevalence and N_2O production were not related to each other in the study site. Furthermore, the N_2O predicted values are lower than some flux measurements in previous studies (Brummell et al., 2014, 2012); therefore, the effect of N_2O consumption could be minor in the site. Nevertheless, with polar desert evolution under a warming climate, it could be more critical to link N_2O consumption to production processes to better estimate surface fluxes as N_2O consumption increases with increasing soil moisture (Stewart et al., 2012). Therefore, as permafrost thaw and meltwater production increase, N_2O consumption may be more involved in N_2O flux in polar deserts.

My study suggests that diapirism is a key edaphic factor for the output of N from polar desert ecosystems under a warming climate. Diapiric frost boils emit higher amounts of N_2O under low soil moisture conditions. Under high soil moisture conditions, diapiric frost boils emit N_2O more frequently but at a lower rate, than non-diapiric frost boils. As permafrost thaws, two connected events will increase the amount of labile C in the Bhy horizon: (i) increased meltwater will increase diapirism frequency in frost boils (Callaghan et al., 2005; Klaus et al., 2013; Walker et al., 2008), and (ii) these diapiric extrusions will contain the more labile soil organic C being released at the permafrost boundary (Gillespie et al., 2014). Coupled with an increase in surface N_2-fixation rates due to increased moisture and temperature (Stewart et al., 2014) and the plant-microbe interaction, there is a strong potential for diapiric frost boils to release more N_2O.

5. SPRING PULSE OF GREENHOUSE GASES: CONTRIBUTION OF FREEZE AND SUBSEQUENT THAW TO GREENHOUSE GAS EMISSIONS FROM HIGH ARCTIC POLAR DESERTS

5.1 Preface

I characterized CO_2 and N_2O emissions associated with diapirism. In this chapter, I incorporate the snowmelt season, when it can be logistically challenging to conduct fieldwork. I also characterize CH_4 emissions associated with diapirism and investigate how freeze-thaw alters the main GHG emissions to review the emissions associated with diapirism over the entire growing season. I discuss a potential effect of a freeze-thaw event on the main GHG emissions and implications of distinct GHG emissions pattern during the snowmelt season that may have been missed.

5.2 Abstract

Freeze-thaw cycles are an integral dynamic of biogeochemical processes in the High Arctic polar deserts that cover 26% of the Arctic. Over time, freeze-thaw cycles develop frost boils and in approximately 30% of frost boils, create diapiric intrusions within the soil profiles. Diapiric intrusions increase soil carbon and nitrogen into the upper soil horizons but slow organic matter cycling. In other ecosystems, freeze-thaw events often trigger a pulse of carbon dioxide, transient nitrous oxide, and methane emissions by stimulating soil microbes to decompose necromass or resistant soil organic matter. I hypothesized that freeze-thaw events would enhance greenhouse gas pulses more in frost boils with recalcitrant diapiric organic carbon than those without diapirs because of the priming by necromass. Soil samples from two High Arctic polar deserts near Alexandra Fjord (78°51′N, 75°54′W), Ellesmere Island, Nunavut, Canada were subjected to freeze-thaw treatments at different moisture contents. Freeze-thaw increased the magnitude of carbon dioxide emissions from frost boils by 1.3–3.5 times supporting the priming paradigm of organic matter cycling in Arctic soils. In contrast, freeze-thaw decreased the magnitude but increased the probability of nitrous oxide emissions, increasing the estimated nitrous oxide emissions by 119% (wet conditions) to 204% (dry conditions) within the dolomitic and by 72% (dry conditions) to 177% (wet conditions) within the granitic deserts. Freeze-thaw reduced methane consumption to a greater extent than methane production in diapiric frost boils, reducing the balance between net methane production and consumption. Freeze-thaw events likely led to carbon priming of the recalcitrant diapiric organic matter, and in so doing increased greenhouse gas emissions across the desert frost boils. As my study found, other polar deserts may have a distinct greenhouse gas emission pattern during the snowmelt season, and the knowledge gap may be large considering the area covered by polar deserts (1.4×10^6 km^2) in the Arctic. Despite logistically challenging area during the snowmelt season, my study suggests that field verification of the greenhouse gas emissions interacted with other rapidly changing environmental variables (*i.e.,* soil temperature, thaw depth, and plant activity) may need to assess the contribution of polar deserts to the emissions that are locally small but could be important in total during the potentially important time.

5.3 Introduction

Previous studies have demonstrated the importance of greenhouse gas (GHG) emissions associated with freeze-thaw events (Congreves et al., 2018; Mastepanov et al., 2013; Schimel & Clein, 1996) and provide an indication that I may need to extensively review GHG emissions from frost boils in the High Arctic polar deserts based on previous studies. Frost boils create key biogeochemical cycling related to GHG production and dominate many polar-desert landscapes. Frost boils are repeated and circular patches (often 1–3 meters in diameter) with sparse vegetation cover and commonly develop in polar deserts (Muc et al., 1989). The development of frost boils involves downward and upward movements of nutrients with leaching and frost heave, and thus frost boils create nutrient cycling that leads to GHG emissions in polar deserts (Walker et al., 2004). The bare circular patches increase soil temperature that enhances nutrient decomposition and GHG emissions, which may be accelerated by a rapidly warming climate (Kaiser et al., 2005; Wilson & Humphreys, 2010). In addition to this, approximately 30% of frost boils develop cryoturbic diapirs, subsurface nutrient patches (Muller et al., 2017; Swanson et al., 1999). Diapirs increase subsurface carbon (C) and nitrogen (N) abundance (Muller et al., 2017; Ota et al., 2020) but contain recalcitrant organic C (Ota et al., 2020). Brummell et al. (2015) and Ota et al. (2020) showed that diapirs lowered CO_2 production. Similarly, Ota & Siciliano (2020) showed that diapirs decreased the amount of N_2O emission under wet conditions favouring denitrification, which was linked to recalcitrant C present in diapirs. Thus, the previous research into the deserts seems to coherently explain the role of diapirs. However, freeze-thaw was neglected in the field due to logistical constraints.

High Arctic polar deserts likely have more severe freeze and thaw regimes compared to High Arctic tundra and Subarctic because of the lower vegetation cover and insulation in deserts (Grogan et al., 2004; Ping et al., 2015; Walker et al., 2004). Biogeochemical cycling during active layer thaw plays a primary role on seasonal patterns of GHG production in High Arctic polar deserts (Blaud et al., 2015; Mastepanov et al., 2013). Freezing and a subsequent thaw kill soil microbes and/or damages microbial cells and can decrease metabolic activity. However, these dead cells (necromass) release simple sugars and free amino acids into the surrounding soil, providing nutrients for the surviving microbes (Congreves et al., 2018; Mastepanov et al., 2013; Schimel & Clein, 1996). These processes often lead to a short-lived pulse of carbon dioxide (CO_2), transient nitrous oxide (N_2O) efflux, and methane (CH_4) emitted during the first half of the growing season (Congreves et al., 2018; Grogan et al., 2004; Mastepanov et al., 2013;

Schimel & Clein, 1996). Freeze-thaw cycles create dead microbial biomass that stimulates the remaining soil microbial community to decompose recalcitrant SOM (Wild et al., 2014) or dead microbial biomass (Schimel & Clein, 1996; Wild et al., 2014). Using this framework, I hypothesized that freeze-thaw events would enhance GHG pulses more in frost boils with diapirs—associated with recalcitrant SOM—when compared to frost boils without diapirs.

If this is the case, the previous work may have misinterpreted the effect of diapirism on GHG emissions, especially CO_2 as the snowmelt season has not been included due to the difficulty of accessing the remote study site. For example, Brummell et al. (2015) conducted measurements of soil GHG production in diapiric and non-diapiric frost boils at two polar deserts near Alexandra Fjord and found lower CO_2 production in diapiric-frost boils, but did so three weeks after the first day of snowmelt according to snowmelt data from Assmann et al. (2019). Ota et al. (2020) also showed that diapiric frost boils had lower CO_2 emissions than non-diapiric frost boils under laboratory conditions; however, the incubation system included a pre-incubation period and was designed to provide a similar condition to that in the field when the measurements occurred. As a result, the previous sampling may have missed GHG emissions during the event associated with the thaw (*i.e.,* snowmelt season). A previous study based on eddy covariance flux measurements found the highest ecosystem respiration immediately after snowmelt in a polar semidesert, leading to mostly positive net ecosystem exchange through snowmelt season in June (Emmerton et al., 2016). Similarly, Raz-Yaseef et al. (2017) showed that the pulse of CO_2 during spring thaw offset 46% of the total CO_2 uptake during the growing season at polygonal tundra sites in northern Alaska. Therefore, CO_2 emissions during the snowmelt season or the first half of the growing season likely contribute to a large portion of total CO_2 emissions; however, how diapirism would regulate the spring pulse of CO_2 is not clear. Freeze-thaw events are not only important for CO_2 production but also important for N_2O and CH_4 emissions as neglecting the pulses during spring thaw could underestimate the annual emissions (Butterbach-Bahl et al., 2013; Hargreaves et al., 2001; Raz-Yaseef et al., 2017; Wagner-Riddle et al., 2017). The objective of this study was to investigate the effect of freezing and a subsequent thaw on GHG emissions from the soil samples collected from diapiric and non-diapiric frost boils.

5.4 Materials and Methods

5.4.1 Study site and soil sampling

The study site was on a mountain plateau 5 km southwest of Alexandra Fjord (78º51′ N, 75º54′ W), Ellesmere Island, in the Canadian High Arctic. Field description and soil sampling methods are described in Ota et al., 2020. Briefly, the site included two distinct polar deserts (*i.e.,* dolomitic and granitic deserts). The dolomitic desert plant community is described as cryptogam, herb barren by the CAVM (Walker et al., 2002) whereas the granitic desert is described as noncarbonated mountain complexes (Walker et al., 2002). Soil sampling was conducted during July and August 2013. To cover the variation in frost-boil feature and vegetation characteristics, I adopted a randomized block design and divided the dolomitic (five blocks) and the granitic (12 blocks) deserts for soil sampling. I collected 1 kg of soil samples from subsurface horizons in diapiric frost boils where SOC abruptly increased and those in non-diapiric frost boils where the increase in SOC with depth was absent within the dolomitic (n = 40) and the granitic (n = 40) deserts.

5.4.2 Cumulative CO_2, N_2O, and CH_4

The incubation used the soil cores that were frozen after the previous incubation study (Ota & Siciliano, 2020). The soil core and the microcosm bottle are detailed in Ota & Siciliano (2020). Briefly, three soil cores were created from a soil sample by packing soil in polystyrene cores (2.8 × 1.4 cm internal diameter) with a bulk density of 1.3 g cm^{-3} (Brummell et al., 2014) and was pre-incubated for three weeks at 10ºC in the dark. Then, autoclaved distilled water was added to the core to adjust the soil moisture to 45% or 75% water-filled pore space (WFPS), with 45% WFPS considered to favour nitrification (Well et al., 2008) and 75% WFPS considered to favour denitrification (Gil et al., 2017). The microcosm bottle was a 100-mL glass bottle (VWR International, Radnor, Pennsylvania) with the cap equipped with a brass compression tube straight adapter for 1/4” OD tubing × 1/8” male pipe (McMaster-Carr Supply Company, Elmhurst, Illinois), sandwiching Thermogreen™ LB-2 septa (9.5 mm) (Sigma-Aldrich Co., St. Louis, Missouri) for gas sampling. After the incubation, the soil cores were immediately taken from the microcosm bottles and frozen at −20ºC for this incubation study for more than two months. Throughout the incubation, the water losses from the cores were minor. During freezing, the soil cores were sealed with Parafilm.

Three frozen cores of each sample were placed in the microcosm bottle. For CO_2 and N_2O assays, the 45% WFPS and the 75% WFPS cores were used whereas only the 75% WFPS

cores were used for CH_4 assays. The gas sampling for day zero was conducted immediately after the cap was closed. As described in Ota & Siciliano (2020), each gas sample was transferred into a pre-evaluated 12-mL Exetainer vial (Labco, Lampeter, Wales, UK) to quantify each of the GHGs at days 0, 9, and 14 using a standard 50-mL polypropylene syringe fitted with a 25-gauge needle. Between each of the sampling times, the microcosm bottles were incubated in the dark at 10ºC. Gas samples were analyzed as post-freeze treatment using a gas chromatograph (Scion 456-GC, Bruker Biosciences, Billerica, Massachusetts) equipped with a thermal conductivity detector for CO_2, ^{63}Ni electron capture detector for N_2O, and flame ionizer detector for CH_4. The GHG measurements ($\mu L\ L^{-1}$) were converted to the mass units for CO_2 ($\mu g\ CO_2$-C), N_2O (ng N_2O-N), and CH_4 (ng CH_4-C) using the Ideal Gas Law, and then normalized to dry soil mass (g). Each of the cumulative GHGs were represented as the slope of a line incorporating the series of normalized measurements against the three sampling time points. Slopes with poor linearity (*i.e.,* $R^2 < 0.85$) were removed from further analysis. Due to the low measurements of N_2O and CH_4, I used the 95% confidence intervals constructed by the slopes of the controls (*i.e.,* microcosm bottles without soil cores for the background concentrations) (n = four) for the thresholds (*i.e.,* detection limits) of N_2O production, CH_4 production, and CH_4 consumption, and the measurements below detection limits were truncated to zero for statistical analysis (Ota & Siciliano, 2020); the detail is stated in the method section for statistical analysis.

Each of the cumulative GHGs in the post-freeze treatment was compared with that in the pre-freeze treatment. For the pre-freeze treatment, I analyzed the CO_2 and the CH_4 measurements and used the N_2O results under the identical incubation condition from a previous study (Ota & Siciliano, 2020). The slopes of the controls, however, varied between the pre-freeze and post-freeze treatments due apparently to the instrumental variability, which in turn altered the detection limits between the treatments. The slope value of N_2O controls (*i.e.,* the background N_2O) in post-freeze treatment increased about twice as high as that in pre-freeze treatments, which led to a concern that the magnitudes of the cumulative N_2O expressed as slope values in post-freeze treatment may have also artificially increased. Therefore, I normalized the N_2O slope values (*i.e.,* cumulative N_2O) in post-freeze to those in pre-freeze by multiplying a fixed value obtained in Eq. 5.1 using the control slope values in pre-freeze and post-freeze treatments when comparing the slope values between these treatments.

$$Fixed\ value\ =\ Control_{pre}/Control_{post} \quad \text{(Eq. 5.1)}$$

where $Control_{pre}$ and $Control_{post}$ were the control slope value in pre-freeze treatment and the control slope value in post-freeze treatment, respectively.

5.4.3 Statistical analysis

All statistical analyses were performed using R version 3.3.3 (R Core Team, 2017), and effects were considered significant at $p < 0.05$. The effects of diapirism and the freeze-thaw treatment on the cumulative CO_2 were tested by linear mixed models using the nlme R package version 3.1-131 (Pinheiro et al., 2017). Outliers (n = six in the dolomitic desert and six in the granitic desert) were removed when they were greater than ±2.5 standard deviations or when they largely deviated from the majority of observations (Zuur et al., 2010). Linear mixed models included frost-boil type (diapiric versus non-diapiric) as a fixed effect and block nested within sampling time as a random effect for each of the pre-freeze data and the post-freeze data. I also created a dataset including both pre-freeze and post-freeze treatments and ran linear mixed models included frost-boil type and freeze-thaw treatment (pre-freeze versus post-freeze) as fixed effects and block nested within sampling time as a random effect. These linear mixed models incorporated the varIdent function to allow different variances per stratum (Zuur et al., 2009). Akaike information criterion and the likelihood ration testing approach were used to select the optimal varIdent variance structure (Zuur et al., 2009). The heterogeneity of variance of each of the selected models was checked by plotting residuals against fitted values.

To analyze the left-censored cumulative N_2O, a hurdle model was used following Ota & Siciliano (2020). Briefly, the hurdle model was comprised of generalized linear mixed models (GLMM) for the Bernoulli and gamma distributions using the lme4 package (Bates et al., 2015). The Bernoulli component modeled whether the slope values (*i.e.,* cumulative N_2O) were below the detection limit to be censored ("zero") or above the detection limit to be uncensored ("one"). The gamma component modeled the detected slope values above the detection limit (*i.e.,* the magnitude of cumulative N_2O). For the post-freeze data, the GLMMs for the Bernoulli and gamma distributions included the same fixed and random terms as the selected models for 45% WFPS and 75% WFPS (pre-freeze treatment) in the previous study (Ota & Siciliano, 2020) and were combined to estimate the predicted values. There were no significant effects of the covariates in either 45% or 75% WFPS in post-freeze-treatment; these p values are not reported.

A new dataset was created by combining the post-freeze data with the pre-freeze data from Ota & Siciliano (2020) and was analyzed using the hurdle model. The fixed terms of GLMMs for the Bernoulli and gamma distributions were the frost-boil type and the freeze-thaw treatment. Due to the low sample size, I selected random terms for each of the GLMMs (block or block nested by sampling time) based on data exploration. The effects of diapirism and freeze-thaw treatment on the magnitude of cumulative N_2O were assessed using least-squares means (LS means) (Lenth, 2016) from GLMM for gamma distribution.

Likewise, cumulative CH_4 was analyzed using GLMMs for the Bernoulli and gamma distributions. CH_4 slope values (*i.e.,* cumulative CH_4) were distributed below the lower limit of 95% confidential interval—indicative of net CH_4 consumption—as well as above the upper limit. However, each sample size of net CH_4 production ($7 \leq n \leq 13$) and consumption (zero $\leq n \leq$ four) was low, which made it impossible to separately perform the statistical analysis for net CH_4 production and consumption. As a reasonable trade-off between the sample sizes and the statistical analysis, these samples were grouped together. The instrumental variability also altered the slope value of CH_4 controls in post-freeze from that in pre-freeze, which may reflect altering the magnitudes of cumulative CH_4 in post-freeze. However, due to the small sample size and grouping the net production and consumption together, normalization of the magnitude—in the same way as N_2O analysis—made statistical analysis difficult. Thus, I solely compared the pattern of cumulative CH_4 from diapiric and non-diapiric frost boils between pre-freeze and post-freeze instead of testing the effect of freeze-thaw treatment. To achieve the gamma analysis, I used the minimal detectable difference—the smallest difference that can be statistically detected—for an imaginal detection limit. The minimal detectable difference was obtained using the power.t.test function in R by setting significance level and statistical power to 0.05 and 0.95, respectively under the condition of the particular sample size and standard deviation. A fixed value was set to bring the lowest CH_4 slope value (*i.e.,* the highest net CH_4 consumption) up to the value of the minimal detectable difference, and then added to each of the CH_4 slope values to create a left-censored data set to test the effect of diapirism. For data presentation, the fixed value was subtracted from the estimates obtained from the gamma model. There was also a limitation for the Bernoulli analysis as the Bernoulli estimate for censored data included both the production and the consumption probability that could not be distinguished from each other. As a result, the values below the detection limit could not be replaced with the estimates obtained by

combining the Bernoulli and gamma processes. Therefore, I analyzed the data (> detection limit) using the Bernoulli and gamma GLMMs separately and did not obtain predicted values using the hurdle model as I did for the N_2O emissions.

5.5 Results

5.5.1 CO_2 emissions

Freezing and a subsequent thaw altered the pattern of CO_2 emissions from diapiric and non-diapiric frost boils which were found in previous studies (Brummell et al., 2015; Ota et al., 2020). Before the freeze-thaw treatment, CO_2 emissions from the non-diapiric frost boils were slightly greater ($p < 0.001$) than those from the diapiric frost boils at both 45% and 75% WFPS within both of the dolomitic and the granitic deserts (Fig. 5.1); consistent with the results from previous studies (Brummell et al., 2015; Ota et al., 2020). After the freeze-thaw treatment, non-diapiric frost boils continued to have significantly higher emissions compared with diapiric frost boils at 75% WFPS within the dolomitic desert ($p < 0.001$) and at 45% WFPS within the granitic desert ($p < 0.001$) (Fig. 5.1 B, C). However, non-diapiric frost boils had moderately lower emissions than diapiric frost boils at 45% WFPS within the dolomitic desert ($p = 0.05$) and had significantly lower CO_2 emissions at 75% WFPS within the granitic desert ($p < 0.001$) (Fig. 5.1 A, D).

Freeze and a subsequent thaw also increased the amount of CO_2 emissions from both diapiric and non-diapiric frost boils. After the freeze-thaw treatment, CO_2 emissions increased by 1.3–3.5 times relative to those before the freeze-thaw treatment (Fig. 5.2). The increase in the emissions was greater for the non-diapiric frost boils than the diapiric frost boils ($p < 0.001$) at 75% WFPS within the dolomitic desert (Fig. 5.2 A). Conversely, the emissions from the diapiric frost boils increased more than those from non-diapiric frost boils at 45% WFPS within the dolomitic desert ($p < 0.001$) and at 75% WFPS within the granitic desert ($p = 0.0016$).

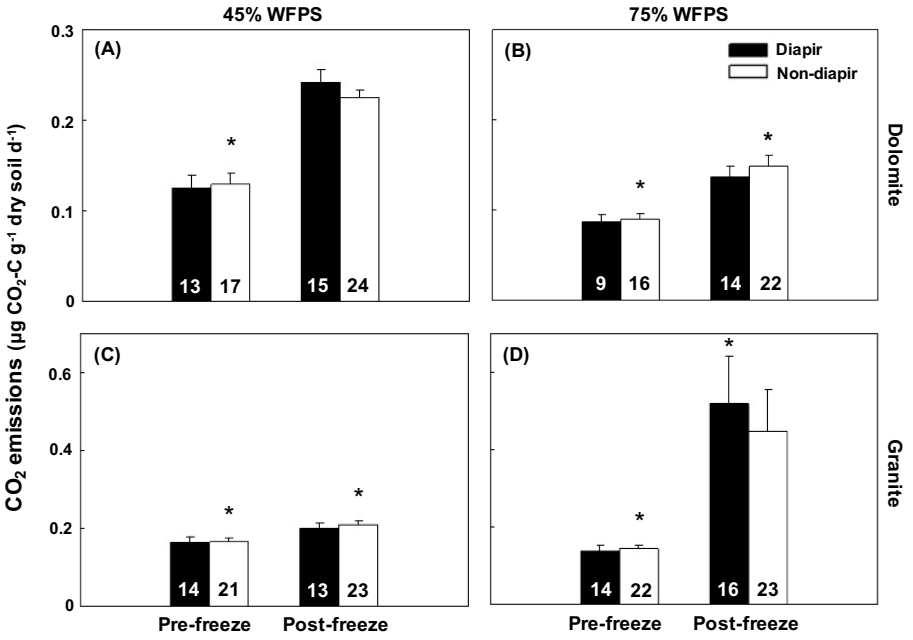

Fig. 5.1 Mean values for CO_2 emissions with standard errors from the (A, B) dolomitic and (C, D) granitic deserts at (A, C) 45% and (B, D) 75% WFPS. Numbers in each column indicate sample sizes. * indicates $p < 0.05$ significance. Note the scale difference in y-axes between (A, B) and (C, D).

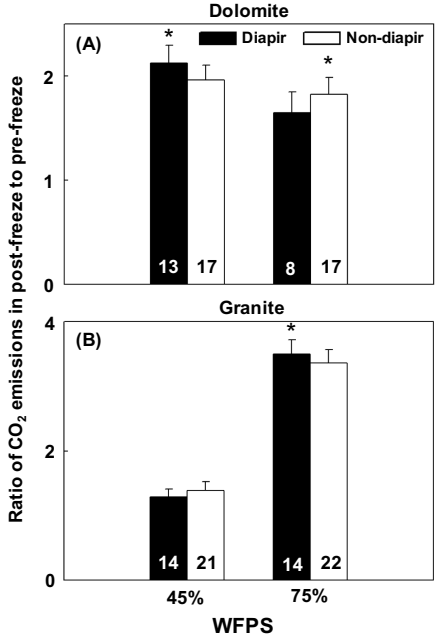

Fig. 5.2 Mean values with standard errors for the ratio of CO_2 emissions in post-freeze to pre-freeze from the dolomitic desert (A) and the granitic desert (B) at 45% WFPS and 75% WFPS. Numbers in each column indicate sample sizes. Note the change in y-axis scale between upper and lower panels. * indicates $p < 0.05$.

5.5.2 N_2O emissions

Overall, freeze and a subsequent thaw decreased LS means of N_2O emissions but increased the probability and predicted values of the emissions. As expected, there were a large number of values below the detection limit, with 18–40% of N_2O emissions below the detection limit under conditions favouring nitrification and 8–21% under conditions favouring denitrification. Within the dolomitic desert, the freeze-thaw treatment decreased the magnitude of the emissions under conditions favouring nitrification ($p = 0.006$) (Fig. A5.2 A). On the other hand, the freeze-thaw treatment increased emission probability ($p = 0.001$) and predicted values by 204% (Fig. A5.2 C, E). Under conditions favouring denitrification, the freeze-thaw treatment had little effect on the magnitude of the emissions ($p = 0.08$) but increased the probability of the emissions ($p < 0.001$) and predicted values by 119% (Fig. A5.2 B, D, F). The granitic desert was similar to the dolomitic desert with respect to N_2O emissions after the freeze-thaw treatment (Fig. A5.3). Under conditions favouring both nitrification and denitrification, the freeze-thaw treatment decreased the magnitude of the emissions ($p < 0.001$) but increased the probability of the emissions ($p < 0.001$) and predicted values (72% and 177% for nitrification and denitrification, respectively).

After the freeze-thaw treatment, LS means of N_2O emissions and the probability were comparable between diapiric and non-diapiric frost boils within the dolomitic desert. Before the freeze-thaw treatment, diapiric frost boils have lower magnitudes of the emission but higher probability compared with non-diapiric frost boils under conditions favouring denitrification (Fig. 5.3 C, G) (Ota & Siciliano, 2020). After the treatment, diapiric frost boils had similar magnitudes of the emission whereas the magnitudes from non-diapiric frost boils decreased and became similar rate to diapiric frost boils (Fig. 5.3 D). The probability of the emissions increased in diapiric frost boils by 66% and in non-diapiric frost boils by 186% after the treatment, and both of the frost boils had comparable probability (Fig. 5.3 G, H). Both diapiric and non-diapiric frost boils increased predicted values by 79% and 193%, respectively (Fig. 5.3 K, L). Under conditions favouring nitrification, both the magnitudes and the probability do not differ between diapiric and non-diapiric frost boils before the freeze-thaw treatment (Ota & Siciliano, 2020) and were also comparable between those frost boils after the treatment (Fig. 5.3 A, B, E, F). Within the granitic desert, LS means of N_2O emissions and the probability were also similar between diapiric and non-diapiric frost boils after the freeze-thaw treatment. Before the freeze-thaw

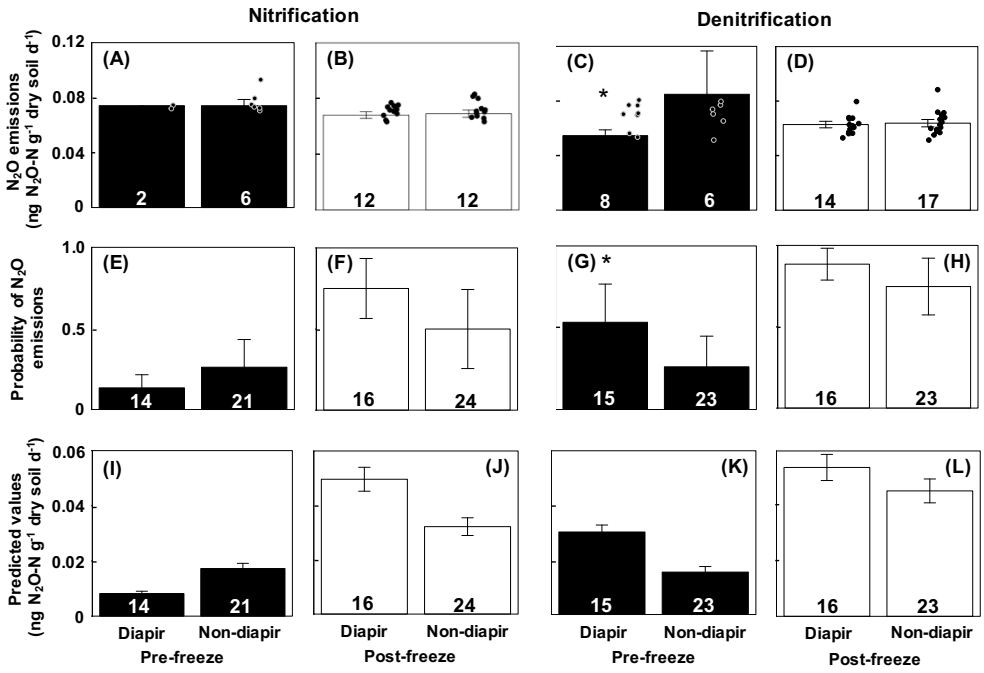

Fig. 5.3 Dolomitic desert N_2O emissions based on GLMM for gamma distribution from diapiric and non-diapiric frost boils. Emissions (A) pre-freeze and (B) post-freeze under condition favouring nitrification. (C) Pre-freeze and (D) post-freeze under conditions favouring denitrification. Jitter plots indicate raw data. Mean probabilities for N_2O emissions based on GLMMs with Bernoulli distributions from diapiric and non-diapiric frost boils during (E, G) pre-freeze and (F, H) post-freeze under (E, F) nitrification and (G, H) denitrification conditions. Predicted values of N_2O emissions from diapiric and non-diapiric frost boils during (I, K) pre-freeze and (J, L) post-freeze under (I, J) nitrification and (K, L) denitrification conditions. Predicted values and their standard errors (I–L) were obtained using the hurdle model incorporating GLMMs with the Bernoulli and gamma components. Numbers in each column indicate sample sizes. Error bars represent standard errors of the mean. * indicates $p < 0.05$ significance. Note: Panel A, C, E, G, I, K were adapted from Supplement 2a and c, and Supplement 1c and a, and Fig. 3a and c, respectively in Ota & Siciliano (2020).

treatment, diapiric frost boils had higher magnitudes of the emission than non-diapiric frost boils under conditions favouring nitrification (Fig. 5.4 A) (Ota & Siciliano, 2020). After the treatment, diapiric frost boils lowered the magnitudes by 53% whereas non-diapiric frost boils did so by 37%, which led to comparable magnitudes between those frost boils (Fig. 5.4 A, B). The probability of the emission was comparable between diapiric and non-diapiric frost boils after the treatment (Fig. 5.4 F). Under conditions favouring denitrification, diapiric frost boils have lower magnitudes of the emissions than non-diapiric frost boils before the freeze-thaw treatment (Fig. 5.4 C, D) (Ota & Siciliano, 2020). After the treatment, the magnitudes decreased by 66% in non-diapiric frost boils and were similar to those in diapiric frost boils (Fig. 5.4 C, D). The probability of the emissions was also comparable between those frost boils after the treatment (Fig. 5.4 H).

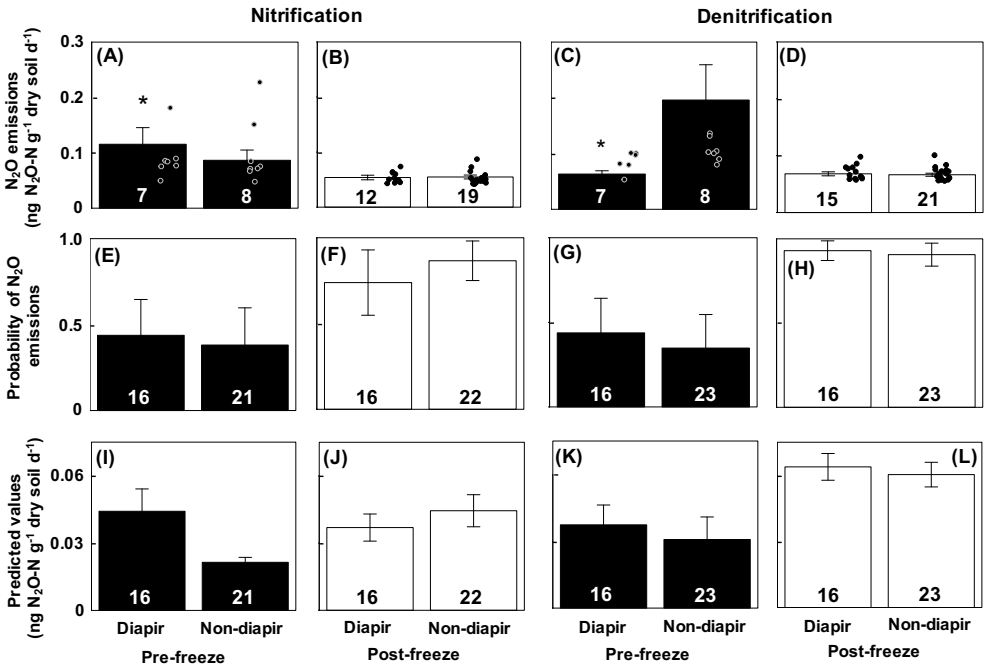

Fig. 5.4 Granitic desert N_2O emissions based on GLMM for gamma distribution from diapiric and non-diapiric frost boils. Emissions (A) pre-freeze and (B) post-freeze under condition favouring nitrification. (C) Pre-freeze and (D) post-freeze under conditions favouring denitrification. Jitter plots indicate raw data. Mean probabilities for N_2O emissions based on GLMMs with Bernoulli distributions from diapiric and non-diapiric frost boils during (E, G) pre-freeze and (F, H) post-freeze under (E, F) nitrification and (G, H) denitrification conditions. Predicted values of N_2O emissions from diapiric and non-diapiric frost boils during (I, K) pre-freeze and (J, L) post-freeze under (I, J) nitrification and (K, L) denitrification conditions. Predicted values and their standard errors (I–L) were obtained using the hurdle model incorporating GLMMs with the Bernoulli and gamma components. Numbers in each column indicate sample sizes. Error bars represent standard errors of the mean. * indicates $p < 0.05$ significance. Note: Panel A, C, E, G, I, K were adapted from Supplement 2b and d, and Supplement 1d and b, and Fig. 3a and c, respectively in Ota & Siciliano (2020).

5.5.3 CH_4 emissions

I treated CH_4 emission data as the balance of production and consumption. The data contained a substantial number of values below the detection limit and those removed due to poor linearity (*i.e.,* $R^2 < 0.85$). The percentage of net methane emissions below the detection limit ranged from 38–51%, and that of removed values ranged from 21–31% within the dolomitic desert. The percentages below the detection limit and the removed values ranged from 36–56% and from 10–26%, respectively within the granitic desert.

Overall, diapiric frost boils had lower net CH_4 emissions than non-diapiric frost boils and the pattern remained after freeze and a subsequent thaw within both of the dolomitic and the granitic deserts. The overall net CH_4 emissions from diapiric frost boils were negative whereas those from non-diapiric frost boils were positive within the dolomitic desert before the freeze-thaw treatment ($p = 0.08$) (Fig. 5.5 A). Diapiric frost boils had net CH_4 consumption higher than net CH_4 production whereas non-diapiric frost boils only had net CH_4 production (Fig. 5.5 C). After the freeze-thaw treatment, only net CH_4 production was observed for the diapiric frost boils and had overall net positive CH_4 emission, thus the difference in overall net emissions between diapiric and non-diapiric frost boils declined (Fig. 5.5 B, D). However, it should be noted that the sample size of diapiric frost boils after the treatment was one. The probability of net CH_4 production and consumption declined after the treatment in both diapiric and non-diapiric frost boils (Fig. 5.5 E, F). Similarly, within the granitic desert, diapiric frost boils had significantly lower overall net CH_4 emissions than non-diapiric frost boils before the freeze-thaw treatment ($p = 0.02$) and after the treatment ($p = 0.04$); however, the difference in the overall emissions between diapiric and non-diapiric frost boils declined after the treatment (Fig. 5.6 A, B). The diapiric frost boils had higher net CH_4 consumption than net CH_4 production before the treatment and had lower net CH_4 consumption after the treatment (Fig. 5.6 C, D). On the other hand, non-diapiric frost boils had no net CH_4 consumption before the treatment but increased the consumption after the treatment (Fig. 5.6 C, D). Diapiric frost boils lowered the probability of both net CH_4 production and consumption after the treatment whereas non-diapiric frost boils had similar probability of the net production and higher probability of the net consumption. However, it should be also noted that the sample sizes of diapiric and non-diapiric frost boils for net CH_4 consumption were one and two, respectively after the treatment.

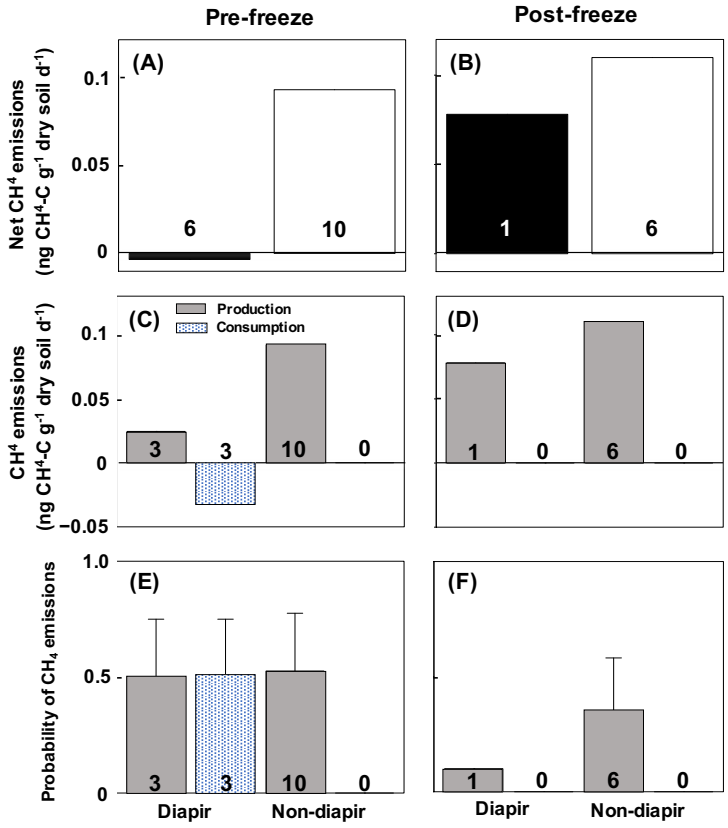

Fig. 5.5 Dolomitic desert net CH_4 emissions and standard errors (SEs) from diapiric and non-diapiric frost boils at 75% WFPS. Emissions (A) pre-freeze (SE = 9.2×10^{-10} for diapir and 9.8×10^{-9} for non-diapir) and (B) post-freeze (SE = 1.4×10^{-8} for non-diapir). Mean estimates of CH_4 production and consumption and SEs based on GLMM with gamma distribution from diapiric and non-diapiric frost boils during (C) pre-freeze (SE = 6.2×10^{-10} for production, 1.2×10^{-9} for consumption in diapir, and 9.8×10^{-9} for production in non-diapir) and (D) post-freeze (SE = 1.4×10^{-8} for production in non-diapir). Mean values and SEs of probability of CH_4 production and consumption based on GLMM with Bernoulli distribution from diapiric and non-diapiric frost boils during (E) pre-freeze and (F) post-freeze. Numbers indicate the sample size of each group.

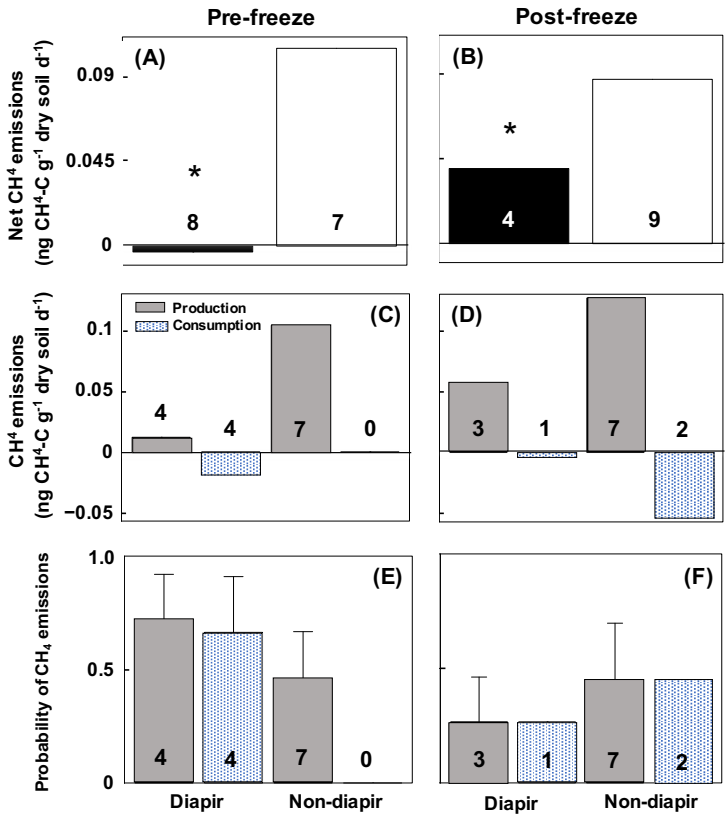

Fig. 5.6 Granitic desert net CH_4 emissions and standard errors (SEs) from diapiric and non-diapiric frost boils at 75% WFPS. Emissions (A) pre-freeze (SE = 2.5×10^{-10} for diapir and 1.1×10^{-8} for non-diapir) and (B) post-freeze (SE = 2.6×10^{-9} for diapir and 1.5×10^{-8} for non-diapir). Mean estimates of CH_4 production and consumption and SEs based on GLMM with gamma distribution from diapiric and non-diapiric frost boils during (C) pre-freeze (SE = 1.6×10^{-10} for production, 3.4×10^{-10} for consumption in diapir, and 1.1×10^{-8} for production in non-diapir) and (D) post-freeze (SE = 3.4×10^{-9} for production in diapir and 1.8×10^{-8} for production in non-diapir). Mean values and SEs of probability of CH_4 production and consumption based on GLMM Bernoulli distribution from diapiric and non-diapiric frost boils during (E) pre-freeze and (F) post-freeze. * indicates $p < 0.05$ significance. Numbers indicate the sample size of each group.

5.6 Discussion

As suspected, previous fieldwork in the mid-summer (Assmann et al., 2019; Brummell et al., 2015) and my laboratory work after pre-incubation (Ota & Siciliano, 2020), only addressed a part of the GHG cycling that occurs following the spring melt at the High Arctic deserts. Snowmelt and growing seasons likely interact with diapiric frost boils to create a GHG emission pattern distinct from that seen previously (Brummell et al., 2015; Ota & Siciliano, 2020). The freeze-thaw treatment increased CO_2 emissions, the probability and the estimated magnitude of potential N_2O emissions, and decreased the relative difference in overall CH_4 emissions between diapiric and non-diapiric frost boils. In the study site, the net production of each GHG has an inter-annually consistent pattern (Brummell et al., 2014). Thus, the emission patterns found in this study may more closely represent those during the snowmelt season whereas the emission patterns obtained after a three-week pre-incubation may represent those during the growing season (Fig. 5.7) (Ota & Siciliano, 2020).

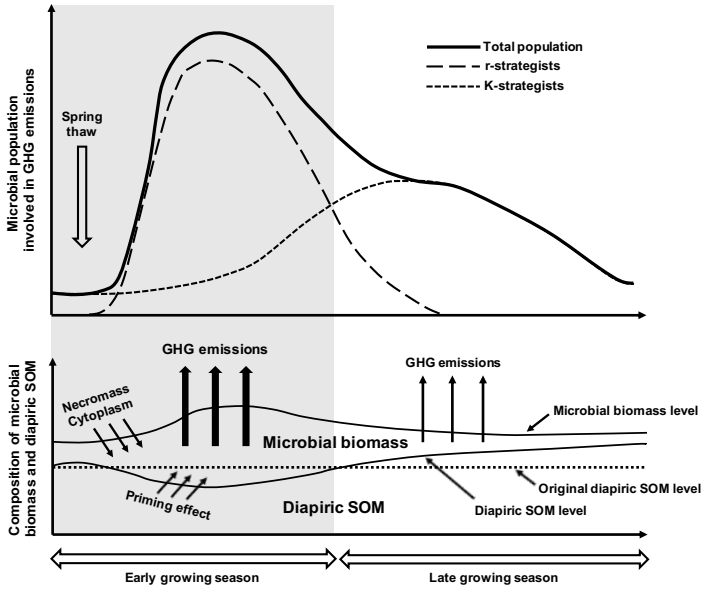

Fig. 5.7 Conceptual diagram of microbial population related to GHG emissions associated with diapirism. GHG emissions upon spring thaw may be due to priming or apparent priming by necromass and/or cytoplasm (Wild et al., 2014) that may awake the dormant state of fast-growing microbes (r-strategists). The priming may stimulate mineralizing diapiric SOM and contribute to GHG emissions during the early growing season. As the labile SOM pool (necromass and/or cytoplasm), slow-growing microbes (K-strategists) may become dominant and slowly decompose recalcitrant diapiric SOM during the later growing season. The length of spring GHG pulses remains to be elucidated. Note: Fig. 5.7 was adapted from Fig. 12.5 in Brady & Weil (2008).

Beyond the two High Arctic polar deserts in the study site, my study outlines some of the fundamental biogeomorphological processes that could reduce uncertainty in forecasting GHG emissions from permafrost C under projected warming (Schuur et al., 2015). The permafrost C pool contains a larger fraction of stable C whose decomposability associated with environmental conditions remains less clear compared with a smaller fraction of labile C that accounts for 5–15% of the total (Schuur et al., 2015). My results suggest that the freeze-thaw event is a key environmental factor that increases GHG emissions from a largely stable C pool. Therefore, ignoring the GHG emissions during the snowmelt season may underestimate the potential for emissions from the stable C pool in the permafrost. Furthermore, a freeze-thaw event may create a key temporal variation in GHG emissions in the Arctic regions near the CAVM bioclimate subzone C and D described by Walker et al. (2005) where the proportion of soil organic C that is less biodegradable cryoturbated C is greatest due to the highest rates of frost heave (Gillespie et al., 2014; Kaiser et al., 2007; Ping et al., 2015; Walker et al., 2008; Wild et al., 2013). Coupled with the C released as CO_2 and CH_4, the present study found that the freeze-thaw event also could increase N_2O emissions. These results indicate that freeze-thaw event is a key environmental parameter occurring at least once a year and that including this in predictive models will lead to a more robust estimation of annual GHG emissions and of the potential C and N feedbacks. To quantify the freeze-thaw processes, the predictive modeling may require ecological parameters such as soil moisture, soil compaction, vegetation since the parameters mainly influence soil insulation capacity, and thus link air temperatures to soil temperatures (Brady & Weil, 2008). In addition to this, microbial taxonomic composition links to the temperature sensitivity of SOM decomposition (Li et al., 2021). Since each landscape type has distinct ecological parameters and microbial taxonomic composition, further investigation would be necessary for the modelling, and my study suggests that how long the freeze-thaw-modified GHG emissions would last be addressed in future investigations.

5.6.1 CO_2 emissions

My results suggest that the freeze-thaw event is critical for the spring CO_2 emissions whose contribution to the CO_2 budget may be strongly related to geomorphological features in the High Arctic polar deserts. The increase in CO_2 emissions from both diapiric and non-diapiric frost boils may result from the soil microbial community being stimulated by the freeze-thaw treatment. Since only soil samples were incubated, the increase in emissions is likely due to

microbial cell lysis and cytoplasm release (Schimel & Clein, 1996). The larger increase in freeze-thaw CO_2 emissions from diapiric frost boils may indicate that the stimulated microbial community decomposed the less biodegradable diapiric organic C (*i.e.,* priming effect) (Ota et al., 2020; Wild et al., 2014). Alternatively, apparent priming where microbes that survive freeze/thaw may consume the released necromass and release CO_2 more than non-diapiric frost boils without decomposing diapiric organic C (Wild et al., 2014). The contribution of freeze-thaw CO_2 emissions to the CO_2 budget may be strongly related to geomorphological features in polar-desert landscapes. For example, Luërs et al. (2014) found CO_2 flux to be mainly positive in High Arctic semideserts during snowmelt season based on eddy covariance flux measurements. After the snowmelt, the ecosystem became a CO_2 sink, which was indicative of the CO_2 assimilation/respiration balance shifting towards assimilation (Luërs et al., 2014) and highlights the importance of vegetation on the spring CO_2 pulse. Further, Wilson & Humphreys (2010) found that both sedge fen areas and well-vegetated frost boils have net CO_2 sequestration whereas sparsely vegetated frost boils were a net source of CO_2. In the sparsely vegetated polar desert landscape, the spring pulse of CO_2 may dominate the annual CO_2 budget. The present study suggests that frost boil density and its vegetation cover should be incorporated into the CO_2 budgets of polar desert ecosystems.

5.6.2 N_2O emissions

During the snowmelt season, transient N_2O emissions may be critical under conditions favouring both nitrification and denitrification. These emissions may be small due to damage of the microbial cells (Schimel & Clein, 1996) though the probability of emissions associated with nutrient release from dead and/or damaged microbial cells increases (Congreves et al., 2018; Grogan et al., 2004; Schimel & Clein, 1996). Afterwards, diapirism may alter the magnitude and probability of the emissions. As the mid-summer approaches and the dead microbial biomass is consumed, the transient emissions may cease, resulting in a decreased probability of emissions. At the same time, under conditions favouring nitrification, archaeal ammonia oxidizer—the dominant ammonia oxidizer in the study site (Brummell et al., 2015)—may recover and increase the magnitude of the emissions according to the abundance in archaeal *amoA* gene that is higher in diapiric frost boils within the granitic desert (Ota & Siciliano, 2020). On the other hand, recalcitrant diapiric C may slow the recovery of heterotrophic denitrifiers, and thus an increase in the magnitude of the emissions may be pronounced only in non-diapiric frost boils during the

later growing season. Nevertheless, with higher C content, diapiric frost boils may maintain a higher probability but a slower rate of the emissions than non-diapiric frost boils during the later growing season as a previous study showed (Ota & Siciliano, 2020).

In response to the freeze-thaw event, N_2O emissions seem to vary between conditions favouring nitrification and those favouring denitrification across the dolomitic and the granitic deserts. I caution that I had to apply different detection limits for the analyses between the soil moisture conditions due to the instrumental variability. Thus, I did not directly compare the emissions but do a relative increase in the emissions from each of the frost boils between the soil moisture conditions. Diapiric frost boils increased the estimate of the emissions with the freeze-thaw event by 6× under dry conditions but only 2× under wet conditions within the dolomitic desert. On the other hand, non-diapiric frost boils increased the estimate by 2× under dry conditions but 3× under wet conditions. Within the granitic desert, diapiric frost boils slightly decreased the estimate with the freeze-thaw event under dry condition but increased it by twice under wet condition. Non-diapiric frost boils increased the estimate at a comparable rate between the dry and the wet conditions. The principles underlying the variability in the emissions between the conditions favouring nitrification and denitrification across the dolomitic and the granitic deserts remain unclear. If the hurdle models incorporate the gamma component modified by Haslauer et al. (2017) to account for multiple detection limits, that may allow to directly compare the emissions associated with the freeze-thaw event between the conditions favouring nitrification and denitrification. The approach may be key for finding covariates that explain the variability in the emissions; however, I was unable to use the hurdle models with the Haslauer-modified gamma component due to the limited sample sizes.

5.6.3 CH_4 emissions

Polar-desert freeze-thaw reduces the contribution of net CH_4 consumption to overall net CH_4 emissions from both diapiric and non-diapiric frost boils. After the freeze-thaw treatment, the differences in overall net CH_4 emissions between diapiric and non-diapiric frost boils became smaller within both dolomitic and granitic deserts. I caution that the number of observed methane fluxes was very low and that instrumental variability made it difficult to compare the magnitudes of the net CH_4 production and consumption between pre-freeze and post-freeze treatments. Thus, I do not directly compare the magnitudes between the treatments. Nevertheless, as Schimel & Clein (1996) proposed—the microbial community recovers from damage caused

by the freeze-thaw event and return the ability of nutrient processes—diapiric frost boils might increase the relative contribution of net CH_4 consumption or methanotrophic process and might turn to net CH_4 sink after the freeze-thaw event. Net CH_4 production may remain lower in diapiric frost boils than in non-diapiric frost boils during the entire growing season within both deserts. Indeed, diapiric frost boils contain recalcitrant organic C (Ota et al., 2020) that due to slow decomposition may limit the substrates available for methanogens. Alternatively, diapirs increase deep (20–30 cm) root biomass (Muller et al., 2017), which might act as ventilation pathways for CH_4 and reduce the amount of CH_4 oxidized to CO_2 (Schuur et al., 2015; Wilson & Humphreys, 2010). Therefore, considering plant-mediated CH_4 emissions, the difference in overall CH_4 emissions between diapiric and non-diapiric frost boils might be less pronounced at the ecosystem level.

6. SUMMARY AND CONCLUSIONS

6.1 Dissertation Overview

The High Arctic polar deserts are subject to rapidly warming climate due to higher rates of warming and permafrost thaw in high-latitude regions (Allan et al., 2014; Schuur et al., 2015) and have a strong potential of positive feedback loops with higher SOC stock than previously estimated (Burnham & Sletten, 2010; Hugelius et al., 2014). Frost-boil development and diapirism are expected to increase with warming climate (Callaghan et al., 2005; Klaus et al., 2013; Walker et al., 2008); thus my study investigated how diapirs within frost-boil profiles would alter key soil properties and the main GHG emissions. My study employed the hurdle model approach to cope with N_2O and CH_4 emissions data that contained an excessive number of zeros and were hard to apply linear regression modelling for. Furthermore, my study considered the main GHG emissions during earlier growing or snowmelt season for understanding the contribution of diapirism to the emissions during the entire growing season. In the following sections, I discuss the overall findings of my study and synthesize the findings from previous studies conducted at the research site (Brummell et al., 2015; Muller et al., 2017) for future research consideration.

The key takeaways from my research are first that biological activity may be contributing to the creation of frost boil diapirs through the production of polysaccharides which increase the viscosity of the active layer. The creation and mining of diapiric intrusions into the active layer creates habitat segregation for the coexistence of different plant species under extremely limited N conditions. Thus, GHG emissions from diapiric frost boils may strongly link to a plant-microbe relationship. Secondly, as my research found that diapirism is an important factor of N_2O production, the hurdle model approach may contribute to the estimate of N_2O emissions that can be near the detection limit in a research site but can be important in the entire Arctic region. These strong geomorphological and ecological feedback loops are maintained during freeze-thaw

events which also drive GHG emissions. Overall, this dissertation outlined the unique nexus that occurs in polar deserts among plants, microbes, and geomorphology.

6.2 Summary of Findings

My study found that diapirism alters the main GHG emissions from frost boils but that the emission rates may not be constant during the growing season. With the pre-incubation period, my study showed that diapirism slows CO_2 emissions from frost boils, which was linked to lower N mineralization and higher abundance of recalcitrant OC. The results were consistent with field measurements at the study site which was conducted three weeks after the first day of snowmelt (Assmann et al., 2019; Brummell et al., 2015; Ota et al., 2020). Likewise, my study showed that diapiric frost boils slow CH_4 emissions within the granitic desert although the limited sample size reduces the confidence in these conclusions. Lower N mineralization may lead to a higher abundance in archaeal ammonia oxidizers (Koper et al., 2010). As a result, diapiric frost boils may increase the magnitude of N_2O emissions and the estimation of emissions under conditions favouring nitrification within the granitic desert (Ota & Siciliano, 2020). Under conditions favouring denitrification, the recalcitrant diapiric C may slow heterotrophic denitrification and slow the magnitude of the emissions (Ota & Siciliano, 2020). At the same time, the increase in OC—an electron donor for denitrification process—with diapirism may increase the probability of the emissions, leading to an increase in the estimated emissions (Ota & Siciliano, 2020). In the field measurements, N_2O emissions did not differ between diapiric and non-diapiric frost boils (Brummell et al., 2015). The contrasting results suggest that heterotrophic soil moisture conditions may have masked the effect of diapirism on N_2O emissions in the field measurements. Furthermore, if the field measurements incorporate the idea of the probability of N_2O being detected, the results might change. However, my study also found that the emission rates differed after freeze-thaw treatment; the implications will be discussed next paragraph. Therefore, the emission characteristics of the main GHGs found in those studies (Brummell et al., 2015; Ota et al., 2020; Ota & Siciliano, 2020) may not represent the entire growing season but only the later growing season.

The freeze-thaw event may alter the nutrient pools in both diapiric and non-diapiric frost boils as Grogan et al. (2004) demonstrated that below-ground nutrient pools alter after the specific freeze-thaw regimes. Indeed, microbial communities are robust to mild freeze-thaw regimes with minimum soil temperature being −8°C (Grogan et al., 2004), which is typical in

sub-arctic heath tundra. However, the study site is located in the High Arctic polar desert and is likely to have more severe freeze-thaw cycling, which could increase the alternation in below-ground C and N cycling by microbial cell lysis and cytoplasm. The increase in necromass may stimulate r-strategists and lead to priming effect during the snowmelt season. As Wild et al. (2014) demonstrated the priming of SOM decomposition in cryoturbic horizons after adding labile organic N, necromass with a low C:N ratio (Kallenbach et al., 2015) might lead to even higher in diapiric horizons. Additional N from necromass might be used for extracellular enzymes required for decomposing diapiric C as Wild et al. (2014) suggested. Alternatively, apparent priming where microbes that survive freeze/thaw may consume the necromass and release CO_2 without decomposing diapiric organic C (Wild et al., 2014). As necromass can account for a significant fraction of SOM (Kallenbach et al., 2015), there may be key nutrient dynamics involved in the main GHG emissions during the early growing season in the Arctic regions with severe freeze-thaw regimes.

Interestingly, in the study site, diapiric frost boils increased freeze-thaw CO_2 emissions more than non-diapiric frost boils only under drier conditions within the dolomitic desert whereas diapiric frost boils had increased emissions only under wetter conditions within the granitic desert. The contrasting results might indicate the specific limitation of C decomposition (Kaiser et al., 2005) in the two types of polar desert. Namely, the released nutrients (necromass and cytoplasm) might be the limiting factor for the decomposition process under drier conditions within the dolomitic desert whereas they might be a limiting factor under wetter conditions within the granitic desert.

Likewise, the freeze-thaw treatment may change the relationship between the nutrient pools and N_2O emissions as the covariates of each of the selected models in Ota & Siciliano (2020) were no longer related to either the magnitude or the probability of the N_2O emissions. Though my study does not elucidate nutrient pool dynamics associated with the freeze-thaw treatment, my study suggests that the increase in the probability of N_2O emissions is key for rising N_2O emissions from the High Arctic polar desert. Furthermore, considering that both the magnitude and the probability of N_2O emissions were comparable after the freeze-thaw event, as an ecological role, diapirism might also alter trends in the magnitude and the probability of the emissions over time during the growing season. As the necromass and cytoplasm released by freeze-thaw event decline, the microbial taxa might shift to K-strategists, which might lead to

CO_2 and N_2O emissions patterns found in previous studies (Ota et al., 2020; Ota & Siciliano, 2020).

My study found the distinct pattern of each of the main GHG emissions after the freeze-thaw treatment. Grogan et al. (2004) indicated that different types of freeze-thaw regimes led to different nutrient pool dynamics immediately after the final thaw. Microbial communities store a substantial portion of total ecosystem nutrients in a frost-boil tundra ecosystem in Siberia, and even slight fluctuations in the microbial population can release a substantial amount of the nutrients (Kaiser et al., 2005). Therefore, as the climate warms winter temperatures and alters the freeze-thaw regime in polar deserts, the GHG emission patterns may also alter at the beginning of the growing season, and subsequently those patterns in the later growing season. It is critical to identify potential changes in the freeze-thaw regime and to assess the GHG emissions associated with the changes during the growing season in the High Arctic polar deserts. Coupled with the variation in nutrient pool dynamics, my study suggests that a particular freeze-thaw regime affects nutrient cycling in relation to diapirism and frost-boil development; thus is strongly tied to the main GHG emissions from the High Arctic polar deserts and potential polar-desert feedbacks to the current warming climate.

My study found a possibility of a plant-microbe relationship in diapiric horizons in the High Arctic polar deserts. A previous study found that *Salix arctica*, the dominant vascular plant in the study site, increased root biomass and N uptake within diapirs (Muller et al., 2017). Since N availability is critical for plant community development in polar deserts (Gold & Bliss, 1995), the increase in N uptake indicates that diapirs play an important role in sustaining the plant community in the study site. However, my study suggests that diapiric N is taken up as a result of investments of plants that stimulate microbial mining of N from diapirs, which decrease C and N mineralization and have a recalcitrant OC compound (Ota et al., 2020). It has been known that root exudates released by plants enhance the decomposition of organic matter (Meier et al., 2017; Wild et al., 2016). A common mechanistic explanation is that the N in root exudates is used for the synthesis of extracellular enzymes for breaking down recalcitrant SOM and that the C is used as an energy source for the microbes to facilitate the decomposition of the energy-poor SOM (Meier et al., 2017; Wild et al., 2016). Thus, *Salix arctica* might also provide microbes with additional C and N to increase microbial mining of N from diapirs. Also, *Salix arctica* is known to establish a mutually beneficial association with ectomycorrhiza in the High Arctic tundra near

Alexandra Fjord (Kohn & Stasovski, 1990). In addition to *Salix arctica*, *Dryas integrifolia* and *Cassiope tetragona*, which grow in the polar-desert site, are also found to be colonized by ectomycorrhiza in the High Arctic tundra (Kohn & Stasovski, 1990; Muller et al., 2017). To maintain the association, plants allocate approximately 5–30% of the total photosynthate production to provide ectomycorrhiza with C compounds (Brady & Weil, 2008). With 24-hour daylight in the study site during the growing season, the energy cost might not as high as other terrestrial regions where midnight sun does not occur. Muller et al. (2017) found *Salix arctica* dominated *Dryas integrifolia* and *Cassiope tetragona* in the polar-desert site, which might reflect that *Salix arctica* can establish the mutualistic relationship better than the others. As those vascular plants target diapirs for N, competition for N in the surface ground might decrease. In polar deserts, plants typically have shallow root systems (Muller et al., 2017), and thus might not have to compete for N derived from biological soil crusts with *Salix arctica*, *Dryas integrifolia*, and *Cassiope tetragona*. Therefore, diapirism might be critical in terms of creating habitat segregation for the coexistence of different plant species under extremely limited N conditions.

My study suggests that biological factors are involved in diapirism. A previous study explains that diapiric movement is initiated by unstable bulk density profiles containing low-density ice-rich layer and high-density overlying layer and showed that higher viscosity of the overlying layer facilitates diapiric movement (Swanson et al., 1999). However, what would cause the viscosity has not been explained. My study indicated that diapiric frost boils increase polysaccharides (Ota et al., 2020), which are known to enhance soil aggregation and increase soil viscosity (Calderón et al., 2011; Hayes, 2009). The presence of polysaccharides reflects biological activities. Microbes produce polysaccharides as they decompose plant residues (Brady & Weil, 2008) and protect their cells from environmental stress (Arco et al., 2005). Also, microbes contain polysaccharides in their cell walls (Rodrigues et al., 2011). Furthermore, polysaccharides account for a large portion of root exudates to enhance root colonization (Akhtar et al., 2018; Bais et al., 2006). Therefore, soil microbes and/or plants may contribute to diapirism. It is still not clear whether diapirs occur first, and then plants and microbes facilitate further diapiric flow or plants and/or microbes initiate diapirism. After soil materials in the ice-rich horizon start intruding into the overlying soil layer, plants might forage for diapiric nutrients, and then polysaccharides derived from root exudates and/or microbial processes facilitate further diapiric flow. Alternatively, plants might forage for nutrients from temporal

nutrient patches that somehow already exist and increase the viscosity of the overlying layer with the accumulation of polysaccharides, and then trigger the upward movement of the underlying low-density materials. A developing stage of diapirism might be evidence to answer the question. In the former case, diapirs might not have plant roots in the stage whereas diapirs might already have plant roots in the latter case. As the viscosity of the overlying layer is higher than the underlying ice-rich horizon, diapiric flow more easily occurs (Swanson et al., 1999); thus the latter case might be a more possible condition.

6.3 Future Research Directions

Diapirism is likely critical for a feedback loop of GHG emissions in the Arctic regions under a rapidly warming climate. My study characterized the main GHG emissions associated with diapirism; however, it is still not clear how much diapirs emit the GHGs over the entire growing season and in the presence of plants. Diapirism is a consequence of deeper permafrost thaw (Ping et al., 2015; Swanson et al., 1999). On a decadal scale, the ice-rich horizon of the uppermost permafrost thaws due to extreme climate, which results in larger diapiric movement (*i.e.,* several decimeters) (Ping et al., 2015; Swanson et al., 1999). In addition to this, diapirism has been found to occur after deeper permafrost thaw due to forest fire in Alaska (Swanson et al., 1999). Warming climate thickens the active layer and increases the frequency of forest fires, and thus increases the magnitude of diapir formation (Allan et al., 2014; Ping et al., 2015; Swanson et al., 1999). Considering that diapirs are high in soil C and N (Muller et al., 2017), diapirism can be regarded as redistribution of C and N and can alter C and N cycling within the active layer as a response to the warming climate. My study found that diapirism slows CO_2 emissions (Ota et al., 2020), which is consistent with the field measurements in the study site (Brummell et al., 2015). For N_2O emissions, my study found that higher estimated N_2O emissions from diapiric frost boils reflected higher magnitudes of the emissions under conditions favouring nitrification whereas higher estimated N_2O emissions from diapiric frost boils reflected higher probability of the emissions under conditions favouring denitrification (Ota & Siciliano, 2020). However, Chapter 5 suggests that the CO_2 and N_2O emission patterns in diapiric and non-diapiric frost boils characterized by those studies (Brummell et al., 2015; Ota et al., 2020; Ota & Siciliano, 2020) solely represent the later growing season. My Chapter 5 suggests that diapiric frost boils could emit more CO_2 than non-diapiric frost boils and increase the estimated N_2O emissions during the snowmelt season due to freeze-thaw events. In addition to this, Chapter 5 suggests

that the change in net CH_4 consumption may be key for overall net CH_4 emissions from diapiric and non-diapiric frost boils during the entire growing season; the analysis of CH_4 emissions will be discussed further below. My entire study suggests that the amounts of CO_2, N_2O, and CH_4 emissions from diapiric frost boils are not constant during the growing season. However, the fate of each of the main GHG emissions is not clear over the growing season. Also, as diapirs increase root biomass (Muller et al., 2017), the GHG emissions from diapiric frost boils might be more subject to root exudates and root ventilation pathways compared with non-diapiric frost boils. As the permafrost thaw increases in the Arctic region, diapirism might play a critical role in incorporating previously stored labile SOM into geochemical cycling within the active layer. Under favourable conditions, a large diapir could form within a single growing season (Swanson et al., 1999). Therefore, diapirism should be monitored to assess feedbacks with GHG production in the Arctic, and future research should include snowmelt season and plant-microbe relationship for a more robust evaluation of diapirism-GHG production.

Diapiric horizons may harbour key principles for a plant-microbe relationship which are useful for agricultural management. My study suggests that increased N uptake by *Salix arctica* shown by Muller et al. (2017) may be due to a mutually beneficial association with certain microbes. It has been known that in both native and agricultural lands, some plants increase N uptake by providing some photosynthate to certain microbes and stimulating their N mining from recalcitrant SOM that is not ready for plant uptake (Bais et al., 2006; Brady & Weil, 2008; Kohn & Stasovski, 1990; Wild et al., 2017). However, confounding interactions among plants, microbes, and the surrounding environment below-ground prevent researchers from unveiling the whole picture of the mutualistic symbiosis (Bais et al., 2006; Craine et al., 2007; Wild et al., 2017). For example, increases in soil N availability suppress microbial N mining (Craine et al., 2007). The suppression might be reasonable since microbes do not need to synthesize extracellular enzymes that break down recalcitrant SOM, and thus no longer need to rely on root exudates from plants. At the same time, plants no longer have the photosynthate cost to uptake N. Furthermore, Wild et al. (2017) found labile C addition as a root exudate increased not N mining but efficient use of already available N, which might reflect that threshold for N mining exists. Indeed, mutualistic symbiosis is one of the survival strategies that plants and microbes have developed and would not occur once they find another way that allows them to acquire nutrients with less energy cost. However, in the High Arctic polar deserts, plants and microbes

may have much fewer options for nutrient acquisition and result in establishing a mutualistic relationship to survive. Thus, it would be worthwhile to investigate the plant-microbe relationship in diapiric horizons. Similarly, cryoturbic horizons in other Arctic regions also contain recalcitrant SOM (Gillespie et al., 2014; Kaiser et al., 2007; Wild et al., 2013); however, it has not been investigated yet if any plants forage and increase nutrient uptake from the horizons. If a mutualistic relationship exists in cryoturbic horizons, the investigation of the relationship would contribute to the identification of specific microbes, chemical structures of root exudates to attract the microbes, and desired environmental conditions that initiate the plant-microbe association. The knowledge could be applied for agricultural management to maximize the benefit from the mutualistic symbiosis and to minimize necessary amounts of fertilizer application and environmental stress.

The hurdle model provided insight into N_2O and CH_4 emissions from polar-desert environments that are near the instrumental detection limit. Thus, my study suggests that future studies consider applying and further develop the hurdle model to cope with zero-inflated continuous data in different fields. To my knowledge, this is the first study that adopted the hurdle model to assess the effects of diapirism and freeze-thaw events on N_2O and CH_4 emissions in polar deserts. Using the hurdle-model approach, the N_2O data suggests that the probability of detecting N_2O emissions is critical for interpreting the effect of the diapirism and the freeze-thaw event on the emissions. Therefore, my study suggests that the number of zeros reflects the probability of crossing the detection limit or hurdle and is ecologically meaningful and that the zeros should not be omitted from the environmental data as the omission could reduce the whole picture of the ecological principle that research is trying to reveal. Despite the advantage of the hurdle model, my study faced with the difficulty of CH_4 analysis since CH_4 emissions are the balance between CH_4 production and consumption, which is not exceptional in the study site (Brummell, 2015; Brummell et al., 2014; Conrad, 2009). A larger sample size may improve the CH_4 analysis using the hurdle model as a larger sample size could allow to separately obtain the estimates of net CH_4 production and net consumption in order to calculate the estimate of net CH_4 emissions as the total of the estimates of production and consumption. Besides the N_2O and CH_4 analyses, the gross N transformation rates in my study could be revisited using the hurdle model. Each of the gross N transformation rates had a substantial number of zeros, which partially contributed to the heterogeneity of variance; the varIdent

function was incorporated into a linear mixed model to deal with the issue (Ota et al., 2020; Zuur et al., 2009). Alternatively, by assuming the negative values within the range of three standard deviations from the mean as the negligible rates or rates that did not cross the hurdle (Ota et al., 2020; Piper et al., 2015; Zuur & Ieno, 2016), each of the gross N transformation rates could be analyzed in a way that assesses the probability of being detected and the rate once it is detected. When I applied the hurdle model for N_2O and CH_4 data, there was no package available to fit the model. As a result, I had to separately fit a Bernoulli and a gamma models to the data. Thus, the development of the R package for the zero-altered gamma model would facilitate the expansion of the hurdle model and assist the analysis of continuous data with a large number of zeros, which commonly occur in environmental studies.

7. REFERENCES

Akhtar, J., Galloway, A. F., Nikolopoulos, G., Field, K. J., & Knox, P. (2018). A quantitative method for the high throughput screening for the soil adhesion properties of plant and microbial polysaccharides and exudates. *Plant and Soil*, *428*, 57–65.

Allan, J., Ronholm, J., Mykytczuk, N. C. S., Greer, C. W., Onstott, T. C., & Whyte, L. G. (2014). Methanogen community composition and rates of methane consumption in Canadian High Arctic permafrost soils. *Environmental Microbiology Reports*, *6*(2), 136–144. https://doi.org/10.1111/1758-2229.12139

Altshuler, I., Ronholm, J., Layton, A., Onstott, T. C., Greer, C. W., & Whyte, L. G. (2019). Denitrifiers , nitrogen-fixing bacteria and N 2 O soil gas flux in high Arctic ice-wedge polygon cryosols. *FEMS Microbiology Ecology*, *95*(5), 1–12.

Alves, R. J. E., Wanek, W., Zappe, A., Richter, A., Svenning, M. M., Schleper, C., & Urich, T. (2013). Nitrification rates in Arctic soils are associated with functionally distinct populations of ammonia-oxidizing archaea. *The ISME Journal*, *7*(8), 1620–1631.

Arco, Y., Llamas, I., Martínez-Checa, F., Argandoña, M., Quesada, E., & del Moral, A. (2005). epsABCJ genes are involved in the biosynthesis of the exopolysaccharide mauran produced by Halomonas maura. *Microbiology*, *151*(9), 2841–2851. https://doi.org/10.1099/mic.0.27981-0

Arft, A. M., Walker, M. D., Gurevitch, J., Alatalo, J. M., Bret-Harte, M. S., Dale, M., Diemer, M., Gugerli, F., Henry, G. H. R., Jones, M. H., Hollister, R. D., Jónsdóttir, I. S., Laine, K., Lévesque, E., Marion, G. M., Molau, U., Mølgaard, P., Nordenhäll, U., Raszhivin, V., … Wookey, P. A. (1999). Responses of tundra plants to experimental warming: meta-analysis of the international tundra experiment. *Ecological Monographs*, *69*(4), 491–511. https://esajournals.onlinelibrary.wiley.com/doi/abs/10.1890/0012-9615%281999%29069%5B0491%3AROTPTE%5D2.0.CO%3B2

Assmann, J. J., Myers-Smith, I. H., Phillimore, A. B., Bjorkman, A. D., Ennos, R. E., Prevéy, J. S., Henry, G. H. R., Schmidt, N. M., & Hollister, R. D. (2019). Local snow melt and temperature—but not regional sea ice—explain variation in spring phenology in coastal Arctic tundra. *Global Change Biology*, *25*(7), 2258–2274. https://doi.org/10.1111/gcb.14639

Bais, H. P., Weir, T. L., Perry, L. G., Gilroy, S., & Vivanco, J. M. (2006). The role of root exudates in rhizosphere interactions with plants and other organisms. *Annual Review of Plant Biology*, *57*, 233–266. https://doi.org/10.1146/annurev.arplant.57.032905.105159

Bates, D., Machler, M., Bolker, B., & Steve, W. (2015). Fitting linear mixed-effects models Using lme4. *Journal of Statistical Software*, *67*(1), 1–48.

Beamish, A. L., Nijland, W., Edwards, M., Coops, N. C., & Henry, G. H. R. (2016). Phenology and vegetation change measurements from true colour digital photography in high Arctic tundra. *Arctic Science*, *2*, 33–49.

Bedard-Haughn, A, Tate, K. W., & van Kessel, C. (2004). Using nitrogen-15 to quantify

vegetative buffer effectiveness for sequestering nitrogen in runoff. *Journal of Environmental Quality*, *33*(6), 2252–2262.
Bedard-Haughn, A., Comeau, L.-P., & Sangster, A. (2013). Gross nitrogen mineralization in pulse-crop rotations on the Northern Great Plains. *Nutrient Cycling in Agroecosystems*, *95*(2), 159–174. https://doi.org/10.1007/s10705-013-9555-z
Biskaborn, B. K., Smith, S. L., Noetzli, J., Matthes, H., Vieira, G., Streletskiy, D. A., Schoeneich, P., Romanovsky, V. E., Lewkowicz, A. G., Abramov, A., Allard, M., Boike, J., Cable, W. L., Christiansen, H. H., Delaloye, R., Diekmann, B., Drozdov, D., Etzelmüller, B., Grosse, G., … Lantuit, H. (2019). Permafrost is warming at a global scale. *Nature Communications*, *10*(1), 1–11. https://doi.org/10.1038/s41467-018-08240-4
Blaud, A., Lerch, T. Z., Phoenix, G. K., & Osborn, A. M. (2015). Arctic soil microbial diversity in a changing world. *Research in Microbiology*, *166*(10), 796–813. https://doi.org/10.1016/j.resmic.2015.07.013
Bliss, L. C., Henry, G. H. R., Svoboda, J., & Bliss, D. I. (1994). Patterns of plant distribution within two polar desert landscapes. *Arctic and Alpine Research*, *26*(1), 46–55.
Bliss, L. C., & Matveyeva, N. V. (1992). Circumpolar Arctic vegetation. In F. S. Chapin III, R. L. Jefferies, J. F. Reynolds, G. R. Shaver, J. Svoboda, & E. W. Chu (Eds.), *Arctic Ecosystems in a Changing Climate* (pp. 59–89). Academic.
Boike, J., Ippisch, O., Overduin, P. P., Hagedorn, B., & Roth, K. (2008). Water, heat and solute dynamics of a mud boil, Spitsbergen. *Geomorphology*, *95*(1–2), 61–73.
Boulanger-Lapointe, N., Levesque, E., Boudreau, S., Henry, G. H. R., & Schmidt, N. M. (2014). Population structure and dynamics of Arctic willow (Salix arctica) in the High Arctic. *Journal of Biogeography*, *41*(10), 1967–1978.
Brady, N. C., & Weil, R. R. (2008). *The Nature and Properties of Soils* (V. R. Anthony, S. Kottcamp, & A. B. Wolf (eds); 14th ed.) Pearson Prentice Hall.
Brummell, M. E. (2015). *Greenhouse Gas Production and Consumption in Soils of the Canadian High Arctic*. University of Saskatchewan, Saskatoon, Canada.
Brummell, M. E., Farrell, R. E., Hardy, S. P., & Siciliano, S. D. (2014). Greenhouse gas production and consumption in High Arctic deserts. *Soil Biology and Biochemistry*, *68*, 158–165.
Brummell, M. E., Farrell, R. E., & Siciliano, S. D. (2012). Greenhouse gas soil production and surface fluxes at a High Arctic polar oasis. *Soil Biology and Biochemistry*, *52*, 1–12. http://dx.doi.org/10.1016/j.soilbio.2012.03.019
Brummell, M. E., Guy, A., & Siciliano, S. D. (2015). Does diapirism influence greenhouse gas production on patterned ground in the High Arctic? *Soil Science Society of America Journal*, *79*(3), 889–895.
Burnham, J. H., & Sletten, R. S. (2010). Spatial distribution of soil organic carbon in northwest Greenland and underestimates of High Arctic carbon stores. *Global Biogeochemical Cycles*, *24*(3).
Butterbach-Bahl, K., Baggs, E. M., Dannenmann, M., Kiese, R., & Zechmeister-Boltenstern, S. (2013). Nitrous oxide emissions from soils: How well do we understand the processes and their controls? *Philosophical Transactions of the Royal Society B*, *368*(1621). https://doi.org/10.1098/rstb.2013.0122
Calderón, F. J., Reeves, J. B., Collins, H. P., & Paul, E. A. (2011). Chemical differences in soil organic matter fractions determined by diffuse-reflectance mid-infrared spectroscopy. *Soil Science Society of America Journal*, *75*(2), 568–579.

https://www.soils.org/publications/sssaj/abstracts/75/2/568
Callaghan, T. V., Björn, L. O., Chaplin III, F. S., Chernov, Y., Christensen, T. R., Huntley, B., Ims, R., Johansson, M., Riedlinger, D. J., Jonasson, S., Matveyeva, N., Oechel, W., Panikov, N., & Shaver, G. (2005). Arctic tundra and polar desert ecosystems. In C. Symon, L. Arris, & B. Heal (Eds.), *Arctic Climate Impact Assessment* (pp. 243–352). Cambridge Univsersity Press. http://www.acia.uaf.edu/pages/scientific.html
Cannone, N., Guglielmin, M., & Gerdol, R. (2004). Relationships between vegetation patterns and periglacial landforms in northwestern Svalbard. *Polar Biology*, *27*(9), 562–571.
Chantigny, M. H., Angers, D. A., Kaiser, K., & Karsten, K. (2008). Extraction and characterization of dissolved organic matter. In M. R. Carter & E. G. Gregorich (Eds.), *Soil Sampling and Methods of Analysis* (pp. 617–634). CRC Press.
Ciais, P., Sabine, C., Bala, G., Bopp, L., Brovkin, V., Canadell, J., Chhabra, A., DeFries, R., Galloway, J., Heimann, M., Jones, C., Le Quéré, C., Myneni, R. B., Piao, S., & Thornton, P. (2013). Carbon and Other Biogeochemical Cycles. In: Climate Change 2013: The Physical Science Basis. Contribution of Working Group I to the Fifth Assessment Report of the Intergovernmental Panel on Climate Change. In T. F. Stocker, D. Qin, G.-K. Plattner, M. Tignor, S. K. Allen, J. Boschung, A. Nauels, Y. Xia, V. Bex, & P. M. Midgley (Eds.), *Cambridge University Press*. https://doi.org/10.1017/CBO9781107415324.015
Congreves, K. A., Wagner-Riddle, C., Si, B. C., & Clough, T. J. (2018). Nitrous oxide emissions and biogeochemical responses to soil freezing-thawing and drying-wetting. *Soil Biology and Biochemistry*, *117*, 5–15. https://doi.org/10.1016/j.soilbio.2017.10.040
Conrad, R. (2007). Microbial ecology of methanogens and methanotrophs. *Advances in Agronomy*, *96*, 1–63.
Conrad, R. (2009). The global methane cycle: Recent advances in understanding the microbial processes involved. *Environmental Microbiology Reports*, *1*(5), 285–292. https://doi.org/10.1111/j.1758-2229.2009.00038.x
Corradi, C., Kolle, O., Walter, K., Zimov, S. A., & Schulze, E. D. (2005). Carbon dioxide and methane exchange of a north-east Siberian tussock tundra. *Global Change Biology*, *11*(11), 1910–1925. https://doi.org/10.1111/j.1365-2486.2005.01023.x
Craine, J. M., Morrow, C., & Fierer, N. (2007). Microbial Nitrogen Limitation Increases Decomposition. *Ecology*, *88*(8), 2105–2113.
Dhillon, G. S., Amichev, B. Y., Freitas, R. De, & van Rees, K. (2015). Communications in Soil Science and Plant Analysis Accurate and Precise Measurement of Organic Carbon Content in Carbonate-Rich Soils Accurate and Precise Measurement of Organic Carbon Content in Carbonate-Rich Soils. *Communications in Soil Science and Plant Analysis*, *46*(21), 2707–2720.
Dhillon, G. S., Gillespie, A., Peak, D., & Van Rees, K. C. J. (2017). Spectroscopic investigation of soil organic matter composition for shelterbelt agroforestry systems. *Geoderma*, *298*, 1–13. http://dx.doi.org/10.1016/j.geoderma.2017.03.016
Dlugokencky, E. (2021a). *Trends in atmospheric methane*. NOAA/GML. www.esrl.noaa.gov/gmd/ccgg/trends_ch4/
Dlugokencky, E. (2021b). *Trends in atmospheric nitrous oxide*. NOAA/GML. www.esrl.noaa.gov/gmd/ccgg/trends_n2o/
Dlugokencky, E., & Tans, P. (2021). *Trends in atmospheric carbon dioxide*. NOAA/GML. www.esrl.noaa.gov/gmd/ccgg/trends/
Elberling, B., Christiansen, H. H., & Hansen, B. U. (2010). High nitrous oxide production from

thawing permafrost. *Nature Geoscience*, *3*, 332–335. https://doi.org/10.1038/ngeo803
Emmerton, C. A., St. Louis, V. L., Humphreys, E. R., Gamon, J. A., Barker, J. D., & Pastorello, G. Z. (2016). Net ecosystem exchange of CO2 with rapidly changing high Arctic landscapes. *Global Change Biology*, *22*(3), 1185–1200. https://doi.org/10.1111/gcb.13064
Ernakovich, J. G., Wallenstein, M. D., & Calderón, F. J. (2015). Chemical indicators of cryoturbation and microbial processing throughout an Alaskan permafrost soil depth profile. *Soil Science Society of America Journal*, *79*(3), 783–793. https://dl.sciencesocieties.org/publications/sssaj/abstracts/79/3/783
Expert Committee on Soil Survey. (1987). *The Canadian system of soil classification* (2nd ed.). Research Branch, Agruculture and Agri-Food Canada.
Fontaine, S., Henault, C., Aamor, A., Bdioui, N., Bloor, J. M. G., Maire, V., Mary, B., Revaillot, S., & Maron, P. A. (2011). Soil Biology & Biochemistry Fungi mediate long term sequestration of carbon and nitrogen in soil through their priming effect. *Soil Biology and Biochemistry*, *43*, 86–96. http://dx.doi.org/10.1016/j.soilbio.2010.09.017
Fontaine, S., Mariotti, A., & Abbadie, L. (2003). The priming effect of organic matter : a question of microbial competition ? *Soil Biology and Biochemistry*, *35*(6), 837–843.
Friborg, T., Soegaard, H., Christensen, T. R., Lloyd, C. R., & Panikov, N. S. (2003). Siberian wetlands: Where a sink is a source. *Geophysical Research Letters*, *30*(21), 1–4. https://doi.org/10.1029/2003GL017797
Gabler, C. A., & Siemann, E. (2013). Timing of favorable conditions, competition and fertility interact to govern recruitment of invasive Chinese Tallow Tree in stressful environments. *PLOS ONE*, *8*(8), 1–9. https://doi.org/10.1371/journal.pone.0071446
Gil, J., Pérez, T., Boering, K., Martikainen, P. J., & Biasi, C. (2017). Mechanisms responsible for high N2O emissions from subarctic permafrost peatlands studied via stable isotope techniques. *Global Biogeochemical Cycles*, *31*(1), 172–189. https://doi.org/10.1002/2015GB005370
Gillespie, A. W., Sanei, H., Diochon, A., Ellert, B. H., Regier, T. Z., Chevrier, D., Dynes, J. J., Tarnocai, C., & Gregorich, E. G. (2014). Perennially and annually frozen soil carbon differ in their susceptibility to decomposition: analysis of subarctic earth hummocks by bioassay, XANES and pyrolysis. *Soil Biology and Biochemistry*, *68*, 106–116. http://dx.doi.org/10.1016/j.soilbio.2013.09.021
Gold, W. G., & Bliss, L. C. (1995). Water limitations and plant community development in a polar desert. *Ecology*, *76*(5), 1558–1568.
Grogan, P., Michelsen, A., Ambus, P., & Jonasson, S. (2004). Freeze-thaw regime effects on carbon and nitrogen dynamics in sub-arctic heath tundra mesocosms. *Soil Biology and Biochemistry*, *36*(4), 641–654. https://doi.org/10.1016/j.soilbio.2003.12.007
Guy, A. L., Siciliano, S. D., & Lamb, E. G. (2015). Spiking regional vis-NIR calibration models with local samples to predict soil organic carbon in two High Arctic polar deserts using a vis-NIR probe. *Canadian Journal of Soil Science*, *95*(3), 237–249. http://pubs.aic.ca/doi/10.4141/cjss-2015-004
Haberhauer, G., Feigl, B., Gerzabek, M. H., & Cerri, C. (2000). *FT-IR spectroscopy of organic matter in tropical soils: changes induced through deforestation*. *54*(2), 221–224.
Hargreaves, K. J., Fowler, D., Pitcairn, C. E. R., & Aurela, M. (2001). Annual methane emission from Finnish mires estimated from eddy covariance campaign measurements. *Theoretical and Applied Climatology*, *70*(1), 203–213. https://doi.org/10.1007/s007040170015
Hart, S. C., Stark, J. M., Davidson, E. A., & Firestone, M. K. (1994). Nitrogen mineralization,

immobilization, and nitrification. In *Methods of Soil Analysis, Part 2. Microbiological and Biochemical Properties* (pp. 985–1018). SSSA Book Series, no. 5.

Haslauer, C. P., Meyer, J. R., Bárdossy, A., & Parker, B. L. (2017). Estimating a Representative Value and Proportion of True Zeros for Censored Analytical Data with Applications to Contaminated Site Assessment. *Environmental Science and Technology*, *51*(13), 7502–7510. https://doi.org/10.1021/acs.est.6b05385

Hayashi, K., Shimomura, Y., Morimoto, S., Uchida, M., Nakatsubo, T., & Hayatsu, M. (2016). Characteristics of ammonia oxidation potentials and ammonia oxidizers in mineral soil under Salix polaris–moss vegetation in Ny-Ålesund, Svalbard. *Polar Biology*, *39*(4), 725–741.

Hayatsu, M., Tago, K., & Saito, M. (2008). Various players in the nitrogen cycle: diversity and functions of the microorganisms involved in nitrification and denitrification. *Soil Science and Plant Nutrition*, *54*(1), 33–45.

Hayes, M. H. B. (2009). Evolution of concepts of environmental natural nonliving organic matter. In N. Senesi, B. Xing, & P. M. Huang (Eds.), *Biophysico-Chemical Processes Involving Natural Nonliving Organic Matter in Environmental Systems* (pp. 1–39). John Wiley & Sons.

Henry, G. H. R., Freedman, B., & Svoboda, J. (1986). Effects of fertilization on 3 tundra plant-communities of a polar desert oasis. *Canadian Journal of Botany-Revue Canadienne De Botanique*, *64*, 2502–2507.

Hofstetter, H., Dusseldorp, E., Zeileis, A., & Schuller, A. A. (2016). Modeling Caries Experience: Advantages of the use of the hurdle model. *Caries Research*, *50*(6), 517–526. https://doi.org/10.1159/000448197

Hu, H. W., Chen, D., & He, J. Z. (2015). Microbial regulation of terrestrial nitrous oxide formation: Understanding the biological pathways for prediction of emission rates. *FEMS Microbiology Reviews*, *39*(5), 729–749. https://doi.org/10.1093/femsre/fuv021

Huang, L., Bradshaw, K., Grosskleg, J., & Siciliano, S. D. (2019). Assessing Space, Time, and Remediation Contribution to Soil Pollutant Variation near the Detection Limit Using Hurdle Models to Account for a Large Proportion of Nondetectable Results. *Environmental Science and Technology*, *53*(12), 6824–6833. https://doi.org/10.1021/acs.est.8b07110

Hugelius, G., Strauss, J., Zubrzycki, S., Harden, J. W., Schuur, E. A. G., Ping, C. L., Schirrmeister, L., Grosse, G., Michaelson, G. J., Koven, C. D., O'Donnell, J. A., Elberling, B., Mishra, U., Camill, P., Yu, Z., Palmtag, J., & Kuhry, P. (2014). Estimated stocks of circumpolar permafrost carbon with quantified uncertainty ranges and identified data gaps. *Biogeosciences*, *11*(23), 6573–6593.

Intergovernmental Panel on Climate Change. (2014). *Climate Change 2014: Mitigation of Climate Change. Contribution of Working Group III to the Fifth Assessment Report of the Intergovernment Panel on Climate Change* (O. Edenhofer, R. Pichs-Madruga, Y. Sokona, E. Farahani, S. Kadner, K. Seyboth, A. Adler, I. Baum, S. Brunner, P. Eickemeier, B. Kriemann, J. Savolainen, S. Schlomer, C. von Stechow, T. Zwickel, & J. C. Minx (Eds.)).

IPCC. (2014). *Climate Change 2014: Synthesis Report. Contritution of Working Groups I, II, and III to the Fifth Assessment Report of the Intergovernmental Panel on Climate Change* (Core Writing Team, R. K. Pachauri, & L. A. Meyer (Eds.)). IPCC.

Jones, C. M., Graf, D. R. H., Bru, D., Philippot, L., & Hallin, S. (2013). The unaccounted yet abundant nitrous oxide-reducing microbial community: A potential nitrous oxide sink. *ISME Journal*, *7*(2), 417–426. https://doi.org/10.1038/ismej.2012.125

Jones, D. L., & Kielland, K. (2012). Amino acid, peptide and protein mineralization dynamics in a taiga forest soil. *Soil Biology and Biochemistry*, *55*(3), 60–69. https://doi.org/10.1016/j.soilbio.2012.06.005

Kade, A., & Walker, D. A. (2008). Experimental Alteration of Vegetation on Nonsorted Circles : Effects on Cryogenic Activity and Implications for Climate Change in the Arctic. *Arctic, Antarctic, and Alpine Research*, *40*(1), 96–103. https://doi.org/10.1657/1523-0430(06-029)

Kaiser, C., Meyer, H., Biasi, C., Rusalimova, O., Barsukov, P., & Richter, A. (2005). Storage and mineralization of carbon and nitrogen in soils of a frost-boil tundra ecosystem in Siberia. *Applied Soil Ecology*, *29*(2), 173–183. https://doi.org/10.1016/j.apsoil.2004.10.005

Kaiser, C., Meyer, H., Biasi, C., Rusalimova, O., Barsukov, P., & Richter, A. (2007). Conservation of soil organic matter through cryoturbation in arctic soils in Siberia. *Journal of Geophysical Research: Biogeosciences*, *112*(G2), 1–8.

Kallenbach, C. M., Grandy, A. S., Frey, S. D., & Diefendorf, A. F. (2015). Microbial physiology and necromass regulate agricultural soil carbon accumulation. *Soil Biology and Biochemistry*, *91*, 279–290. https://doi.org/10.1016/j.soilbio.2015.09.005

Klaus, M., Becher, M., & Klaminder, J. (2013). Cryogenic soil activity along bioclimatic gradients in northern Sweden: insights from eight different proxies. *Permafrost and Periglacial Processes*, *24*(3), 210–223.

Kohn, L. M., & Stasovski, E. (1990). Mycological Society of America Mycological Society of America. *Mycologia*, *82*(1), 23–35.

Koper, T. E., Stark, J. M., Habteselassie, M. Y., & Norton, J. M. (2010). Nitrification exhibits Haldane kinetics inan agricultural soil treated with ammoniumsulfate or dairy-waste compost. *FEMS Microbiology Ecology*, *74*(2), 316–322. https://doi.org/10.1111/j.1574-6941.2010.00960.x

Kuhnert, P. M., Martin, T. G., Mengersen, K., & Possingham, H. P. (2005). Assessing the impacts of grazing levels on bird density in woodland habitat: A Bayesian approach using expert opinion. *Environmetrics*, *16*(7), 717–747. https://doi.org/10.1002/env.732

Lamb, E. G., Han, S., Lanoil, B. D., Henry, G. H. R., Brummell, M. E., Banerjee, S., & Siciliano, S. D. (2011). A High Arctic soil ecosystem resists long-term environmental manipulations. *Global Change Biology*, *17*(10), 3187–3194.

Lenth, V. R. (2016). Least-Squares Means: The R Package lsmeans. *Journal of Statistical Software*, *69*(1), 1–33.

Li, H., Yang, S., Semenov, M. V., Yao, F., Ye, J., Bu, R., Ma, R., Lin, J., Kurganova, I., Wang, X., Deng, Y., Kravchenko, I., Jiang, Y., & Kuzyakov, Y. (2021). Temperature sensitivity of SOM decomposition is linked with a K-selected microbial community. *Global Change Biology*, 1–17. https://doi.org/10.1111/gcb.15593

Linn, D. M., & Doran, J. W. (1984). Effect of water-filled pore space on carbon dioxide and nitrous oxide production in tilled and nontilled soils. *Soil Science Society of America Journal*, *48*(6), 1267–1272.

Lloyd, C. R. (2001). On the physical controls of the carbon dioxide balance at a high Arctic site in Svalbard. *Theoretical and Applied Climatology*, *70*, 167–182. https://doi.org/10.1046/j.1365-2486.2001.00422.x

Luërs, J., Westermann, S., Piel, K., & Boike, J. (2014). Annual CO2 budget and seasonal CO2 exchange signals at a high Arctic permafrost site on Spitsbergen, Svalbard archipelago. *Biogeosciences*, *11*, 6307–6322. https://doi.org/10.5194/bg-11-6307-2014

Lynch, L. M., Machmuller, M. B., Cotrufo, M. F., Paul, E. A., & Wallenstein, M. D. (2018).

Tracking the fate of fresh carbon in the Arctic tundra: will shrub expansion alter responses of soil organic matter to warming? *Soil Biology and Biochemistry*, *120*, 134–144. https://doi.org/10.1016/j.soilbio.2018.02.002

Ma, W. K., Bedard-Haughn, A., Siciliano, S. D., & Farrell, R. E. (2008). Relationship between nitrifier and denitrifier community composition and abundance in predicting nitrous oxide emissions from ephemeral wetland soils. *Soil Biology and Biochemistry*, *40*(5), 1114–1123. https://doi.org/10.1016/j.soilbio.2007.12.004

Ma, W. K., Farrell, R. E., & Siciliano, S. D. (2008). Soil formate regulates the fungal nitrous oxide emission pathway. *Applied and Environmental Microbiology*, *74*(21), 6690–6696. https://doi.org/10.1128/AEM.00797-08

Ma, W. K., Schautz, A., Fishback, L.-A. E., Bedard-Haughn, A., Farrell, R. E., & Siciliano, S. D. (2007). Assessing the potential of ammonia oxidizing bacteria to produce nitrous oxide in soils of a high arctic lowland ecosystem on Devon Island, Canada. *Soil Biology and Biochemistry*, *39*(8), 2001–2013.

Martin, T. G., Wintle, B. A., Rhodes, J. R., Kuhnert, P. M., Field, S. A., Low-Choy, S. J., Tyre, A. J., & Possingham, H. P. (2005). Zero tolerance ecology: Improving ecological inference by modelling the source of zero observations. *Ecology Letters*, *8*(11), 1235–1246. https://doi.org/10.1111/j.1461-0248.2005.00826.x

Marushchak, M. E., Pitkamaki, A., Koponen, H., Biasi, C., Seppala, M., & Martikainen, P. J. (2011). Hot spots for nitrous oxide emissions found in different types of permafrost peatlands. *Global Change Biology*, *17*(8), 2601–2614.

Mastepanov, M., Sigsgaard, C., Tagesson, T., Ström, L., Tamstorf, M. P., Lund, M., & Christensen, T. R. (2013). Revisiting factors controlling methane emissions from high-Arctic tundra. *Biogeosciences*, *10*(11), 5139–5158. https://doi.org/10.5194/bg-10-5139-2013

Meier, I. C., Finzi, A. C., & Phillips, R. P. (2017). Root exudates increase N availability by stimulating microbial turnover of fast-cycling N pools. *Soil Biology and Biochemistry*, *106*, 119–128. https://doi.org/10.1016/j.soilbio.2016.12.004

Miller, J. J., & Curtin, D. (2008). Electrical conductivity and soluble ions. In M. R. Carter & E. G. Gregorich (Eds.), *Soil Sampling and Methods of Analysis* (pp. 161–171). CRC Press.

Muc, M., Freedman, B., & Svoboda, J. (1989). Vascular plant communities of a polar oasis at Alexandra Fiord (79° N), Ellesmere Island, Canada. *Canadian Journal of Botany*, *67*(4), 1126–1136. https://doi.org/10.1139/b89-147

Muller, A. L., Hardy, S. P., Mamet, S. D., Ota, M., Lamb, E. G., & Siciliano, S. D. (2017). Salix arctica changes root distribution and nutrient uptake in response to subsurface nutrients in High Arctic deserts. *Ecology*, *98*(8), 2158–2169.

Myhre, G., Shindell, D., Bréon, F.-M., Collins, W., Fuglestvedt, J., Huang, J., Koch, D., Lamarque, J.-F., Lee, D., Mendoza, B., Nakajima, T., Robock, A., Stephens, G., Takemura, T., & Zhang, H. (2013). *Anthropogenic and Natural Radiative Forcing. In: Climate Change 2013: The Physical Science Basis. Contribution of Working Group I to the Fifth Assessment Report of the Intergovernmental Panel on Climate Change* (T. F. Stocker, D. Qin, G.-K. Plattner, M. Tignor, S. K. Allen, J. Boschung, A. Nauels, Y. Xia, V. Bex, & P. M. Midgley (Eds.)). Cambridge University Press.

Ota, M., Mamet, S. D., Muller, A. L., Lamb, E. G., Dhillon, G., Peak, D., & Siciliano, S. D. (2020). Could cryoturbic diapirs be key for understanding ecological feedbacks to climate change in High Arctic polar deserts? *Journal of Geophysical Research: Biogeosciences*,

125, 1–13. https://doi.org/10.1029/2019jg005263
Ota, M., & Siciliano, S. D. (2020). Biology and carbon lability of sub-surface nutrient patches in High Arctic polar deserts drives the probability and magnitude of nitrous oxide emissions. *Soil Biology and Biochemistry*, *150*, 1–8. https://doi.org/10.1016/j.soilbio.2020.108001
Park, S., Pérez, T., Boering, K. A., Trumbore, S. E., Gil, J., Marquina, S., & Tyler, S. C. (2011). Can N2O stable isotopes and isotopomers be useful tools to characterize sources and microbial pathways of N2O production and consumption in tropical soils? *Global Biogeochemical Cycles*, *25*(1), 1–16. https://doi.org/10.1029/2009GB003615
Pautler, B. G., Simpson, A. J., Mcnally, D. J., Lamoureux, S. F., & Simpson, M. J. (2010). Arctic permafrost active layer detachments stimulate microbial activity and degradation of soil organic matter. *Environmental Science & Technology*, *44*(11), 4076–4082. papers2://publication/uuid/EB518091-84C2-44BD-B04C-1516081F351B
Ping, C. L., Jastrow, J. D., Jorgenson, M. T., Michaelson, G. J., & Shur, Y. L. (2015). Permafrost soils and carbon cycling. *Soil*, *1*(1), 147–171. https://doi.org/10.5194/soil-1-147-2015
Ping, C. L., Michaelson, G. J., Jorgenson, M. T., Kimble, J. M., Epstein, H., Romanovsky, V. E., & Walker, D. A. (2008). High stocks of soil organic carbon in the North American Arctic region. *Nature Geoscience*, *1*(9), 615–619. https://doi.org/10.1038/ngeo284
Pinheiro, J., Bates, D., DebRoy, S., & Sarkar, D. (2017). *nlme: linear and nonlinear mixed effects models. R package version 3.1-131. https://cran.r-project.org/package=nlme*. https://cran.r-project.org/package=nlme
Piper, C. L., Lamb, E. G., & Siciliano, S. D. (2015). Smooth brome changes gross soil nitrogen cycling processes during invasion of a rough fescue grassland. *Plant Ecology*, *216*(2), 235–246.
Prosser, J. I., & Nicol, G. W. (2012). Archaeal and bacterial ammonia-oxidisers in soil: The quest for niche specialisation and differentiation. *Trends in Microbiology*, *20*(11), 523–531. https://doi.org/10.1016/j.tim.2012.08.001
R Core Team. (2017). *R: a language and environment for statistical computing*. R Foundation for Statistical Computing. https://www.r-project.org/
Ravishankara, A. R., Daniel, J. S., & Portmann, R. W. (2009). *Nitrous Oxide (N 2 O): The Dominant Ozone-Depleting Substance Emitted in the 21st Century*. *326*(October 2), 123–125.
Raz-Yaseef, N., Torn, M. S., Wu, Y., Billesbach, D. P., Liljedahl, A. K., Kneafsey, T., Romanovsky, V. E., Cook, D. R., & Wullschleger, S. D. (2017). Large CO 2 and CH 4 emissions from polygonal tundra during spring thaw in northern Alaska. *Geophysical Research Letters*, *44*(1), 504–513.
Rodrigues, M. L., Nimrichter, L., Cordero, R. J. B., & Casadevall, A. (2011). Fungal polysaccharides : biological activity beyond the usual structural properties. *Frontiers in Microbiology*, *2*(171), 1–4.
Schaeffer, S. M., Sharp, E., Schimel, J. P., & Welker, J. M. (2013). Soil-plant N processes in a High Arctic ecosystem, NW Greenland are altered by long-term experimental warming and higher rainfall. *Global Change Biology*, *19*(11), 3529–3539.
Schauss, K., Focks, A., Leininger, S., Kotzerke, A., Heuer, H., Thiele-bruhn, S., Sharma, S., Wilke, B., Matthies, M., Smalla, K., Munch, J. C., Amelung, W., Kaupenjohann, M., Schloter, M., & Schleper, C. (2009). Dynamics and functional relevance of ammonia-oxidizing archaea in two agricultural soils. *Environmental Microbiology*, *11*(2), 446–456. https://doi.org/10.1111/j.1462-2920.2008.01783.x

Schimel, J. P., & Clein, J. S. (1996). Microbial response to freeze-thaw cycles in tundra and taiga soils. *Soil Biology and Biochemistry*, *28*(8), 1061–1066.
Schimel, J. P., & Schaeffer, S. M. (2012). Microbial control over carbon cycling in soil. *Frontiers in Microbiology*, *3*, 1–11.
Schoenau, J. J., & O'Halloran, I. P. (2008). Sodium bicarbonate extractable phosphorus. In M. R. Carter & E. G. Gregorich (Eds.), *Soil Sampling and Methods of Analysis* (pp. 89–94). CRC Press.
Schuur, E. A. G., McGuire, A. D., Schadel, C., Grosse, G., Harden, J. W., Hayes, D. J., Hugelius, G., Koven, C. D., Kuhry, P., Lawrence, D. M., Natali, S. M., Olefeldt, D., Romanovsky, V. E., Schaefer, K., Turetsky, M. R., Treat, C. C., & Vonk, J. E. (2015). Climate change and the permafrost carbon feedback. *Nature*, *520*, 171–179.
Shilts, W. W. (1978). Nature and genesis of mudboils, Central Keewatin, Canada. *Canadian Journal of Earth Science*, *15*(7), 1053–1068.
Siciliano, S. D., Ma, W. K., Ferguson, S., & Farrell, R. E. (2009). Nitrifier dominance of Arctic soil nitrous oxide emissions arises due to fungal competition with denitrifiers for nitrate. *Soil Biology and Biochemistry*, *41*(6), 1104–1110.
Siljanen, H. M. P., Alves, R. J. E., Ronkainen, J. G., Lamprecht, R. E., Bhattarai, H. R., Bagnoud, A., Marushchak, M. E., Martikainen, P. J., Schleper, C., & Biasi, C. (2019). Archaeal nitrification is a key driver of high nitrous oxide emissions from arctic peatlands. *Soil Biology and Biochemistry*, *137*, 1–10. https://doi.org/10.1016/j.soilbio.2019.107539
Silver, W. L., Herman, D. J., & Firestone, M. K. (2001). Dissimilatory nitrate reduction to ammonium in upland tropical forest soils. *Ecology*, *82*(9), 2410–2416.
Šimek, M., & Cooper, J. E. (2002). The influence of soil pH on denitrification: Progress towards the understanding of this interaction over the last 50 years. *European Journal of Soil Science*, *53*(3), 345–354. https://doi.org/10.1046/j.1365-2389.2002.00461.x
Slater, A. G., & Lawrence, D. M. (2013). Diagnosing present and future permafrost from climate models. *Journal of Climate*, *26*(15), 5608–5623. https://doi.org/10.1175/JCLI-D-12-00341.1
Soil Survey Staff. (1999). Soil Taxonomy: A Basic System of Soil Classification for Making and Interpreting Soil Surveys. In *Agriculture Handbook* (2nd ed.). USDA-NRCS, US Gov. Print. Office.
Stark, J. M., & Hart, S. C. (1996). Diffusion technique for preparing salt solutions, Kjeldahl digests, and persulfate digests for nitrogen-15 analysis. *Soil Science Society of America Journal*, *60*(6), 1846–1855.
Stein, L. Y. (2011). Surveying N2O-producing pathways in bacteria. In M. G. Klotz (Ed.), *Methods in Enzymology* (Vol. 486, pp. 131–152). Elsevier.
Stewart, K. J., Brummell, M. E., Coxson, D. S., & Siciliano, S. D. (2013). How is nitrogen fixation in the High Arctic linked to greenhouse gas emissions? *Plant and Soil*, *362*(1), 215–229.
Stewart, K. J., Brummell, M. E., Farrell, R. E., & Siciliano, S. D. (2012). N 2O flux from plant-soil systems in polar deserts switch between sources and sinks under different light conditions. *Soil Biology and Biochemistry*, *48*, 69–77.
Stewart, K. J., Grogan, P., Coxson, D. S., & Siciliano, S. D. (2014). Topography as a key factor driving atmospheric nitrogen exchanges in arctic terrestrial ecosystems. *Soil Biology and Biochemistry*, *70*(3), 96–112. https://doi.org/10.1016/j.soilbio.2013.12.005
Swanson, D. K., Ping, C. L., & Michaelson, G. J. (1999). Diapirism in soils due to thaw of ice-

rich material near the permafrost table. *Permafrost and Periglacial Processes*, *10*(4), 349–367.
Szymański, W. (2017). Quantity and chemistry of water-extractable organic matter in surface horizons of Arctic soils under different types of tundra vegetation – a case study from the Fuglebergsletta coastal plain (SW Spitsbergen). *Geoderma*, *305*, 30–39.
Tatzber, M., Stemmer, M., Spiegel, H., Katzlberger, C., Haberhauer, G., Mentler, A., & Gerzabek, M. H. (2007). FTIR-spectroscopic characterization of humic acids and humin fractions obtained by advanced NaOH, Na4P2O7, and Na2CO3 extraction procedures. *Journal of Plant Nutrition and Soil Science*, *170*(4), 522–529.
Torrance, J. K., & Schellekens, F. J. (2006). Chemical factors in soil freezing and frost heave. *Polar Record*, *42*(220), 33–42. https://doi.org/10.1017/S0032247405004894
Tourna, M., Freitag, T. E., Nicol, G. W., & Prosser, J. I. (2008). Growth, activity and temperature responses of ammonia-oxidizing archaea and bacteria in soil microcosms. *Environmental Microbiology*, *10*(5), 1357–1364. https://doi.org/10.1111/j.1462-2920.2007.01563.x
Toyoda, S., & Yoshida, N. (1999). Determination of nitrogen isotopomers of nitrous oxide on a modified isotope ratio mass spectrometer. *Analytical Chemistry*, *71*(20), 4711–4718. https://doi.org/10.1021/ac9904563
Treusch, A. H., Leininger, S., Kletzin, A., Schuster, S. C., Klenk, H.-P., & Schleper, C. (2005). Novel genes for nitrite reductase and Amo-related proteins indicate a role of uncultivated mesophilic crenarchaeota in nitrogen cycling. *Environmental Microbiology*, *7*(12), 1985–1995. https://doi.org/10.1111/j.1462-2920.2005.00906.x
Tye, A. M., Young, S. D., Crout, N. M. J., West, H. M., Stapleton, L. M., Poulton, P. R., & Laybourn-Parry, J. (2005). The fate of 15N added to high Arctic tundra to mimic increased inputs of atmospheric nitrogen released from a melting snowpack. *Global Change Biology*, *11*(10), 1640–1654.
van Everdingen, R. (Ed.). (1998). *Multi-language glossary of permafrost and related ground-ice terms. revised 2015.* International Permafrost Association. www.nsidc.org/fgdc/glossary/
Verhoeven, E., Decock, C., Barthel, M., Bertora, C., Sacco, D., Romani, M., Sleutel, S., & Six, J. (2018). Nitrification and coupled nitrification-denitrification at shallow depths are responsible for early season N2O emissions under alternate wetting and drying management in an Italian rice paddy system. *Soil Biology and Biochemistry*, *120*, 58–69. https://doi.org/10.1016/j.soilbio.2018.01.032
Voigt, C., Lamprecht, R. E., Marushchak, M. E., Lind, S. E., Novakovskiy, A., Aurela, M., Martikainen, P. J., & Biasi, C. (2017). Warming of subarctic tundra increases emissions of all three important greenhouse gases – carbon dioxide, methane, and nitrous oxide. *Global Change Biology*, *23*(8), 3121–3138. https://doi.org/10.1111/gcb.13563
Voigt, C., Marushchak, M. E., Abbott, B. W., Biasi, C., Elberling, B., Siciliano, S. D., Sonnentag, O., Stewart, K. J., Yang, Y., & Martikainen, P. J. (2020). Nitrous oxide emissions from permafrost-affected soils. *Nature Reviews Earth & Environment*, *1*(8), 420–434. https://doi.org/10.1038/s43017-020-0063-9
Wagner-Riddle, C., Congreves, K. A., Abalos, D., Berg, A. A., Brown, S. E., Ambadan, J. T., Gao, X., & Tenuta, M. (2017). Globally important nitrous oxide emissions from croplands induced by freeze-thaw cycles. *Nature Geoscience*, *10*(4), 279–283. https://doi.org/10.1038/ngeo2907
Walker, D. A., Epstein, H. E., Romanovsky, V. E., Ping, C. L., Michaelson, G. J., Daanen, R. P.,

Shur, Y., Peterson, R. A., Krantz, W. B., Raynolds, M. K., Gould, W. A., Gonzalez, G., Nicolsky, D. J., Vonlanthen, C. M., Kade, A. N., Kuss, P., Kelley, A. M., Munger, C. A., Tarnocai, C. T., … Daniëls, F. J. A. (2008). Arctic patterned-ground ecosystems: a synthesis of field studies and models along a North American Arctic transect. In *Journal of Geophysical Research: Biogeosciences* (Vol. 113, Issue 3, pp. 1–17).

Walker, D. A., Gould, W. A., Maier, H. A., & Raynolds, M. K. (2002). The circumpolar Arctic vegetation map: AVHRR-derived base maps, environmental controls, and integrated mapping procedures. *International Journal of Remote Sensing*, *23*(21), 4551–4570.

Walker, D. A., Epstein, H. E., Gould, W. A., Kelley, A. M., Kade, A. N., Knudson, J. A., Krantz, W. B., Michaelson, G., Peterson, R. A., Ping, C. L., Raynolds, M. K., Romanovsky, V. E., & Shur, Y. (2004). Frost-boil ecosystems: complex interactions between landforms, soil, vegetation and climate. *Permafrost and Periglacial Processes*, *15*(2), 171–188.

Walker, D. A, Raynolds, M. K., Daniëls, F. J. A., Einarsson, E., Elvebakk, A., Gould, W. A., Katenin, A. E., Kholod, S. S., Markon, C. J., Melnikov, E. S., Moskalenko, N. G., Talbot, S. S., Yurtsev, B. A., & Team, C. (2005). The Circumpolar Arctic Vegetation Map Stable. *Journal of Vegetation Science*, *16*(3), 267–282.

Well, R., & Flessa, H. (2009). Isotopologue signatures of N2O produced by denitrification in soils. *Journal of Geophysical Research: Biogeosciences*, *114*(2), 1–11. https://doi.org/10.1029/2008JG000804

Well, R., Flessa, H., Xing, L., Xiaotang, J., & Römheld, V. (2008). Isotopologue ratios of N2O emitted from microcosms with NH4+ fertilized arable soils under conditions favoring nitrification. *Soil Biology and Biochemistry*, *40*(9), 2416–2426. https://doi.org/10.1016/j.soilbio.2008.06.003

Well, R., Kurganova, I., De Gerenyu, V. L., & Flessa, H. (2006). Isotopomer signatures of soil-emitted N2O under different moisture conditions - A microcosm study with arable loess soil. *Soil Biology and Biochemistry*, *38*(9), 2923–2933. https://doi.org/10.1016/j.soilbio.2006.05.003

Wild, B., Alaei, S., Bengtson, P., Bodé, S., Boeckx, P., Schnecker, J., Mayerhofer, W., & Rütting, T. (2017). Short-term carbon input increases microbial nitrogen demand, but not microbial nitrogen mining, in a set of boreal forest soils. *Biogeochemistry*, *136*(3), 261–278. https://doi.org/10.1007/s10533-017-0391-0

Wild, B., Gentsch, N., Capek, P., Diáková, K., Alves, R. J. E., Bárta, J., Gittel, A., Hugelius, G., Knoltsch, A., Kuhry, P., Lashchinskiy, N., Mikutta, R., Palmtag, J., Schleper, C., Schnecker, J., Shibistova, O., Takriti, M., Torsvik, V. L., Urich, T., … Richter, A. (2016). Plant-derived compounds stimulate the decomposition of organic matter in arctic permafrost soils. *Scientific Reports*, *6*, 1–11. https://doi.org/10.1038/srep25607

Wild, B., Schnecker, J., Alves, R. J. E., Barsukov, P., Bárta, J., Čapek, P., Gentsch, N., Gittel, A., Guggenberger, G., Lashchinskiy, N., Mikutta, R., Rusalimova, O., Šantrůčková, H., Shibistova, O., Urich, T., Watzka, M., Zrazhevskaya, G., & Richter, A. (2014). Input of easily available organic C and N stimulates microbial decomposition of soil organic matter in arctic permafrost soil. *Soil Biology and Biochemistry*, *75*, 143–151. https://doi.org/10.1016/j.soilbio.2014.04.014

Wild, B., Schnecker, J., Bárta, J., Čapek, P., Guggenberger, G., Hofhansl, F., Kaiser, C., Lashchinsky, N., Mikutta, R., Mooshammer, M., Šantrůčková, H., Shibistova, O., Urich, T., Zimov, S. A., & Richter, A. (2013). Nitrogen dynamics in turbic cryosols from Siberia and Greenland. *Soil Biology and Biochemistry*, *67*, 85–93.

Wille, C., Kutzbach, L., Sachs, T., Wagner, D., & Pfeiffer, E.-M. (2008). Methane emission from Siberian arctic polygonal tundra: Eddy covariance measurements and modeling. *Global Change Biology*, *14*(6), 1395–1408. https://doi.org/10.1111/j.1365-2486.2008.01586.x

Wilson, K. S., & Humphreys, E. R. (2010). Carbon dioxide and methane fluxes from Arctic mudboils. *Canadian Journal of Soil Science*, *90*(3), 441–449. https://doi.org/10.4141/CJSS09073

Wojdyr, M. (2010). Fityk: a general-purpose peak fitting program. *Journal of Applied Crystallography*, *43*(5), 1126–1128.

Wrage, N., Velthof, G. L., van Beusichem, M. L., & Oenema, O. (2001). Role of nitrifier denitrification in the production of nitrous oxide. *Soil Biology and Biochemistry*, *33*(12–13), 1723–1732. https://doi.org/10.1016/S0038-0717(01)00096-7

Zumft, W. (1997). Cell biology and molecular basis of denitrification. *Microbiol Mol Biol Rev*, *61*(4), 533–616. http://mmbr.asm.org/cgi/reprint/61/4/533?view=long&pmid=9409151

Zuur, A. F., Ieno, E. N., Walker, N. J., Saveliev, A. A., & Smith, G. M. (2009). *Mixed effects models and extentions in ecology wit R*. Springer Science+Business Media LLC.

Zuur, A. F., & Ieno, E. N. (2016). *Beginner's Guide to Zero-Inflated Models with R* (C. Andreasen (Ed.)). Highland Statistics Ltd.

Zuur, A. F., Ieno, E. N., & Elphick, C. S. (2010). A protocol for data exploration to avoid common statistical problems. *Methods in Ecology and Evolution*, *1*, 3–14. https://doi.org/10.1111/j.2041-210x.2009.00001.x

Zuur, A. F, & Ieno, E. N. (2016). Beginner's Guide to Zero-Inflated Models with R. In *Highland Statistics' Beginner's Guide Series* (Issue May). http://highstat.com/index.php/beginner-s-guide-to-zero-inflated-models

APPENDICES

APPENDIX 1

Calculations for corrected $\delta^{15}N$ and ^{15}N SP values of N_2O

1. δ^{15}N value

The δ^{15}N value was defined by

$$\delta^{15}N = \left(\frac{15N/14N}{R\ standard} - 1\right) \times 1000 \quad \text{(A1.1)}$$

where δ^{15}N is instrumental measurement, R standard is international reference standard (0.00367), 15N is ^{15}N, and 14N is ^{14}N.

In my study, ^{15}N and ^{14}N were defined by

$$15N + 14N = 1 \quad \text{(A.1.2).}$$

Using A1.1 and A1.2, ^{15}N was solved.

First of all, A.1.1 was modified by

$$\frac{15N/14N}{R\ standard} - 1 = \delta^{15}N/1000 \quad \text{(A.1.3)}$$

followed by

$$15N/14N = (\delta^{15}N/1000 + 1) \times R\ standard \quad \text{(A.1.4)}$$

followed by

$$15N/14N = \frac{\delta^{15}N + 1000}{1000} \times R\ standard \quad \text{(A.1.5)}$$

followed by

$$15N/14N = (\delta^{15}N + 1000) \times R\ standard/1000 \quad \text{(A.1.6).}$$

Then, A.1.2 was modified by

$$14N = 1 - 15N \quad \text{(A.1.7)}$$

to substitute ^{14}N into A.1.6, which led to

$$15N/(1 - 15N) = (\delta^{15}N + 1000) \times R\ standard/1000 \quad \text{(A.1.8).}$$

To solve ^{15}N,

$$A = (\delta^{15}N + 1000) \times R\ standard/1000 \quad \text{(A.1.9)}$$

was substituted into A.1.8, which led to

$$15N/(1 - 15N) = A \quad \text{(A.1.10).}$$

A.1.9 was modified by

$$15N = A \times (1 - 15N) \quad \text{(A.1.11);}$$

thus, ^{15}N was solved by

$$15N = A/(1 + A) \quad \text{(A.1.12).}$$

A.1.9 was substituted into A.1.12, which led to

$$15N = \frac{(\delta^{15}N + 1000) \times R\ standard/1000}{1 + (\delta^{15}N + 1000) \times R\ standard/1000} \quad \text{(A.1.13).}$$

The denominator and the numerator in the right side of A.1.13 were multiplied by *R standard/1000*; thus ^{15}N was solved by

$$15N = \frac{\delta^{15}N + 1000}{1000/R\ standard + \delta^{15}N + 1000} \quad \text{(A.1.14).}$$

Using the ^{15}N value from A.1.14, each amount of $^{15}N_2O$ and $^{14}N_2O$ was calculated in both the beginning and the end of the incubation (*i.e.,* day zero and 14), and each production of $^{15}N_2O$ and $^{14}N_2O$ were obtained. The production values were used to obtain corrected δ^{15}N values in the same manner as A.1.1.

2. ^{15}N SP value

$$\delta^{15}N^{\alpha} = \left(\frac{14N-15N-O/14N-14N-O}{R\ standard} - 1\right) \times 1000 \quad \text{(A.1.15)}$$

where $\delta^{15}N^{\alpha}$ is the instrumental measurement.

Using the ^{15}N value obtained in the process of solving the corrected δ^{15}N value, the amount of ^{14}N-^{14}N-O is obtained. As $\delta^{15}N^{\alpha}$ is solved,

$$14N - 15N - O = \frac{\delta^{15}N^{\alpha} + 1000}{1000} \times R\ standard \times 14N - 14N - O \quad \text{(A.1.16).}$$

By obtaining the amount of ^{14}N-^{14}N-O at day zero and day 14, the production of ^{14}N-^{15}N-O was obtained and the corrected $\delta^{15}N^{\alpha}$ value was calculated. The corrected $\delta^{15}N^{\beta}$ value was obtained in the same way.

Site preference was calculated by this equation.

$$SP = corrected\ \delta^{15}N^{\alpha} - corrected\ \delta^{15}N^{\beta} \quad \text{(A.1.17).}$$

APPENDIX 2

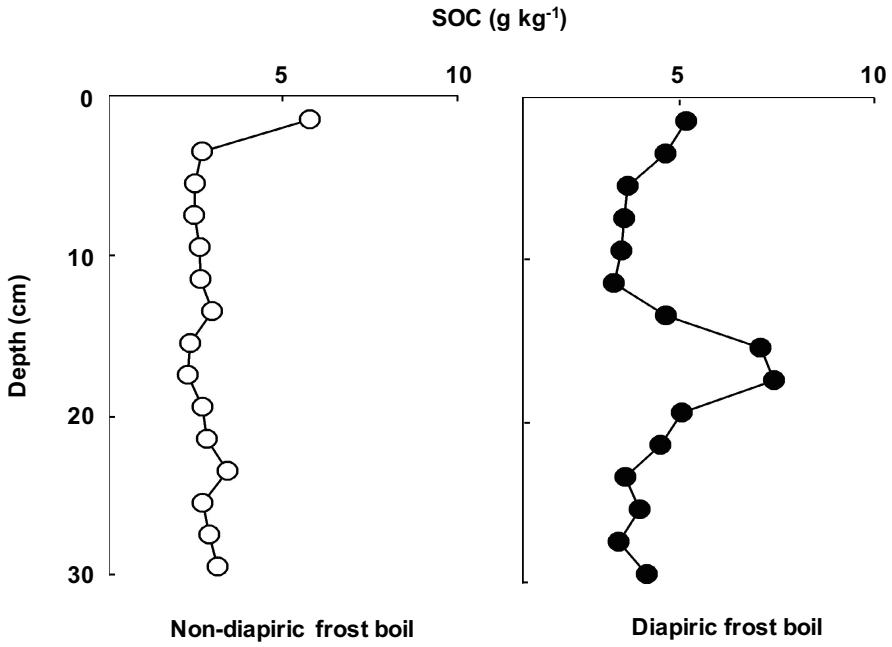

Fig. A3.1 SOC profiles of diapiric and non-diapiric frost boils based surveyed using the vis-NIR spectrometer. The data are from Muller et al. (2017).

APPENDIX 3

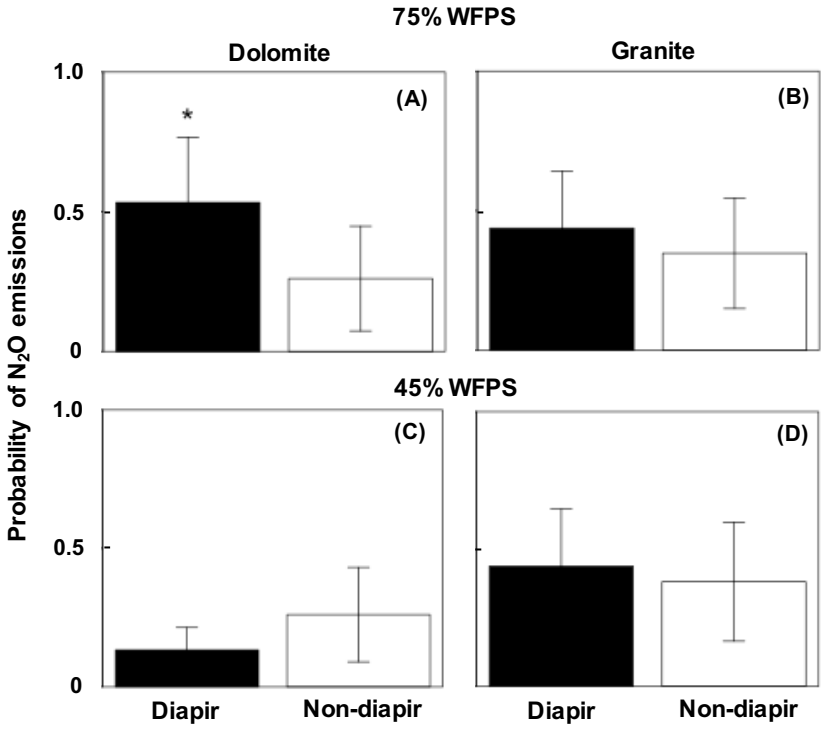

Fig. A4.1 The probability of N_2O emissions based on GLMM for the Bernoulli distribution from diapiric and non-diapiric frost boils within each of the dolomitic (A) (15 diapiric and 23 non-diapiric frost boils) and the granitic (B) (16 diapiric and 23 non-diapiric frost boils) deserts at 75% WFPS condition, and the probability from diapiric and non-diapiric frost boils within each of the dolomitic (C) (14 diapiric and 21 non-diapiric frost boils) and the granitic (D) (16 diapiric and 21 non-diapirc) deserts at 45% WFPS. * indicates $p < 0.05$ significance between diapiric and non-diapiric frost boils.

APPENDIX 4

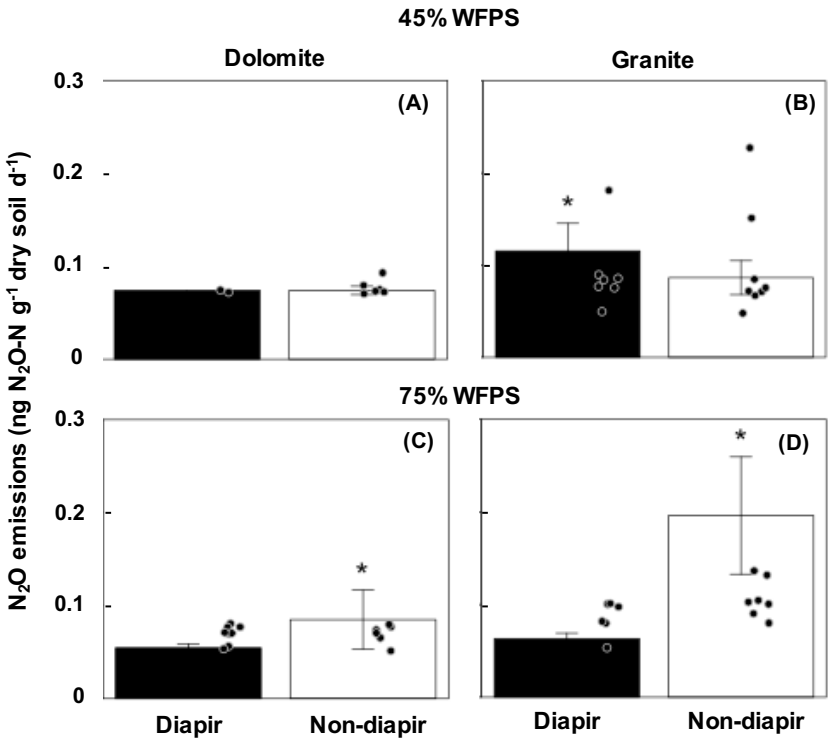

Fig. A4.2 LS means of N_2O emissions based on GLMM for gamma distribution (above detection limit) from diapiric and non-diapiric frost boils within each of the dolomitic (a) (two diapiric and six non-diapiric frost boils) and the granitic (b) (seven diapiric and eight non-diapiric frost boils) deserts at 45% WFPS, and those from diapiric and non-diapiric frost boils within each of the dolomitic (c) (eight diapiric and six non-diapiric frost boils) and the granitic (d) (seven diapiric and eight non-diapiric frost boils) deserts at 75% WFPS. There was one value higher than the y-axis upper limit in each of diapiric (0.35) and non-diapiric (0.44) frost boils within the granitic desert. * indicates $p < 0.05$ significant between diapiric and non-diapiric frost boils.

APPENDIX 5

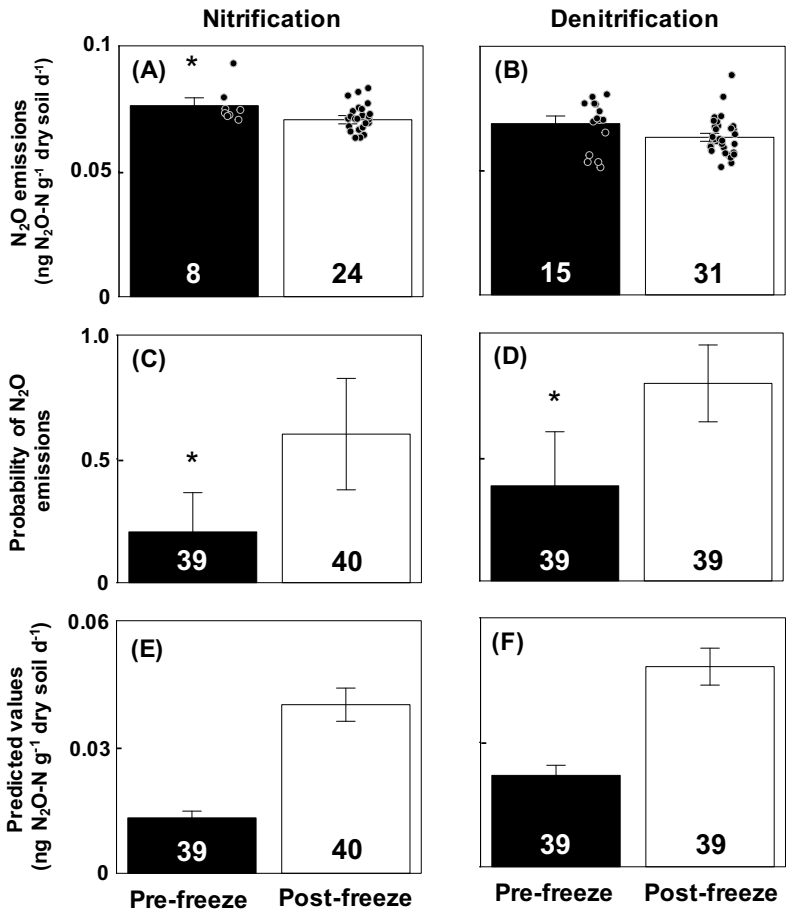

Fig. A5.2 LS means of N_2O emissions based on GLMM with a gamma distribution from pre-freeze and post-freeze in the dolomitic desert. Emissions under conditions favouring (A) nitrification and (B) denitrification. Mean values for the probability of N_2O emissions based on GLMM with Bernoulli distribution from pre-freeze and post-freeze under conditions favouring (C) nitrification and (D) denitrification. Predicted values for N_2O emissions from pre-freeze and post-freeze under favouring (E) nitrification and (F) denitrification. The predicted values and their standard errors were obtained using the hurdle model incorporating GLMMs with the Bernoulli and gamma components. Numbers in each column indicate sample sizes. Error bars represent standard errors of the mean. * indicates $p < 0.05$ significance.

APPENDIX 6

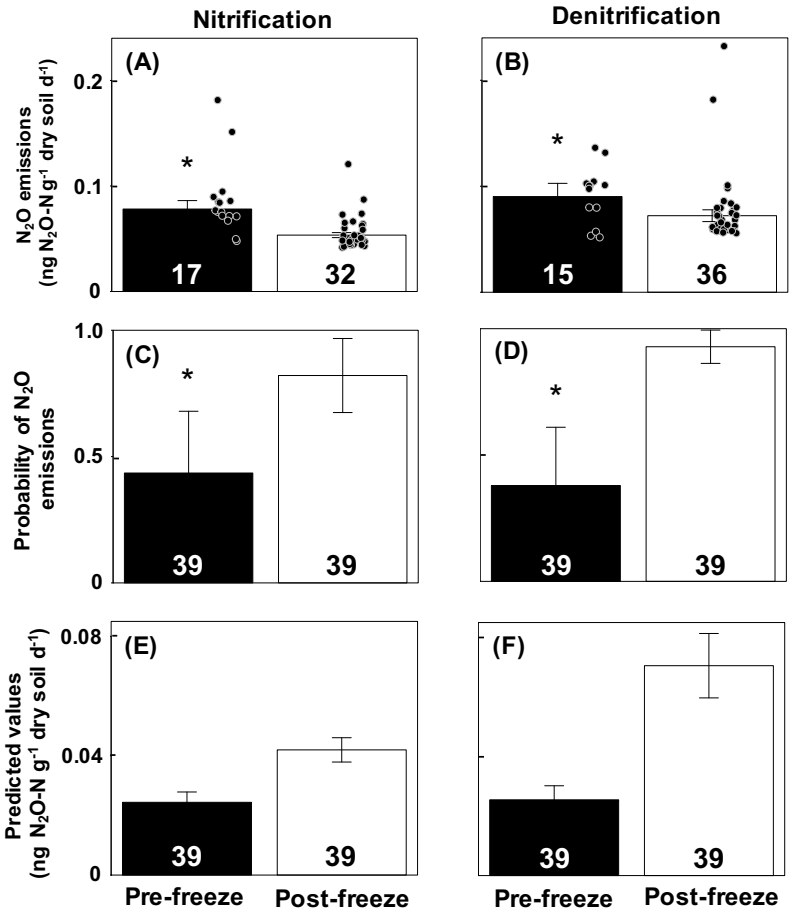

Fig. A5.3 LS means of N_2O emissions based on GLMM with a gamma distribution from pre-freeze and post-freeze in the granitic desert. Emissions under conditions favouring (A) nitrification and (B) denitrification. Mean values for the probability of N_2O emissions based on GLMM with Bernoulli distribution from pre-freeze and post-freeze under conditions favouring (C) nitrification and (D) denitrification. Predicted values for N_2O emissions from pre-freeze and post-freeze under conditions favouring (E) nitrification and (F) denitrification. The predicted values and their standard errors were obtained using the hurdle model incorporating GLMMs with the Bernoulli and gamma components. Numbers in each column indicate sample sizes. Error bars represent standard errors of the mean. * indicates $p < 0.05$ significance.